UC Berkeley

Title

Quantum Gravity Beyond Equilibrium

Permalink

https://escholarship.org/uc/item/76r544z4

Author

Mogni, Christopher

Publication Date

2021

Quantum Gravity Beyond Equilibrium

by

Christopher Mogni

A dissertation submitted in partial satisfaction of the

requirements for the degree of

Doctor of Philosophy

in

Physics

in the

Graduate Division

of the

University of California, Berkeley

Committee in charge:

Professor Petr Horava, Chair
Professor Richard Borcherds
Professor Holger Mueller

Summer 2021

Quantum Gravity Beyond Equilibrium

Abstract

Quantum Gravity Beyond Equilibrium

by

Christopher Mogni

Doctor of Philosophy in Physics

University of California, Berkeley

Professor Petr Horava, Chair

In this thesis, we explore the intersection between relativistic quantum gravity and non-equilibrium physics. We demonstrate a scenario where non-equilibrium physics can provide important insights into quantum gravity by non-perturbatively proving a weak gravity conjecture using entropic considerations. We take a different approach to extending string theory to describe scenarios where the universe is not assumed to be static and eternal by applying the Schwinger-Keldysh technique to Large-N gauge theories. We use the correspondence between Large-N gauge theories and string theory to derive a universal structure that worldsheets must follow out of equilibrium.

To Marie Hepfer

Thank you for your love and patience while I spent my sweet time finishing graduate school. Staying so long was not what we planned for, but you kept me sane and fed and happy throughout it all. I promise to give you the same love and support for your dreams too, even if that means figuring out how to keep our apartment in tip top shape all by myself!

Contents

List of Figures

Acknowledgments

I want to thank Petr Horava for providing kind, patient mentorship throughout my doctoral program. Petr is a great physicist and even greater person.

I want to thank my collaborators; Zach Fisher, Ziqi Yan, and Kevin Grosvenor; for working on very fun and exciting projects with me, especially as I learned how to be a good collaborator myself.

Most importantly, thank you mom and dad for supporting me in so many ways while I took the time to complete my program.

I would like to thank Oleg Tchernyshyov for being the first professor to take me on as a research student and Marc Kamionkowski for providing very good and humorous advice during my final year as an undergraduate. I would also like to thank the high school teachers for whom I am grateful for pushing me academically: Robert Rozzi, Priscilla Durkin, and Regina Levine.

Finally, I would like to thank John Brown and Xiaobei Wei for providing a second home at Sophie's Cuppa Tea.

Chapter 1

Introduction

Non-equilibrium many-body systems are of central interest in remarkably many areas of physics, across a vast range of scales: From the micoscopic scales of particle physics, to mesoscopic phenomena and condensed matter physics, to the cosmological scales of the cosmic microwave background and the large-scale structure of the Universe. Moreover, the fluctuations governing the collective behavior in such systems may be either quantum or classical, thermal in nature.

In the past few decades, the paradigm of string theory has proven to be a powerful generator of novel theoretical concepts which have found their way into remarkably many areas of physics and mathematics, not only to quantum gravity and particle phenomenology beyond the standard model, but also to condensed matter in holographic dualities and AdS/CFT correspondence [1, 2], or in helping with the topological classification of new topological states and phases of matter [3]. One naturally wonders, can this useful influence of string theory be extended to non-equilibrium systems?

A direct attempt to formulate string theory far away from equilibrium faces a strong, historically rooted obstacle: String theory originated [4] from the theory of the S-matrix, which is itself strongly based on the assumption of the static, stable, eternal relativistic vacuum.

Generally, in many-body physics such an assumption is far from necessary. The more general formulation, which could simply be called "quantum mechanics without simplifying assumptions" about the vacuum, is known as the Schwinger-Keldysh (SK) formalism [5, 6] (see [7] for a comprehensive list of reviews). The system is evolved forward and then backward, along a doubled time contour called the Schwinger-Keldysh (SK) time contour. Equivalently, this doubling can be viewed as a doubling of fields on the single-valued time t. This formalism has been the leading go-to technique for handling non-equilibrium many-body systems in condensed matter and a broad range of related areas for many decades. It also plays an increasingly important role in gravity and cosmology, which goes back to the early pioneering and insightful work by Hájíček [8], and later by Jordan [9]. In this century, the importance of the SK "in-in" formalism for inflationary cosmology has been particularly stressed by Weinberg [10, 11, 12] (see also [13]).

The purpose of this thesis is twofold: to show why non-equilibrium physics can lead to novel insights about quantum gravity and to explore what a non-equilibrium formulation of string theory should look like. The structure of this thesis is as follows.

The second chapter of this thesis demonstrates how studying non-equilibrium scenarios in semi-classical gravity can lead to deep insights about constraints on a UV complete theory of quantum gravity. This chapter uses entropic considerations to study a non-perturbative proof of a weak gravity conjecture by studying the evolution of near equilibrium (near-extremal) black holes. We show that the evolution of a black hole from its near-extremal to extremal state violates the second law of thermodynamics when a non-gravitational force is weaker than gravity. The extremal state in the theory we consider is unstable when gravity is the weakest force, which prevents the violation from occurring.

The third and forth chapters of this thesis focus on understanding how string theory relates to the SK formalism. Some work on SK formalism and strings already exists in the literature, primarily from the spacetime point of view [14, 15, 16, 17]. Here we follow a different strategy: In equilibrium, the structure of the large-N expansion in theories with interacting matrix degrees of freedom predicts a string coupling expansion, as a sum over connected worldsheet topologies Σ of increasing genus,

$$\mathcal{Z} = \sum_{h=0}^{\infty} \left(\frac{1}{N}\right)^{2h-2} \mathcal{F}_h(\lambda, \ldots). \tag{1.1}$$

Here $g_s \equiv 1/N$ plays the role of the string coupling constant, with the power of N given by the Euler number $\chi(\Sigma) = 2 - 2h$. The 't Hooft coupling λ is a worldsheet coupling analogous to α' of critical strings, with "$\ldots$" suggesting there might be more than one such worldsheet coupling. The importance of this duality, first developed by 't Hooft [18, 19], was further advocated over the years by Polyakov (see, *e.g.*, [20]), and others. It turned out that at least in special circumstances, when combined with additional spacetime symmetries, this relationship reveals a lot about the dual string theory, eventually leading to such milestones as AdS/CFT correspondence [21]. Can this relationship be extended away from equilibrium, and if so, what does it reveal about the perturbative expansion of the dual string theory?

The advantage of asking this question first on the large-N side is that we understand conceptually quite well how to take that system out of equilibrium: Simply apply the SK formalism. On the string dual side, much less is known about non-equilibrium, and we can hope to learn something new by taking the correspondence seriously.

Finally, the fifth chapter provides some concluding remarks concerning future research directions.

Chapter 2

An Entropic Proof of a Weak Gravity Conjecture

2.1. Introduction

In its simplest incarnation [22], the weak gravity conjecture states that a consistent, quantized theory of gravity coupled to an Abelian gauge theory must contain at least one charged, massive particle satisfying

$$m \leq q M_{\mathrm{Pl}}, \tag{2.1}$$

where m is the particle mass and q the particle charge. Because Newton's constant $G_N = 1/M_{\mathrm{Pl}}^2$, the bound implies gravity is the weakest force. All known string compactifications with Abelian gauge forces satisfy the conjecture. Moreover, it reconciles the absence of global symmetries in string theory with the $q \to 0$ limit of Abelian gauge theories. Within the context of perturbative string theory, the authors of [23] demonstrate that modular invariance of effective worldsheet theories evidently implies a version of the conjecture. Extensions of the weak gravity conjecture apply to p-form gauge fields of any $p \geq 0$ in arbitrary spacetime dimensions $D \geq 3$ [22]. In this chapter, we focus on $p = 1$, $D = 4$.

Although string theory automatically satisfies the weak gravity conjecture, the authors of [22] use black holes to argue that all healthy effective field theories should obey a weak gravity conjecture. Suppose a black hole has charge Q and mass M. Assuming cosmic censorship, $M \geq Q M_{\mathrm{Pl}}$. The black hole may decay via Hawking radiation or Schwinger pair production. For black holes far from extremality, Hawking radiation dominates. If the black hole only emits charged particles with charge q, and mass m, then conservation of charge implies that Q/q particles are produced. The black hole evolves to a state with mass mQ/q, which is less than M by conservation of energy. Through this process, the black hole approaches extremality, $Q/M = 1$.[1] At extremality, the black hole's temperature is zero, and Hawking radiation ceases. Such a black hole is stable unless there is a charged particle with $q/m > 1$, in which case particle-antiparticle pairs are produced via Schwinger

---

[1]We work in Planck units, i.e. $M_{\mathrm{Pl}} = 1$.

pair production. Pair production emits charged matter from the black hole; the black hole is no longer extremal. On the other hand, if the weak gravity conjecture is violated, a large number of stable extremal black hole states exist in the full quantum theory.[2] While a proliferation of stable quantum states does not itself signal a sickness from the effective field theory's perspective, it does appear physically undesirable.

Recent research directions have focused on sharpening and defining the weak gravity conjecture using effective field theory. The authors of [26] propose a stronger form of the weak gravity conjecture by studying matter gauged under a $U(1)^N$ symmetry group. They claim that the convex hull of the charge-to-mass vectors z_i for each species i of particles gauged under the $U(1)^N$ group must contain the unit ball $|z_i| \leq 1$. The same authors also attempt to frame the conjecture in terms of unitarity and causality of infrared scattering amplitudes [27], but [28] discusses counterexamples to their original argument. A series of chapters [29, 30, 23] combine intuition from black hole physics with considerations from effective field theory to sharpen the conjecture and to cast doubt on the consistency of field theories that violate it, such as large field axion inflationary models.

Nonetheless, an inherent sickness in effective field theories violating the weak gravity conjecture has eluded discovery. Proving the conjecture from a "bottom-up" perspective within the realm of flat space effective field theory may prove too difficult, or impossible. Consequently, effective field theories on large black hole backgrounds provide an ideal setting to test the conjecture without needing to invoke assumptions or intuition from some unknown UV theory. Presumably, we should be able to treat the near horizon physics of large black holes semi-classically due to the smallness of the Ricci curvature. One expects that entanglement of macroscopic fields across the horizon should tell us something about the underlying gravitational theory, even in a semi-classical setup.

Let us suppose a proliferation of stable black hole states is a property of sick effective field theories. It is plausible that the sickness would manifest itself by violating known properties of semi-classical entropy. The past decade has seen immense progress in unravelling entropy inequalities that encode deep connections between field theory and semi-classical gravity [25, 31, 32, 33, 34]. It is natural to speculate that macroscopic entropy might be powerful enough to discriminate between effective field theories that live in the landscape or swampland.

Sen *et al.* laid the foundation to study black hole entropy in effective field theory [35, 36, 37, 38, 39, 40]. They calculate logarithmic corrections to black hole entropy from the Euclidean path integral over the near horizon black hole geometry. One may work with the near horizon geometry directly because of the attractor mechanism, which Sen *et al.* also show applies to non-BPS black holes in the near-extremal limit. They further justify their methodology by matching the macroscopic entropy results with microscopic state counting using the $\text{AdS}_2/\text{CFT}_1$ duality. In low energy effective theories descending from string theory, the results match on both sides of the duality.

---

[2]Previously, it was believed that the presence of a large number of stable, Planck sized extremal black hole states would violate known entropy bounds [24]. However, Casini [25] casts doubt on this assertion by carefully examining properties of relative entropy, showing that entropy bounds may not necessarily rule out remnants.

These chapters do not address the macroscopic entropy due to fields interacting with the background field strength. The presence of a background electric flux modifies the effective masses of the matter fields near the horizon. The flux depends on the radius of the black hole. If the fields have sufficiently small mass relative to their charge, the coupling to the flux renders the near-horizon geometry unstable. It decays rapidly due to Schwinger pair production of particle-antiparticle pairs, which precludes us from calculating the macroscopic entropy with Sen's formalism. On the contrary, whenever the weak gravity conjecture is violated or saturated, the geometry is stable. No symmetry protects the stability of the extremal black hole in the non-supersymmetric theories we consider. We expect that perturbations of the extremal geometry may alter the black hole entropy in a way incompatible with known entropy inequalities after we account for quantum effects.

The purpose of this chapter is to confirm this hypothesis. To our knowledge, this is the first concrete demonstration that entropy inequalities may discriminate between effective theories that live in the swampland or landscape in a controlled, semi-classical environment. We consider $D = 4$ scalar matter gauged under a $U(1)^N$ gauge group in a large, extremal black hole background. The scalar matter violates the weak gravity conjecture. The scalar is minimally coupled to the gravitational and gauge fields. We do not include any non-renormalizable interactions or scalar-scalar interactions. We compute the exact, non-perturbative macroscopic contribution of the gauged scalar to the entropy of the black hole.[3] We choose a renormalization condition that sets an extremal black hole solution with large charge $|\vec{Q}|$ to its classical value. We consider a perturbation to the black hole whereby a neutral particle with energy E crosses the black hole horizon. We demonstrate that any small perturbation violates the second law for a sufficiently large initial black hole solution.[4] Consequently, we prove the weak gravity conjecture for a single scalar.

Related work

Qualitatively similar results to our entropy calculation appear in [41]. However, not all of their quantitative results match ours exactly. We believe that this results from the formalism they use to calculate the entropy of the black hole, which is not exactly equivalent to ours. We also believe that their conclusions and interpretation of results differ significantly enough from our own. Moreover, they do not attempt to prove the weak gravity conjecture using entropy inequalities, although they allude to this possibility.

A separate application of the second law towards understanding the weak gravity conjecture appears in [42], which appeared during the preparation of this manuscript. However,

---

[3]We hold the external gauge and gravitational fields fixed. Determining the full macroscopic entropy requires the gauge and gravitational sectors as well. Note however that the quantum corrections of fields neutral under the gauge symmetry are generically subleading. The calculation is exact in the semiclassical limit because the action is quadratic in the gauged scalar field.

[4]What we refer to as the second law is typically referred to as the generalized second law in the literature. We omit the word "generalized" because the generalized second law is the second law once one accounts for all sources of entropy.

their calculation is orthogonal to ours. Their chapter argues for the weak gravity conjecture using a bound on relaxation rates of quasinormal modes of near-extremal black holes. Although related to the second law, the connection is indirect: the second law implies the relaxation rate bound, which in turn implies the weak gravity conjecture. In this chapter, we present a a more direct link between the second law and the weak gravity conjecture.

2.2. Setup

Consider a charged, non-rotating black hole. The metric is

$$ds^2 = -\frac{(r - r_+)(r - r_-)}{r^2}dt^2 + \frac{r^2}{(r - r_+)(r - r_-)}dr^2 + r^2 d\Omega^2_{S^{D-2}}, \tag{2.2}$$

where

$$r_\pm = M \pm \sqrt{M^2 - |\vec{Q}|^2} \tag{2.3}$$

are the outer and inner horizons of the black hole in units where $M_{\text{Pl}} = 1$. M is the ADM mass of the black hole spacetime. The black hole is a solution of Einstein's equations, where the stress-energy tensor descends from a $U(1)^N$ gauge theory action. The classical action is

$$S_0 = \frac{1}{16\pi} \int d^D x \sqrt{\det g} \left(M_{\text{Pl}}^2 R - \sum_{n=1}^N F_{\mu\nu}^{(n)} F^{(n)\,\mu\nu} \right). \tag{2.4}$$

where g is the determinant of the spacetime metric, R is the Ricci scalar, and $F^{(n)}$ is the field strength for the nth gauge field. The background gauge fields $A_\mu^{(n)}$ are a Coulomb potential in the appropriate gauge:

$$A_\mu^{(n)} = \left(\frac{Q^{(n)}}{r}, 0, \dots, 0 \right). \tag{2.5}$$

In the extremal limit, $M \to |\vec{Q}|$, the coordinates of the horizons degenerate to

$$r_E^2 = |\vec{Q}|^2. \tag{2.6}$$

We may compute the macroscopic entropy of the classical geometry and quantum fluctuations about it using the near-horizon geometry [38].[5] After an appropriate choice of coordinates and Wick rotation to Euclidean signature, the near-horizon geometry in $D = 4$ spacetime dimensions is described by[6]

$$ds^2 = r_E^2 \left(d\eta^2 + \sinh^2 \eta \, d\theta^2 + d\psi^2 + \sin^2 \psi \, d\varphi^2 \right), \tag{2.7}$$

---

[5]This is computationally beneficial because there are no conifold singularities in the near-horizon geometry.

[6]Roughly, $\cosh \eta$ corresponds to the proper distance from the outer horizon in the near-horizon geometry. Details on deriving this form of the metric by taking the near-horizon and extremal limits may be found in [39]. The utility of working with this form of the metric is that there are no conical singularities.

where θ is 2π-periodic.[7] The near-horizon extremal metric factorizes as $\text{AdS}_2 \times S^2$.

The macroscopic entropy of the black hole may be calculated by calculating the effective action for the quantum fluctuations about the classical background. We work with the normalization of the Euclidean action in [38]. The effective action splits into a classical (S_0) and quantum (ΔW_{eff}) component:

$$W_{\text{eff}} = S_0 + \Delta W_{\text{eff}}. \tag{2.8}$$

Using

$$F_{\eta\theta}^{(n)} = Q^{(n)} \sinh \eta \tag{2.9}$$

and

$$R = 2/r_E^2, \tag{2.10}$$

we obtain

$$S_0 = -2\beta r_E - 4\pi r_E^2, \tag{2.11}$$

where $\beta = 4\pi r_E \cosh \eta_0$ is the inverse temperature of the near-extremal black hole induced by the $\text{AdS}_2 \times S^2$ boundary cutoff.[8] The first term in the classical part of the effective action is the classical entropy. The second is the classical black hole energy multiplied by the inverse temperature of the black hole.

Quantum corrections to the effective action may be calculated by splitting each field Φ into their classical background value Φ_{cl} and fluctuations about the background Φ_{q}:

$$\Phi(x) = \Phi_c(x) + \Phi_q(x). \tag{2.12}$$

If we truncate the action for the fluctuations about the background at quadratic order, we may calculate the one-loop contribution to the effective action. This classical action changes by ΔW_{eff} [38]:

$$\Delta W_{\text{eff}} = \int d^4x \sqrt{\det g} \, \Delta \mathcal{L}_{\text{eff}} = \frac{1}{2}\pi r_E^4 \left(\cosh \eta_0 - 1\right) \Delta \mathcal{L}_{\text{eff}}, \tag{2.13}$$

where $\Delta \mathcal{L}_{\text{eff}}$ is the effective Lagrangian. The first term corrects the ground state energy, regularized by an infrared cutoff η_0.[9] The second term corrects the macroscopic entropy [38]:

$$S_{\text{quant}} = -\frac{1}{2}\pi r_E^4 \Delta \mathcal{L}_{\text{eff}}. \tag{2.14}$$

From this expression, it is explicitly clear that in the near-extremal limit, where we can take $\beta \to \infty$, that the difference in entropies between two near-extremal geometries automatically satisfies the first law of thermodynamics.

---

[7]The coordinate θ is related to Euclidean time by a rescaling. The Euclidean time coordinate has infinite periodicity for extremal black holes. The normalization of Euclidean time such that it has period 2π permits us to find a finite result for the macroscopic entropy.

[8]The cutoff is implicitly taken to infinity, indicating that the black hole has a temperature that limits to zero, as expected for near-extremal black holes.

[9]This IR cutoff renders the volume of EAdS_2 finite.

Calculating the quantum correction to the macroscopic entropy reduces to calculating $\Delta\mathcal{L}_{\text{eff}}$.[10] The evolution operator along Euclidean worldline time for a particle with worldline Hamiltonian $\widehat{H}$ is the heat kernel [43, 44]

$$K(x, x'; s) = \langle x' | e^{-s\widehat{H}} | x \rangle. \tag{2.15}$$

To derive $\widehat{H}$ for fluctuations of a scalar field about a classical background, consider the minimally gauged scalar field action:

$$S_\phi = \int d^4x \sqrt{\det g} \left(-g^{\mu\nu} \overline{\phi} \left(\nabla_\mu + qA_\mu \right) \left(\nabla_\nu + qA_\nu \right) \phi + m^2 \overline{\phi}\phi \right), \tag{2.16}$$

where ∇_μ is the covariant derivative compatible with the metric $g_{\mu\nu}$. The worldline Hamiltonian for the ϕ field is

$$\widehat{H} = -g^{\mu\nu} \left(\nabla_\mu + qA_\mu \right) \left(\nabla_\nu + qA_\nu \right) + m^2. \tag{2.17}$$

Inserting $\widehat{H}$ into the heat kernel, we obtain the quantum correction to the effective action:

$$\Delta\mathcal{L}_{\text{eff}} = \frac{1}{2} \int_\varepsilon^\infty \frac{ds}{s} \int d^4x \sqrt{\det g} \, K(s), \tag{2.18}$$

where $K(s) \equiv K(x, x; s)$.[11] A small distance cutoff ε[12] must be imposed due to divergences at the lower bound of the s integral.

We may calculate the heat kernel in two ways. Perturbatively, we may perform an expansion of the heat kernel for small s [44, 45]. We express the heat kernel in powers of the Riemann curvature, field strengths, and their contractions, multiplied by the appropriate power of s. The geometric expansion yields the perturbative, one-loop contribution to the effective action. This is the familiar small s expansion of the heat kernel. For an arbitrary scalar field, this expansion reads

To find an *exact* solution, we decompose the heat kernel as a sum of the eigenfunctions $f_n(x)$ and eigenvalues κ_n of $\widehat{H}$ [44]:

$$K(x, x'; s) = \sum_n f_n(x) f_n^*(x) e^{-\kappa_n s}. \tag{2.19}$$

By performing the sum, we obtain the resummed one-loop contribution to the effective action. If the action is quadratic in the field Φ, then the resummed one-loop correction is the *exact* correction to the effective action for the Φ field in the presence of *fixed, external*

---

[10]Some places in the literature refers to the quantum correction we compute as S_{out}, and the macroscopic entropy as S_{gen}.

[11]$K(s)$ is independent of x by translational symmetry.

[12]With dimensions length squared.

$A_\mu^{(n)}$ and $g_{\mu\nu}$. Although the heat kernel only resums one-loop diagrams, the effects of higher loop processes from internal gravitons and gauge particles are encoded in effective vertices, which may be verified in a Feynman diagrammatic expansion.[13]

Armed with the exact effective action, we extract its logarithmic corrections in the limit where $|\vec{Q}|$ and $|\vec{q}\cdot\vec{Q}|$ are large, but $|\vec{q}|$ is small. After choosing a renormalization scheme or redefining couplings by appropriately absorbing the effective field theory cutoff, we obtain the macroscopic entropy due to the Φ field. Note that because A_μ and $g_{\mu\nu}$ are held fixed, their contribution to the entropy must be estimated from their separate one-loop contribution to the effective action. Additionally, one must characterize the backreaction on the gauge and gravitational fields induced by the scalar fluctuations.[14]

2.3. Macroscopic Entropy

Contribution to Entanglement Entropy from Neutral Scalars

We want to compute the quantum correction to the macroscopic entropy due to a gauged scalar. Let us review the calculation for a neutral, massless scalar. For each field, there are four contributions to the entropy:

$$S = S_0 + S_{\text{div}} + S_{\text{CT}} + S_{\text{fin}} \tag{2.20}$$

where S_0 is the classical contribution to the entropy, S_{div} is the UV divergent quantum correction, S_{CT} is the entropy from counterterms that regulate UV divergences, and S_{fin} is from finite quantum corrections to the entropy. Because the heat kernels of the individual fields add at one-loop, the total entropy is the sum of the individual fields' contributions to the entropy. Beyond one-loop, we must estimate the magnitude of entropic contributions from quantum fluctuations of the background geometry backreacting on one-another.

To compute the heat kernel of the scalar field in the $\text{AdS}_2 \times S^2$ geometry, we express $\widehat{H}$ as the sum of the scalar Laplacian operator on AdS_2 and the scalar Laplacian on S^2. The heat kernel factorizes as

$$K(s) = K_{\text{AdS}_2}(s) K_{\text{S}^2}(s). \tag{2.21}$$

The eigenfunctions of S^2 are the spherical harmonics $Y_{\ell m}(\psi, \varphi)/r_E^2$. Only the $m = 0$ eigenfunctions contribute to $K(s)$. At $\psi = 0$,

$$Y_{\ell 0}(0) = \sqrt{\frac{2\ell + 1}{4\pi}}, \tag{2.22}$$

---

[13] The same phenomenon occurs in the Euler-Heisenberg Lagrangian, cf. [43].

[14] We may calculate the semiclassical backreaction by solving Einstein's equations with the stress-tensor replaced by its one-loop corrected expectation value. We later show backreaction effects to be negligible for the perturbations of the renormalized effective action for the specific geometry we study.

and $Y_{\ell 0}$ has eigenvalues $\ell(\ell + 1)/r_E^2$. Therefore,

$$K_{S^2}(s) = \frac{1}{4\pi r_E^2} \sum_{\ell=0}^{\infty} (2\ell + 1)e^{-s\ell(\ell+1)/r_E^2}. \tag{2.23}$$

The eigenvalues and eigenfunctions of the S^2 Laplacian are unaffected by the gauge covariant coupling of the ϕ field to the background gauge field.

The eigenfunctions of the neutral, massless scalar Laplacian on AdS_2 are given in [38]. The full expression simplifies significantly at the origin of the AdS_2 coordinate system. There, the eigenfunctions are

$$f(\lambda) = \sqrt{\frac{\lambda \tanh(\lambda)}{2\pi r_E^2}}, \tag{2.24}$$

where λ is a positive real number. The eigenvalues are

$$\kappa(\lambda) = \frac{\lambda^2 + 1/4}{r_E^2}. \tag{2.25}$$

Therefore, the heat kernel is

$$K_{AdS_2}(s) = \frac{1}{2\pi r_E^2} \int_0^{\infty} d\lambda \, \lambda \tanh(\pi\lambda) e^{-(\lambda^2 + 1/4)s/r_E^2}. \tag{2.26}$$

We interpret $\lambda \tanh(\pi\lambda)$ as the density of states for the neutral scalar in the AdS_2 background geometry.

Combining these results, we obtain the heat kernel for the neutral, massless scalar on the near-horizon background geometry

$$K(s) = \frac{1}{16\pi^2 r_E^4 \bar{s}^2} \left(1 + \frac{\bar{s}^2}{45}\right). \tag{2.27}$$

Consequently, the divergent contribution to the entropy in the large $|\vec{Q}|$ limit in Planck units is

$$S_{\mathrm{div}} = +\frac{r_E^2}{4\varepsilon^2} + \frac{1}{180} \log(\varepsilon/r_E^2). \tag{2.28}$$

This is the *exact* divergent correction to the macroscopic entropy of the black hole due to the quantum fluctuations of a neutral scalar, previously derived in [38].[15] The result is exact because the action is quadratic in the scalar field, and we formally solved for the heat kernel using equation (2.19) without a perturbative expansion.

---

[15]Up to exponentially suppressed terms and backreaction of the background fields.

The result matches the familiar small s expansion of the heat kernel in powers and contractions of curvature invariants. The coefficients of the heat kernel expanded in s are related to local quantities computed in the background geometry,

$$K(s) = \sum_{n=0}^{\infty} a_{2n}(R_{\mu\nu\rho\sigma}, F_{\mu\nu}) s^{n-2} e^{-sm^2}, \tag{2.29}$$

where, for a massive scalar field in an arbitrary background geometry the coefficients are

$$a_0 = \frac{1}{8\pi^2} \int d^4x \sqrt{\det g} \tag{2.30}$$

$$a_2 = \frac{1}{8\pi^2} \int d^4x \sqrt{\det g} \, \frac{1}{6} R \tag{2.31}$$

$$a_4 = \frac{1}{8\pi^2} \int d^4x \sqrt{\det g} \left(12 \nabla_\mu \nabla^\mu + 5R^2 - 2R_{\mu\nu} R^{\mu\nu} + 2R_{\mu\nu\rho\sigma} R^{\mu\nu\rho\sigma} - 30q^2 F_{\mu\nu} F^{\mu\nu} \right). \tag{2.32}$$

For the near-horizon geometry, the constant part of $K(s)$, which is $a_4(s)$ in four-dimensions, may be reduced to

$$a_4 = \frac{1}{720\pi^2} R_{\mu\nu} R^{\mu\nu} = \frac{1}{720\pi^2 r_E^2}, \tag{2.33}$$

as expected. We have set $m^2 = 0$ for the massless field considered in this section. For a massive field, the logarithmic divergence is damped:

$$S_{\text{div,log}} = \frac{1}{180} \log\left(\frac{\varepsilon}{m^2}\right). \tag{2.34}$$

If the mass is smaller the inverse radius of the extremal black hole, it is appropriate to expand the exponential for small s. The logarithmic divergence is a modification of the massless scalar's logarithmic divergence:

$$S_{\text{div,log}} = \left(\frac{1}{180} + \frac{1}{8} m^2 r_E^2 \right) \log\left(\frac{\varepsilon}{r_E^2}\right). \tag{2.35}$$

It may be checked [44] that this extra term contributes to the renormalization of the cosmological constant. When we study the gauged scalar, it is important to note that the extra divergence present in that answer takes the form of a divergent cosmological constant contribution *without* any expansion of the exponential.

Because the expression for the entropy is UV divergent, we must append counterterms to the effective action to cancel the divergences. Schematically denote each counterterm by $\delta_{\mathcal{O}}\mathcal{O}$, where $\mathcal{O}$ is the operator which receives a divergent correction, and $\delta_{\mathcal{O}}$ is the counterterm. The heat kernel in the small effective mass limit has no exponential suppression. Therefore, the counterterm $\delta_{\mathcal{O}}$ introduces an arbitrary length scale ℓ satisfying $\varepsilon < \ell^2 < r_E^2$ to cancel

the divergence in the logarithmic term that occurs when we take $\varepsilon \to 0$. Schematically, each counterterm takes the form

$$\delta_{\mathcal{O}}\mathcal{O} = -\sum_{n=1}^{d/2} c_{\mathcal{O}}^{(n)} \varepsilon^{-2n} - c_{\mathcal{O}}^{(0)} \log(\ell^2/\varepsilon) = -\sum_{n=1}^{d/2} c_{\mathcal{O}}^{(n)} \varepsilon^{-2n} - c_{\mathcal{O}}^{(0)} \left[\log(\ell_0^2/\varepsilon) + \log(\ell^2/\ell_0^2) \right]. \quad (2.36)$$

The $c_{\mathcal{O}}^{(n)}$ coefficients represent the coefficients of the divergent parts of the ε^{-2n} portions of the effective action in the $\varepsilon \to 0$ limit. We introduce two arbitrary length scales ℓ and ℓ_0. The length scale ℓ_0 does not contribute to the entropy of the initial extremal black hole solution we consider, as it cancels out. However, to simplify calculations, we fix the last term in the above expression for all black hole solutions. When we renormalize both black hole solutions, this fixes both ℓ and ℓ_0. Because ℓ_0 does not appear in the entropy for the extremal black hole, choosing a renormalization condition for the initial extremal black hole fixes ℓ. When we apply a linearized perturbation to the extremal black hole, we have chosen a convention where all terms in the entropy above change except for the last, finite counterterm. We then renormalize this black hole solution, which fixes ℓ_0. All other black hole solutions obtained from further perturbations of the renormalized solution run with changes in the black hole parameters (charge, gauge coupling, radius) as dictated by our initially chosen renormalization conditions.

We implicitly choose a renormalization condition that exactly cancels any non-logarithmic divergences. We only discuss the logarithmically divergent counterterms in what follows, unless otherwise specifed. For the massless scalar, we must add a counterterm for the $R_{\mu\nu}R^{\mu\nu}$ operator. Its contribution to the expression for the entropy is

$$S_{\text{CT,log}} = -\frac{1}{180} \log(\varepsilon/\ell^2), \quad (2.37)$$

where ℓ is the arbitrary renormalization scale, in units of length. The renormalized quantum contribution to the entropy is

$$S_{\text{qu}} = \frac{1}{180} \log(\ell^2/r_E^2), \quad (2.38)$$

at extremality. If we can trust the extremal approximation near-extremality, we may simply replace the extremal radius with the outer radius of the black hole, $r_E \to r_+$. We do this when we consider small, linear perturbations to the near horizon geometry. Because ℓ is an ambiguous scale, we fix it by specifying our renormalization condition. For example, we may choose a condition that for a black hole of charge $\vec{Q}_0$ at extremality, the quantum corretion to the black hole entropy vanishes exactly. Because the entropy depends on the radius of the black hole, the quantum entropy of another extremal black hole of charge $\vec{Q}_0' \neq \vec{Q}_0$ or of a near-extremal black hole of charge $\vec{Q}_0$ is non-zero. In other words, the entropy runs with the radius of the black hole.

The case of a massive scalar is different. For a massive scalar with $m > 1/r_E$, we may not expand the exponential term that suppresses the heat kernel. The logarithmic contribution

to the entropy is, therefore,

$$S_{\text{div,log}} = \frac{1}{180} \log(\varepsilon/m^2). \tag{2.39}$$

Up to a finite term that is independent of the black hole radius, we may choose a logarithmically divergent counterterm for $R_{\mu\nu}R^{\mu\nu}$ whose contribution to the entropy is

$$S_{\text{CT,log}} = \frac{1}{180} \log(m^2/\varepsilon), \tag{2.40}$$

which cancels the divergence exactly. There is no ambiguous renormalization scale that must be specified. This is in line with the reasoning that only massless neutral particles contribute to the entropy of large black holes. The exception is for particles with very small mass, i.e. $m < r_E^{-1}$. In that case, the renormalization to the $R_{\mu\nu}R^{\mu\nu}$ operator proceeds in the same way. An extra operator must be renormalized to absorb the extra divergent contributions to the heat kernel. The structure of the divergent terms exactly matches the contribution to the cosmological constant. We renormalize the cosmological constant to absorb its divergence [44]. Its counterterm contributes a logarithmically divergent term to the entropy

$$S_{\text{CT,log}} = \frac{1}{360} m^4 r_E^4 \log(\ell^2/\varepsilon). \tag{2.41}$$

The renormalized correction to the entropy is

$$S_{\text{qu}} = \left(\frac{1}{180} + \frac{1}{360} m^4 r_E^4 \right) \log(\ell^2/r_E^2). \tag{2.42}$$

Entropy of Gauged Scalars

The coupling of the gauged scalar to the background field modifies the eigenvalues and eigenfunctions of the scalar AdS_2 Laplacian [46]. In the near-horizon geometry, the background field strength for the nth gauge field in the Wick rotated spacetime is

$$F_{\eta\theta}^{(n)} = iQ^{(n)} \sinh\eta. \tag{2.43}$$

Suppose instead that the scalar is coupled to a constant background magnetic monopole field $\vec{B} = \vec{q} \cdot \vec{Q} \sin(\psi) \widehat{\psi} \times \widehat{\varphi}/r_E^2$. There is a continuous and discrete delta-function normalizable spectrum. The continuous eigenvalues are

$$\kappa(\lambda)_B = \frac{(\lambda - \vec{q} \cdot \vec{Q})^2 + (\vec{q} \cdot \vec{Q})^2 + 1/4}{r_E^2}. \tag{2.44}$$

The density of continuous states becomes

$$\lambda \tanh(\pi\lambda) \to \lambda \frac{\sinh(2\pi\lambda)}{\cosh(2\pi\lambda) + \cos(2\pi\vec{q} \cdot \vec{Q})}. \tag{2.45}$$

Wick rotating $\vec{q} \cdot \vec{Q} \to i\vec{q} \cdot \vec{Q}$, where $\vec{q}$ is the elementary charge vector of the ϕ field, we obtain the density of states for the ϕ field in the constant background electric field:

$$\lambda \tanh(\pi\lambda) \to \lambda \frac{\sinh(2\pi\lambda)}{\cosh(2\pi\lambda) + \cosh(2\pi\vec{q} \cdot \vec{Q})}. \tag{2.46}$$

The scalar heat kernel for the near-horizon geometry is

$$K(s) = \frac{1}{8\pi^2 r_E^4} \sum_{\ell=0}^{\infty} (2\ell+1) \int_0^\infty d\lambda \frac{\lambda \sinh(2\pi\lambda)}{\cosh(2\pi\lambda) + \cosh(2\pi\vec{q} \cdot \vec{Q})} e^{-s(\lambda^2 + \ell(\ell+1) + \frac{1}{4} + r_E^2 m^2 - (\vec{q} \cdot \vec{Q})^2)/r_E^2}. \tag{2.47}$$

Because the coupling $\vec{q}$ appears in the argument of a hyperbolic cosine function in the denominator of the density of states, we conclude that the resummed heat kernel represents the non-perturbative scalar field contribution to the effective action in a fixed, constant, external electric field. The result is not, however, the full quantum correction to the heat kernel. The gauge fields and gravitational field themselves contribute to the entropy. Furthermore, allowing the external gauge and gravitational fields to vary induces backreaction effects on the scalar's effective action.

Let us compute the divergent contributions to the effective action. Logarithmic divergences are universal and may be found in the region of integration $\varepsilon \ll s \ll r_E^2$. Therefore, we expand the resummed heat kernels for small $\bar{s} \equiv s/r_E^2$. The total heat kernel is the product of the AdS_2 and S^2 heat kernels, weighted by a factor of $e^{-\bar{s}(r_E^2 m^2 - (\vec{q} \cdot \vec{Q})^2)}$. The expansion of the S^2 heat kernel is [38]:

$$K_{\text{S}^2}(s) = \frac{1}{4\pi r_E^2 \bar{s}} e^{\bar{s}/4} \left(1 + \frac{1}{12}\bar{s} + \frac{7}{480}\bar{s}^2 + \mathcal{O}(\bar{s}^3) \right). \tag{2.48}$$

We perform the small $\bar{s}$ expansion of the AdS_2 heat kernel in its resummed form. The denominator of the AdS_2 density of states has an asymptotic expansion

$$\frac{1}{\cosh(2\pi\lambda) + \cosh(2\pi\vec{q} \cdot \vec{Q})} = 1 + \sum_{n=1}^{\infty} \left(U_n(-\cosh(2\pi\vec{q} \cdot \vec{Q})) - U_{n-2}(-\cosh(2\pi\vec{q} \cdot \vec{Q})) \right) e^{-2\pi n\lambda}, \tag{2.49}$$

where $U_n(x)$ is the nth Chebyshev polynomial of the second kind. The expansion converges when $0 \leq \lambda < |\vec{q} \cdot \vec{Q}|$, regardless of the size of $|\vec{q} \cdot \vec{Q}|$. This may be checked readily by using the ratio test. The first term in the series may be evaluated directly. To evaluate the subsequent terms, we expand $e^{-\lambda^2 \bar{s}}$ for small $\bar{s}$. Denote

$$\mathcal{F}_n(x) = \text{Li}_n(x + \sqrt{x^2 - 1}) + \text{Li}_n(x - \sqrt{x^2 - 1}), \tag{2.50}$$

where Li_n is the nth polylogarithm. We integrate over λ to find the AdS_2 heat kernel:

$$K_{\mathrm{AdS}_2}(s) = -\frac{e^{-\bar{s}/4}}{4\pi r_E^2 \bar{s}}\left[1 + \frac{\bar{s}}{2\pi^2}\mathcal{F}_2(-\cosh(2\pi\vec{q}\cdot\vec{Q}))\right.$$
$$\left. + \bar{s}^2\left(\frac{7}{480} + \frac{1}{24\pi^2}\mathcal{F}_2(-\cosh(2\pi\vec{q}\cdot\vec{Q})) - \frac{3}{4\pi^2}\mathcal{F}_4(-\cosh(2\pi\vec{q}\cdot\vec{Q}))\right)\right].$$
$$(2.51)$$

Through the last step, we have not made any assumptions concerning the size of $|\vec{q}\cdot\vec{Q}|$. All expansions performed have been independent of it. Now, let us take the large $|\vec{q}\cdot\vec{Q}|$ limit. We find that

$$\mathrm{Li}_2(-\cosh(2\pi\vec{q}\cdot\vec{Q})) = -\frac{\pi^2}{6} - 2\pi^2(\vec{q}\cdot\vec{Q})^2 + \mathcal{O}\left(\mathrm{sech}^2(\vec{q}\cdot\vec{Q})\right) \qquad (2.52)$$

$$\mathrm{Li}_4(-\cosh(2\pi\vec{q}\cdot\vec{Q})) = -\frac{7\pi^4}{360} - \frac{\pi^4}{3}(\vec{q}\cdot\vec{Q})^2 - \frac{2\pi^4}{3}(\vec{q}\cdot\vec{Q})^4 + \mathcal{O}\left(\mathrm{sech}^2(\vec{q}\cdot\vec{Q})\right). \qquad (2.53)$$

All together, the unrenormalized, large $|\vec{q}\cdot\vec{Q}|$ heat kernel is

$$K(s) = \frac{e^{-\bar{s}(r_E^2 m^2 - (\vec{q}\cdot\vec{Q})^2)}}{16\pi^2 r_E^4 \bar{s}^2}\left[1 - \bar{s}(\vec{q}\cdot\vec{Q})^2 + \bar{s}^2\left(\frac{1}{45} + \frac{1}{6}(\vec{q}\cdot\vec{Q})^2 + \frac{1}{2}(\vec{q}\cdot\vec{Q})^4\right) + \mathcal{O}(\bar{s}^3)\right]. \quad (2.54)$$

Note that our result reduces to the heat kernel of a single neutral scalar in the extremal black hole near-horizon geometry when $\vec{q} = 0$ [38]. Higher order terms in $\bar{s}$ contribute to finite portions of the effective action, which contribute negligibly to differences in the entropy.[16] A similar, yet quantitatively different, result appears in [41].

Using the heat kernel, we may determine the logarithmic correction to the effective action, and thereby the logarithmic correction to the entropy. To connect with the weak gravity conjecture, we want to know the entropy for the resummed heat kernel, which has the $|\vec{Q}|^4$ dependence. The resummed, unrenormalized logarithmic correction to the macroscopic entropy from a single gauged scalar of mass m and charge $\vec{q}$ in the large $|\vec{q}\cdot\vec{Q}|$ limit for fixed $A_\mu^{(n)}$, $g_{\mu\nu}$ is

$$S_{\mathrm{div,log}} = \frac{1}{4}\left(\frac{1}{45} + \frac{1}{6}(\vec{q}\cdot\vec{Q})^2 + \frac{1}{2}(\vec{q}\cdot\vec{Q})^4\right)\log(\varepsilon/(r_E^4 m^2 - r_E^2(\vec{q}\cdot\vec{Q})^2)). \qquad (2.55)$$

When $r_E^2 m^2 = (\vec{q}\cdot\vec{Q})^2$, there is no exponential suppression, and the logarithmically divergent contribution to the entropy is

$$S_{\mathrm{div,log}} = \frac{1}{4}\left(\frac{1}{45} + \frac{1}{6}(\vec{q}\cdot\vec{Q})^2 + \frac{1}{2}(\vec{q}\cdot\vec{Q})^4\right)\log(\varepsilon/r_E^2). \qquad (2.56)$$

---

[16]One may check that the finite contributions to the entropy scale as $|\vec{q}|^{2n}|\vec{Q}|^4$ for $n > 2$. However, differences between the near-extremal and extremal black hole entropies scale as $|\vec{q}|^{2n}|\vec{Q}|^2$. Because we are interested in the $|\vec{q}| \to 0$ limit, the finite contributions to the entropy are suppressed, as expected. Our logarithmic result, however, does not rely on the smallness of $|\vec{q}\cdot\vec{Q}|$, as shown explicitly in the work outlined above.

Suppose that weak gravity conjecture is satisfied but not saturated. The exponent in the resummed heat kernel before integration over λ

$$\text{Exponent} = e^{-\bar{s}(\lambda^2 + r_+^2 m^2 - (\vec{q}\cdot\vec{Q})^2)} \tag{2.57}$$

grows with increasing $\bar{s}$ for sufficiently small λ. We interpret this as an IR instability in the spectrum. The IR instability yields an imaginary contribution to the effective action [46]. The magnitude of the imaginary contribution corresponds to the amount of pair production that occurs at the near-horizon geometry. We expect that one must resort to a computation of the macroscopic entropy using the Euclidean action defined on the global black hole geometry due to the instability. Additionally, we expect that it is no longer justified to work with the classical black hole background without considering how the instability backreacts on the geometry. We leave this topic for future work.

Renormalization of Gauged Scalar Entropy

Let us specify renormalization conditions for the initial extremal black hole solution. The black hole we consider has charge $\vec{Q}$. We assume that $|\vec{q}|$ is small, $|\vec{Q}|$ is large, and $|\vec{q}\cdot\vec{Q}|$ is large. We choose counterterms that cancel ε^{-n} divergences for $n \geq 1$. The coefficient of the logarithmically divergent term is much larger than the classical contribution to the entropy. However, this does not imply that the correction for *this* black hole solution is large. We choose a renormalization condition that allows us to still work in the semi-classical regime. For the perturbation we consider, we choose a renormalization condition that sets ℓ_0 to the inverse Planck mass. Note that for large perturbations, the quantum corrections to the perturbed black hole become non-negligible.

The entanglement entropy calculated with all loop orders is given by equation (2.55). There are two important pieces of this result. First, we have the divergent term of the form

$$S_{\text{div,log}} = \frac{1}{4}\left(\frac{1}{45} + \frac{1}{6}(\vec{q}\cdot\vec{Q})^2 + \frac{1}{2}(\vec{q}\cdot\vec{Q})^4\right)\log(\varepsilon/r_E^2). \tag{2.58}$$

Comparing this to equation (2.35), we see that this logarithmically divergent contribution resembles the contribution to the entropy from a neutral scalar field with a small mass. There are two important differences. First, the places where the small quantity m/r_E appear in the expansion of the heat kernel are exactly replaced by factors of $(\vec{q}\cdot\vec{Q})^2$. This indicates that unlike the one-loop approximation to the gauged scalar heat kernel (cf appendix), there is an extra divergent contribution to the *exact* heat kernel from a cosmological constant term. As with the massless neutral scalar, we may cancel the divergence from the other two terms by inserting counterterms for $R_{\mu\nu}R^{\mu\nu}$ and $F_{\mu\nu}F^{\mu\nu}$. As may be confirmed in [44], the $(\vec{q}\cdot\vec{Q})^4$ requires renormalization of the cosmological constant.

The second difference is the argument of the logarithm: it depends on $(\vec{q}\cdot\vec{Q})^2$. It becomes clear what to do with the logarithmic divergence if we rewrite its contribution to the entropy

in the following way:

$$S_{\text{div,log}} = \frac{1}{4}\left(\frac{1}{45} + \frac{1}{6}(\vec{q}\cdot\vec{Q})^2 + \frac{1}{2}(\vec{q}\cdot\vec{Q})^4\right)\left(\log(\varepsilon/r_E^2) - \log(r_E^2 m^2) - \log\left(1 - \frac{(\vec{q}\cdot\vec{Q})^2}{r_E^2 m^2}\right)\right).$$
(2.59)

Surprisingly, the divergent terms for a massive gauged scalar look like the divergent terms for a neutral scalar in the small mass limit, with the $r_E^2 m^2$ coefficient swapped for $(\vec{q}\cdot\vec{Q})^2$. The other terms are *resummed, finite* corrections to the entropy. Their contributions come from an infinite sum of $(F_{\mu\nu}F^{\mu\nu})^n$-type operators. They do not require counterterms because of the lack of dependence on ε. Because they depend on the radius of the black hole, their contribution can only be cancelled for a *specific* black hole solution. In general, they contribute a non-zero, *finite* correction to the entropy at arbitrary black hole mass and charge.

We renormalize the entropy as we did for the neutral scalar in the small mass limit, with the only new feature being a $F_{\mu\nu}F^{\mu\nu}$ counterterm. The renormalized entropy is

$$S_{\text{div,log}} = \frac{1}{4}\left(\frac{1}{45} + \frac{1}{6}(\vec{q}\cdot\vec{Q})^2 + \frac{1}{2}(\vec{q}\cdot\vec{Q})^4\right)\left(\log(\ell^2/r_E^2) - \log(r_E^2 m^2) - \log\left(1 - \frac{(\vec{q}\cdot\vec{Q})^2}{r_E^2 m^2}\right)\right).$$
(2.60)

We specify a renormalization condition that sets the finite contributions to the entropy from resummation as well as the divergent terms equal to zero for a black hole of fixed charge $\vec{Q}$ exactly at extremality. This removes the ambiguity for the renormalization scale ℓ and removes all divergences.

2.4. Violating the Second Law

Setup

The second law states that entropy increases under any physical process:

$$dS \geq 0.$$
(2.61)

For healthy semi-classically treated effective field theories in curved space, the second law has been proven within various settings, e.g. [47]. The entropy S has contributions from the classical and quantum parts of the effective action: the Bekenstein-Hawking area term as well as quantum corrections from the macroscopic fields:

$$\mathcal{S} = -W_{\text{eff}} = -(S_0 + S_{\text{quant}}),$$
(2.62)

$$S_{\text{quant}} = S_{\text{div}} + S_{\text{CT}},$$
(2.63)

where we have neglected subleading finite corrections in S_{quant}. In our physical scenario, the entropy changes when the black hole consumes a neutral particle because the black

hole's radius increases. Let subscript f denote final quantities, subscript i initial quantities, $A \equiv 4\pi r_+^2$ the area, and S_{quant} the quantum entropy correction. Then

$$S_{0,f} - S_{0,i} \geq S_{\text{quant},i} - S_{\text{quant},f} \tag{2.64}$$

follows from the second law.

In our thought experiment, we let a single neutral particle crosses the black hole horizon with energy E. This induces a linearized perturbation of the extremal black hole geometry. The black hole charge remains fixed. The initial black hole entropy has been set to its classical entropy S_0 and energy E_0 values by choosing the appropriate renormalization condition:

$$\Delta W_{\text{eff},i} = 0, \tag{2.65}$$

$$S_{0,i} = \pi r_E^2 = \pi |\vec{Q}|^2, \tag{2.66}$$

$$E_{0,i} = r_E = M = |\vec{Q}|. \tag{2.67}$$

By conservation of energy, the black hole mass shifts to

$$M_f = M + \delta M. \tag{2.68}$$

Then

$$M_f > |\vec{Q}|. \tag{2.69}$$

The perturbed black hole receives a quantum contribution to its entropy because we have already specified fixed counterterms for the effective action of the black hole and the divergent contributions to the entropy depend on the radius of the black hole. The quantum contribution to the entropy may be mathematically traced to the fact that it runs with the radius of the horizon of the black hole. Because the quantum contribution to the *exact* contribution of the gauged scalar to the black hole entropy modulo backreaction outscales the classical contribution, we expect large perturbations to the classical geometry may induce large quantum backreaction. We therefore consider small perturbations to the geometry and write the near-extremal radius r_+ of the perturbed black hole as

$$r_+^2 = r_E^2 + \delta r^2. \tag{2.70}$$

Note that in what follows we only consider the gauged scalar matter sector and small perturbations to the geometry in our second law analysis. We justify our result in the next section by demonstrating that effects from all other fields are subleading at one-loop and suppressed at higher loop orders and that quantum backreaction may be neglected for small perturbations of the geometry.

The only modification to the entropy at the level of linearized backreaction arises from the change in the near-horizon electric field, which shifts from $2|\vec{q}|^2 \cos^2(\vartheta) \equiv (\vec{q} \cdot \vec{Q})^2 / r_E^2$ to

$(\vec{q} \cdot \vec{Q})^2 / r_+^2$. The logarithmic correction to the classical entropy of the new black hole is[17]

$$S_{\text{quant}} = \frac{1}{4} \left[\frac{1}{45} + \frac{1}{6} (\vec{q} \cdot \vec{Q})^2 + \frac{1}{2} (\vec{q} \cdot \vec{Q})^4 + \mathcal{O}\left(\text{sech}^2[(\vec{q} \cdot \vec{Q})^2] \right) \right] \log \left(\frac{m^2 r_+^4 - (\vec{q} \cdot \vec{Q})^2 r_+^2}{m^2 r_E^4 - (\vec{q} \cdot \vec{Q})^2 r_E^2} \right).$$
(2.71)

Ignoring exponentially suppressed contributions and keeping only the $\mathcal{O}(|\vec{Q}|^2)$ or higher terms, the bound equation (2.64) becomes

$$|\vec{Q}|^2 \leq \frac{32\pi}{|\vec{q}|^4 \cos^4(\vartheta)} \frac{m^2 - |\vec{q}|^2 \cos^2(\vartheta)}{2m^2 - |\vec{q}|^2 \cos^2(\vartheta)} - \frac{1}{3} \frac{1}{|\vec{q}|^2 \cos^2(\vartheta)},$$
(2.72)

where ϑ is the angle between $\vec{Q}$ and $\vec{q}$. The bound applies to particles violating or saturating $(m^2 = |\vec{q}|^2 \cos^2(\vartheta))$ the conjecture. The dependence on δr^2 cancels on both sides of the bound for small δr^2. We may always choose an initially large, extremal black hole such that we violate the bound. A conservative interpretation of the result is that there is a maximum charge allowed in the macroscopic theories considered. This would require the appearance of some instability for large black holes. There is no evidence that this is the case, however, as we discuss in the next section.

It is natural to wonder if our result is nullified when instanton tunnelling, quantum backreaction, and effects from other fields are accounted for. The answer is no. Because the differences in quantum contributions to the entropy dominate differences in classical contributions to the entropy, large black holes are stable against splitting into multiple black holes whose charge adds up to the charge of the large black hole. This is more general than the statement that no Schwinger pair production occurs for extremal black holes formed in theories violating the weak gravity conjecture. Quantum effects dominate differences in entropy, but do not dominate the classical expressions for the entropy themselves for a suitable renormalization condition. One may worry that changes in energy, related to the backreaction of the quantum fields on the classically perturbed geometry, are important too. In fact, quantum backreaction on the black hole mass only appears at $\mathcal{O}((\delta r^2)^2)$. Moreover, as aforementioned and cited, contributions at one-loop from other massless fields, such as massless matter, other gauge fields, and the gravitational field, are always subleading with respect to the classical entropy of the black hole. For large black holes, only the one-loop answer contributes in the large $|\vec{Q}|$ limit: higher loop contributions are suppressed by factors of inverse radii of the black hole. We leave these results to the appendix.

We cannot emphasize enough that *the answer we have obtained is an exact answer that extends beyond the one-loop approximation*: higher loop factors have in effect been resummed because we computed the full partition function for the scalar field. The reason we could do this is because the action is quadratic in the scalar field, so the Euclidean path integral reduces to a Gaussian integral. Because of the special geometry of the near horizon region, we were able to compute this result analytically. Any error in our result is of order $\mathcal{O}(\text{sech}(|\vec{q} \cdot$

---

[17]In Planck units $M_{\text{Pl}} = 1$.

$\vec{Q}|$)), which is suppressed in the large $|\vec{q} \cdot \vec{Q}|$ limit. As shown in the appendix, quantum backreaction does not affect the classical geometry at order δr^2 after the neutral particle crosses the black hole horizon. This is the only effect that is not explicitly captured by our exact computation.

2.5. Consistency Checks

Subleading Contributions from Neutral Matter, Gauge Fields, and Gravitational Field at All Loop Orders

Our expression for the exact heat kernel of the scalar field indicates a second law violation. We have not included effects from the two other fields present: the $U(1)^N$ gauge field and the gravitational field. This is because these contributions are subleading. The reason that the scalar had such a large contribution to its entropy is because it couples to the background gauge field. Therefore, the action for the ϕ field includes contributions from positive powers of the background black hole charge. This is not the case for the gravitational and gauge actions.

Let us first consider the one-loop contributions to the heat kernel from the gauge and gravitational fields. The total heat kernel for the full theory is the sum of the individual heat kernels, so we can consider each field separately. At one-loop, we only need to consider the quadratic action for each field. The one-loop expression for N $U(1)$ vector fields and the gravitational field has already been known for some time, calculated by Sen in [38]:

$$S = \frac{A}{4} - \frac{1}{180} \left(964 + 62N \right) \log(A).$$
(2.73)

Note that the quantum correction is *subleading*. Moreover, Sen *et al.* demonstrate in [38] that higher loop contributions are suppressed in the large black hole mass limit. Therefore, the one-loop result for the macroscopic answer suffices.

Suppression of Quantum Backreaction for Small Classical Perturbations

In our analysis, we choose renormalization conditions such that the quantum correction to the extremal black hole entropy with charge $\vec{Q}$ is absorbed into the tree-level, classical value for the entropy. The linear perturbation to the black hole induced by a neutral particle crossing the horizon causes the quantum entropy to run, because the entropy depends on the radius of the black hole. The quantum correction to the entropy of the perturbed black hole solution is smaller than the classical entropy of the perturbed black hole. However, the difference between the classical entropies of the initial and final black holes is smaller than the difference in quantum corretions to the entropy. It is for this reason that the second law is violated. We use the exact expression for the scalar field effective action for fixed, external

classical backgrond fields, accounting only for classical backreaction. Here we provide a back of the envelope argument that quantum backreaction does not modify our result at $\mathcal{O}(\delta r^2)$.

The mass of the black hole may be expressed via the first law as

$$M = TS + |\vec{Q}|, \tag{2.74}$$

where T is the temperature, S is the entropy, $\vec{Q}$ is the charge, and we have set the chemical potential to one. We assume that quantum corrections to all quantities written above are factored into this formula. For a stationary, charged black hole, these are the only sources that can contribute to the black hole mass.

Let us consider backreaction on the charge of the black hole. The charge of the perturbed black hole receives quantum corrections that are of order

$$\vec{Q}_{\text{qu}} \propto -|\vec{q}|^4 |\vec{Q}|^0 \delta r^2. \tag{2.75}$$

In the small $|\vec{q}|$ limit, we may assume that these are subleading and ignore these corrections only if the quantum corrections to the mass do not dominate.

The perturbed black hole has a classical correction to its mass proportional to the temperature of the black hole. The classical temperature is

$$T = \frac{1}{2\pi} \left(\frac{1}{r_+} - \frac{|\vec{Q}|^2}{r_+^3} \right), \tag{2.76}$$

which evalutes to

$$T = \frac{\delta r^2}{|\vec{Q}|^3} + \mathcal{O}((\delta r^2)^2). \tag{2.77}$$

It may be checked that quantum corrections do not modify this order of magnitude estimate. The thermal contribution to the mass of the black hole has a classical and quantum component. The classical contribution arises from the classical entropy:

$$M_{cl} = 4\pi T r_+^2 = 4\pi \frac{\delta r^2}{|\vec{Q}|} + \mathcal{O}((\delta r^2)^2). \tag{2.78}$$

The quantum correction to the entropy is proportional to $\mathcal{O}(\delta r^2)|\vec{q}|^4|\vec{Q}|^4$. Therefore, the quantum correction to M is proportional to $(\delta r^2)^2$:

$$M_{qu} \propto -|\vec{q}|^4 |\vec{Q}| \mathcal{O}((\delta r^2)^2). \tag{2.79}$$

In the small δr^2 expansion, this is smaller than the classical backreaction near-extremality. We conclude that we may ignore quantum backreaction effects in our thought experiment. A full analysis should utilize the semi-classical Einstein equations. We leave this to future work.

Stability of the Near Horizon Geometry

A black hole with charge $\vec{Q}$ is not the only classical geometry asymptotic to the $\mathrm{AdS}_2 \times S^2$ in the near-horizon limit. Other geometries that contribute to the path integral are multi-black hole solutions, where the total charge of the black holes equals $\vec{Q}$. When the weak gravity conjecture is satisfied, tunneling processes may occur in which the initial $\mathrm{AdS}_2 \times S^2$ near-horizon geometry fragments into multiple $\mathrm{AdS}_2 \times S^2$ geometries. The simplest example is the Brill instanton, wherein one initial $\mathrm{AdS}_2 \times S^2$ space tunnels into two disconnected spaces. Let us review the calculation using the classical piece of the effective action first, following [48]. For simplicity of presentation, we work with a $U(1)$ gauge group in the remainder of this section. The background gauge field in the two black hole solution is

$$A_t(\vec{x}) = \frac{Q_1}{|\vec{x} - \vec{x}_1|} + \frac{Q_2}{|\vec{x} - \vec{x}_2|}. \tag{2.80}$$

Further details may be found in [48]. The instanton action is half the negative difference of the initial and final black hole entropies,[18]

$$S_{\text{inst}} = -\frac{1}{2}\Delta S. \tag{2.81}$$

Consider the Bekenstein-Hawking term without quantum corrections. The Brill instanton action is

$$S_{\text{inst}} = \pi Q_1 Q_2. \tag{2.82}$$

The transition amplitude from the charge Q black hole to the Q_1 and Q_2 charged black holes is

$$A_{Q \to Q_1 + Q_2} \propto e^{\frac{1}{2}\Delta S}, \tag{2.83}$$

up to normalization. Consequently, the transition probability is

$$P_{Q \to Q_1 + Q_2} \propto e^{-\pi Q_1 Q_2}. \tag{2.84}$$

The probability is less than one for non-zero Q_1 and Q_2, as expected.[19] When $Q_1 \to q$, this answer represents the probability amplitude for brane-antibrane production, i.e. Schwinger pair production. Now consider quantum corrections to the macroscopic entropy from matter neutral under the $U(1)$ gauge symmetry. The logarithmic terms are subleading. Therefore, the instanton action is still positive, because $S(Q) \geq S(Q_1) + S(Q_2)$. We interpret this to mean that large black holes dominate the Euclidean path integral, with an exponentially suppressed probability that the black holes fragment into multi-black hole solutions. Note that fragmentation and Schwinger pair production would preclude us from maintaining a sufficient level of control over the process we consider.

---

[18]The factor of $\frac{1}{2}$ appears because the transition probability between solutions is proportional to $e^{-\Delta S}$.

[19]It is implicit in what follows that Q_1 and Q_2 have the same sign.

Now consider the quantum corrected black hole entropy when the weak gravity conjecture is violated or saturated for a non-supersymmetric gauged scalar. In the large charge limit, one may verify that

$$S(Q) < S(Q_1) + S(Q_2). \tag{2.85}$$

Consequently, the physical instanton process is not fragmentation; rather, it is black hole growth from an initial two black hole state to a single black hole final state. This is consistent with the $Q_1 \to q$ limit: there is no pair production. Similarly, there is no black hole fragmentation. Instead, the correct instanton action corresponds to two initial $\text{AdS}_2 \times S^2$ states transitioning into one final $\text{AdS}_2 \times S^2$ states. In the $Q_1 \to q$ limit, this is a process akin to the thought experiment in the previous section. The combined state of the black hole and a particle eventually transitions to a final state where the black hole consumes the charged particle. In conclusion, the large-charged black hole in our setup does not fragment into a multitude of black holes or charged particles. This is in accord with the kinematics arguments presented in the introduction. The theory contains only subextremal objects in its spectrum, so the extremal black hole has no decay channels. Moreover, the instanton analysis implies that the Euclidean path integral is dominated by small black hole classical saddle points, i.e. remnants. We claim that the absence of a decay channel affords us sufficient control over the process we consider.

It is clear now that black hole growth is the favored physical process in theories violating the weak gravity conjecture. We speculate that the reversal of the Brill instanton violates unitarity. Renormalize the large extremal black hole effective action. One may tune the effective action such that the entropy is positive, despite the seemingly large quantum correction. However, no mechanism exists within the IR theory that prevents the black hole from continuing to grow unbounded. When the black hole grows, the decreasing quantum correction outcompetes the increasing Bekenstein-Hawking term. Counterintuitively, larger black holes hide fewer microscopic states behind the horizon than smaller black holes. Because growth may occur without bound, the entropy eventually becomes negative, indicating that the black hole contains less than one microscopic state. We expect that this behavior is forbidden in a unitary theory. Therefore, we speculate that the scalar violating the weak gravity conjecture is secretly non-unitarity, even at the level of effective field theory.

2.6. Appendix: One-Loop Calculation

The exact heat kernel for the minimally gauged scalar in the presence of fixed external background fields does not match the expected one-loop result. In the one-loop heat kernel Suppose that $m \gg q M_{\text{Pl}}$. Then we may expand the $s(\vec{q} \cdot \vec{Q})^2$ part of the argument of the exponent:

$$K(s) \approx \frac{1}{16\pi^2 r_E^4 \bar{s}^2} \left[1 + \bar{s}^2 \left(\frac{1}{45} + \frac{1}{6} (\vec{q} \cdot \vec{Q})^2 \right) + \mathcal{O}(\bar{s}^4) \right] e^{-\bar{s} r_E^2 m^2}. \tag{2.86}$$

This is exactly what one would obtain in the geometric expansion of the heat kernel in the large $|\vec{Q}|$ limit:

$$K(s) \approx \frac{1}{16\pi^2 \overline{s}^2} \left(1 + \frac{\overline{s}}{6} R + \frac{\overline{s}^2}{45} R_{\mu\nu} R^{\mu\nu} + \frac{1}{6} q^2 F_{\mu\nu} F^{\mu\nu} \right) e^{-\overline{s} r_E^2 m^2}. \tag{2.87}$$

The $(\vec{q} \cdot \vec{Q})^4$ term is cancelled by the background gauge field term when we expand the exponential. Therefore, in the large mass limit, one may verify that only a $q^2 F_{\mu\nu} F^{\mu\nu}$ counterterm is required to cancel the divergence due to powers of $\vec{q} \cdot \vec{Q}$ that appear in the final result, which can be seen by performing the small s expansion or, likewise, expanding the exponent in our exact result.[20]

---

[20]It can be verified that it is only in this limit that the approximation of the integrand made in [41] is justified. Because this is not a focus of our chapter, we refrain from providing further commentary in this chapter on this detail.

Chapter 3

Large-N and String Theory Out of Equilibrium

3.1. Introduction

Our universe is not in equilibrium.[1] The framework of string theory has successfully provided a consistent theoretical picture for describing various aspects of its dynamics, capable of accommodating both the quantum mechanical nature of its constituents and the evolving geometry of its large-scale structure. Yet, somewhat paradoxically, the machinery of string theory as understood today does not appear to be particularly well-suited for describing systems out of equilibrium, such as early-universe cosmology.

Concepts originating from string theory have been very influential in a remarkable number of areas of physics (and even mathematics). This interdisciplinary influence of string theory includes particle phenomenology, with brane-world scenarios, large extra dimensions, the Randall-Sundrum scenario enriching the scene beyond the Standard Model; AdS/CMT and holographic methods for describing strongly-correlated condensed matter systems [1, 2]; the extension of K-theory from a method for classifying D-branes in string theory to classifying stable Fermi surfaces [3] and phases of topological insulators; and the impact of string theory on inflationary cosmology [13] and in quantum gravity, notably leading to the statistical explanation of the Bekenstein-Hawking entropy of various supersymmetric black holes.

In most of these applications, string theory is excellent at describing equilibrium systems, ideally with as many supersymmetries as possible. However, this effectiveness seems to be lost for systems or states away from equilibrium. One naturally wonders why: Is this a fundamental limitation of string theory? Or is it a historical accident, with the proper formulation of string theory away from equilibrium yet to be discovered? Indeed, a glance at the history of string theory reveals a strong bias towards equilibrium states. Since its inception in the 1960's and certainly for much of its early development [4], string theory has been deeply rooted in the ideology of the S-matrix, which depends strongly on the axiom of

---

[1]See, *e.g.*, [49].

a static, stable, eternal vacuum.

Can we uncouple string theory from this assumption of the eternal stable vacuum? While many partial results for string-theory states away from equilibrium have been accumulated – notably, in areas ranging from tachyon condensation to non-equilibrium AdS/CFT dynamics – progress has been rather slow and spotty. It is natural to hope that even in its natural area of quantum gravity, string theory should be able to do better with non-equilibrium systems, to have a more systematic impact of string theory on concepts in early-universe cosmology, or to give new insights into dynamical evaporating black holes.

It may not be immediately clear how to wean critical string theory from its dependence on the S-matrix and equilibrium, or how to formulate non-equilibrium string theory from first principles. However, we do know how to take a general quantum many-body system or quantum field theory out of equilibrium: The basic rules of quantum mechanics can certainly accommodate non-equilibrium states, leading to the formulation known as the Schwinger-Keldysh formalism. In fact, in recent years the methods of the Schwinger-Keldysh formalism have found their way into string theory, primarily in the context of AdS/CFT [15, 16, 14]. However, these approaches are mostly based on the spacetime field theory description, with very little understanding so far of the worldsheet dynamics.

Here we will follow a different strategy: We use the methods of the large-N expansion and its connection to string theory, and extend them to non-equilibrium systems where we can directly apply the Schwinger-Keldysh formalism. In that way, we begin to learn something about the universal rules of non-equilibrium string perturbation theory. Our goal is two-fold: To stimulate string-theory research in directions away from equilibrium, and to encourage further study of possible dual descriptions of non-equilibrium systems across diverse areas of physics in terms of string theory.

This chapter is organized as follows. In the remainder of this introductory Section 1, we briefly review two important topics: The interpretation of the large-N expansion in a quantum theory of matrices in terms of string theory, and the non-equilibrium formalism for quantum systems known as the Schwinger-Keldysh formalism. The reviewed material is well-known to experts in the corresponding fields, but since we wish to make this chapter accessible to a broad audience from a wide range of fields – from string theory to non-equilibrium mesoscopic physics to early-universe cosmology – we include this material to make our chapter relatively self-contained, and to set a uniform stage for the later sections. In Section 2, we connect the two topics reviewed in Section 1, and analyze how the large-N expansion of the non-equilibrium Schwinger-Keldysh formalism leads to a refined expansion in terms of string theory topologies. It is the hallmark of the Schwinger-Keldysh formalism that the system is followed forward and then backward in time, and we analyze how string perturbation theory out of equilibrium reflects this doubling phenomenon. We concentrate on aspect which are universal, and follow solely from the structure of the large-N expansion; we make no assumptions about worldsheet dynamics. We perform our analysis for the case of matrices with $SU(N)$ symmetry, which corresponds to the case of closed oriented strings. We develop the universal structure of non-equilibrium string perturbation theory in terms of a refined sum over worldsheet topologies.

Sections 3 and 4 are then devoted to several generalizations of our main results from Section 2. In Section 3, we consider an important special case, particularly useful for studies of equilibrium systems at finite temperature T. Here the relevant time contour – often referred to as the Kadanoff-Baym contour – contains not only the forward and backward evolution segments in real time familiar from the Schwinger-Keldysh contour, but also a "Matsubara segment"along the imaginary time direction by the amount $\beta = 1/T$. This approach naturally contains both the real-time and imaginary-time approaches to systems at nonzero T. We analyze how large-N theory on the Kadanoff-Baym contour leads to a further refinement of the expected universal features of string perturbation theory. In Section 4, we briefly outline the generalizations of our main results from Section 2 to the case of matrices with $O(N)$ or $Sp(N)$ symmetries, which lead to closed unoriented strings; and the addition of vector-like degrees of freedom, in the fundamental representation of the appropriate symmetry group, which leads to open strings and the presence of worldsheet boundaries. We conclude in Section 5.

Strings from the large-N expansion

The genus expansion into worldsheets of inncreasing topological complexity, weighted by the powers of the string coupling g_s, is a universal hallmark of string theory in its perturbative regime. It is remarkable that the same topological expansion is obtained, quite universally, in the large N limit of theories with degrees of freedom described by matrices of rank N, with $1/N$ playing the role of the string coupling constant g_s. The large-N expansion has turned into an efficient strategy for reorganizing theories that would otherwise be difficult to understand perturbatively. In the context of high-energy physics, the use of this strategy to illuminate QCD dynamics goes back to 1974 and G. 't Hooft [18, 19, 50]. Quite universally, the large-N expansion predicts the existence of a dual description of the same system in terms of string theory. This association with the large-N description of generic systems of fluctuating matrix degrees of freedom is one of the most compelling arguments for the importance of string theory. For readable reviews of the elements of the large-N approach, see [51] (reprinted in [52]), or the more recent [53].

We begin with a system of fluctuating degrees of freedom, described by M which happens to be an $N \times N$ matrix, which we take to be Hermitian and traceless, so that it carries the adjoint representation of our symmetry group $SU(N)$. This matrix may depend on spacetime coordinates, and its dynamics may be relativistic or not; the details are immaterial, and we suppress them in what follows. We will study the system in the perturbative expansion in the powers of $1/N$. The limit of large N will correspond to a new classical limit [54], in a dual theory described by strings. For simplicity, we assume that the system is defined by a path integral, with a classical action $S(M)$. M can be relativistic Yang-Mills gauge fields[2],

---

[2]If M are Yang-Mills gauge fields or if there is any other gauge symmetry, we assume that the gauge symmetry is handled in the BRST formalism, extending the matrix degrees of freedom to include ghosts and antighosts such that each matrix field has a non-degenerate kinetic term and a well-defined propagator, so that the ribbon-diagram expansion discussed below makes sense.

or they can be nonrelativistic matrix fields in some number of spatial dimensions. They can also just be $N \times N$ matrices in quantum mechanics, dependent only on time. The beauty of the large-N expansion argument that we are about to review is in its universality.

In order to set the stage for our arguments, we must choose an action for M. We will mimic the case of Yang-Mills gauge theory, and will take the action to be

$$S(M) = \frac{1}{2g^2} \int dt \, \text{Tr} \left(\dot{M}^2 + M^3 + M^4 + \dots \right). \tag{3.1}$$

In the quadratic term, we indicated explicity only the piece with time derivatives, but generally there will also be terms involving spatial derivatives, as well as mass/chemical potential terms; we keep those implicit, focusing on the univesal features only. The propagator is determined by the full quadratic part in M.

A simple field redefinition to $m = M/g$ would take this action to another, perhaps more familiar form, traditionally used for perturbation theory in g:

$$S(m) = \int dt \, \text{Tr} \left(\frac{1}{2} \dot{m}^2 + \frac{g}{2} m^3 + \frac{g^2}{2} m^4 + \dots \right). \tag{3.2}$$

Here the quadratic term is normalized to $1/2$, and each interaction term is controlled by the appropriate power of g. It is also not difficult to generalize this and make the M^4 coupling constant independent of the coupling that controls the M^3 term. Such cosmetic modifications will not change the line of our reasoning. Importantly, the change from M to m is just a simple change of coordinates, which will not influence the underlying physics. We feel that our arguments will be simplest in the original notation using M, and will use that parametrization in the rest of our analysis.
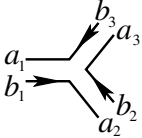
The propagator defined by the full quadratic part of the action in (3.1) is depicted by a ribbon, with each of the two indices associated with one edge of the ribbon,

$$\begin{matrix} a \xleftarrow{\quad} d \\ b \xrightarrow{\quad} c \end{matrix} = \langle M^a{}_b M^c{}_d \rangle = g^2 \, G^{ac}_{bd} = g^2 \, G \, \delta^a_d \delta^b_c. \tag{3.3}$$
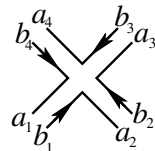
and the arrows at the edges distinguish the upper and lower indices.[3] The bare propagator G can be a function of various suppressed arguments of M, but is independent of g. The

---

[3]A standard word of explanation and caution about the distinction between $U(N)$ and $SU(N)$: By our assumptions, the M degrees of freedom are traceless, and symmetry is $SU(N)$. The correct propagator would then contain also an additive term $-(1/N)\delta^a{}_b\delta^c{}_d$ on the right-hand side of (3.3), in order to maintain the tracelessness of M. We drop this terms systematically in the large-N expansion. Thus, we aproximate $SU(N)$ by $U(N)$, which is permissible as long as the $U(1)$ factor is free and decouples (which we assume throughout this chapter). For further discussion of this standard approach, see [52].

vertices are

$$\vcenter{\hbox{[diagram]}} \quad = \quad -\frac{i}{g^2}\,\delta_{b_1}^{a_2}\delta_{b_2}^{a_3}\delta_{b_3}^{a_1},$$ (3.4)

$$\vcenter{\hbox{[diagram]}} \quad = \quad -\frac{i}{g^2}\,\delta_{b_1}^{a_2}\delta_{b_2}^{a_3}\delta_{b_3}^{a_4}\delta_{b_4}^{a_1},$$ (3.5)

$$\vdots$$ (3.6)

Feynman diagrams built from these propagators are vertices are often called "ribbon diagrams", and this is the terminology we will use in this chapter.[4] Let us focus for simplicity on vacuum ribbon diagrams. For a generic ribbon diagram, we will denote by P its number of propagators, by V the number of vertices and by L the number of closed loops. We will also denote the ribbon diagram itself by Δ.

Each ribbon diagram Δ can be uniquely associated with a compact surface Σ. Loosely speaking, Σ is the lowest-genus surface on which the ribbon diagram can be drawn. More precisely, the constructive prescription for obtaining this Σ for a given ribbon diagram is very simple: Start with the ribbon diagram (as a topological 2-manifold, with boundaries consisting of the edges of the ribbons), and for each closed loop (*i.e.*, a boundary component which is topologically an S^1) glue in a two-dimensional disk D_2, thus closing all holes in the ribbon diagram and producing a compact surface Σ with $\partial\Sigma = \emptyset$. In turn, the ribbon diagram gives a cellular decomposition of Σ, with the vertices and propagators of the diagram serving as the 0-dimensional and 1-dimensional cells, while the glued-in disks – which we will refer to as "plaquettes" – play the role of the 2-dimensional cells in this cellular decomposition of Σ. When we wish to indicate explicitly which ribbon diagram Δ gave rise to a given surface, we will denote that surface by $\Sigma(\Delta)$.

By Feynman rules, the contribution of a given ribbon diagram to the vacuum amplitude depends on g and N as

$$g^{2P-2V}N^L.$$ (3.7)

Importantly, the factor of N^L appears because each plaquette corresponds to a closed loop, and therefore includes the summation over the N values of the index a running around the loop.

We are primarily interested in a meaningful $1/N$ expansion, and therefore have to determine which combination of g and N to hold fixed as $N \to \infty$ in order to Defining the 't Hooft coupling λ

$$\lambda \equiv g^2\,N$$ (3.8)

---

[4]Historically, ribbon diagrams appeared independently in the mathematical literature, where they are often referred to as "fatgraphs" (see, *e.g.*, [55] and references therein).
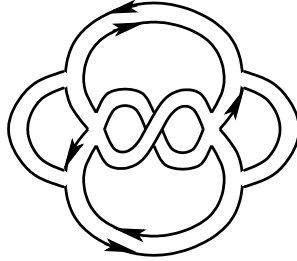
Figure 3.1: A typical ribbon diagram, with 6 vertices, 10 propagators, and 4 closed loops. The Riemann surface associated with this diagram has Euler number $\chi(\Sigma) = V - P + L = 0$, *i.e.*, it is the surface of genus one, $\Sigma = T^2$.

turns this scaling to

$$\lambda^{2P-2V} N^{V-P+L}. \tag{3.9}$$

We recognize the power of N in this expression as

$$\chi(\Sigma) \equiv V - P + L, \tag{3.10}$$

the Euler number $\chi(\Sigma)$ of the surface Σ associated to the ribbon diagram by the construction summarized above. In (3.10), $\chi(\Sigma)$ is expressed in terms of the combinatorial data about Σ. It is crucial however that $\chi(\Sigma)$ is a topological invariant of Σ, in particular independent of the specific cellular decomposition of Σ into a collection of vertices, lines and plaquettes.

Famously, topologically inequivalent compact oriented Riemann surfaces are fully classified by specifying just one non-negative integer, the genus h of the surface, and we have $\chi(\Sigma) = 2 - 2h$. Hence, our $1/N$ expansion is naturally interpreted as organized according to the increasing complexity of the topology of Σ. All diagrams can now be resummed into a perturbative expansion in the powers of $1/N$, and the partition function can be written as

$$\mathcal{Z} = \sum_{h=0}^{\infty} \left(\frac{1}{N}\right)^{2h-2} \mathcal{F}_h(\lambda, \ldots). \tag{3.11}$$

We define the large-N limit by holding the 't Hooft coupling fixed, and identify $1/N$ as the string coupling constant,

$$g_s = \frac{1}{N}. \tag{3.12}$$

We showed the analysis for simplicity for the partition function, but the same conclusion extends to the correlation functions of physical observables in the underlying theory of the matrix degrees of freedom: There is a dual interpretation of this theory as a string theory.

This argument is very convincing in its generality and universality. The catch in this simple universal argument is that it does not give us *a priori* clues as to which string theory is dual to our system. The worldsheet dynamics of the string needs to be found by

other independent means, which are available only in a few rare cases (such as maximally supersymmetric Yang-Mills theories whose additional features allow the dual string theory to be uniquely determined, leading to the celebrated AdS/CFT correspondence [21]).

Quantum theory in real time: Schwinger-Keldysh formalism

The relationship between the large-N expansion and a perturbative string-theory expansion as reviwed in Section 3.1 is derived under a very important implicit assumption, with historical roots in particle physics: The assumption that the system is in a stable, eternal, static vacuum, or in a state not too far from it. Our main goal in this chapter is to relax this assumption, and study the large-N expansion away from equilibrium. Such systems are naturally described by a natural generalization of standard quantum field theory, known as the Schwinger-Keldysh formalism.

Here we give a lightning review of Schwinger-Keldysh formalism, which describes quantum theory for general states, in or out of equilibrium [5, 6]. There are many useful reviews of this formalism, scattered across various fields of physics; see, *e.g.*, [56, 57, 58, 59, 60, 61, 62, 63, 64, 65, 66, 67, 68, 69, 70, 71]. Schwinger-Keldysh formalism is also sometimes referred to as the "in-in" formalism [67], especially in cosmology [10, 11, 12].[5] All these labels for this formalism are largely historical; it would be sensible to think of this formalism simply as "quantum mechanics without simplifying assumptions about the vacuum".

The main highlight of the Schwinger-Keldysh formalism is that it describes the system as evolving on a doubled closed-time contour $\mathscr{C}$ (known as the Schwinger-Keldysh time contour, see Fig. 3.2), starting in the remote past, evolving to the far future $t_\wedge$ along the forward part C_+ of the time contour, and then returning along the backward part C_- of the contour back to the remote past. Often the turn-around point is taken $t_\wedge \to \infty$.

Why such a closed time contour? In fact, this contour is encoded automatically in the rules of quantum mechanics, if one does not make the simplifying assumption of the static vacuum. To see this, let us focus on simple observables: Time-ordered correlation functions of operators in the Heisenberg picture,

$$\langle \psi_{\mathrm{in}} | \mathrm{T}(\phi_{\mathrm{H}}(t_n) \dots \phi_{\mathrm{H}}(t_1)) | \psi_{\mathrm{in}} \rangle, \tag{3.13}$$

in some general initially prepared state $|\psi_{\mathrm{in}}\rangle$. If this state is the static, stable vacuum, the standard LSZ procedure extracts from these correlators the physically observable S-matrix elements. Those are also the natural observables in string theory.

If $|\psi_{\mathrm{in}}\rangle$ is not the static, stable vacuum, we can still apply standard rules of quantum mechanics and develop a perturbative expansion for (3.13). Assume that the Hamiltonian

---

[5]Although the in-in formalism is the consequence of the same quantum mechanics as the Schwinger-Keldysh formalism, it might be appropriate to point out that the physical focus is a bit different: In the cosmological in-in formalism, one concentrates on the correlation functions of observables located at $t_\wedge$, which is interpreted as "the present". In the Schwinger-Keldysh formalism, $t_\wedge$ represents "the end of time" in the future, and the correlators are typically evaluated for observables on the forward time contour before $t_\wedge$ is reached.
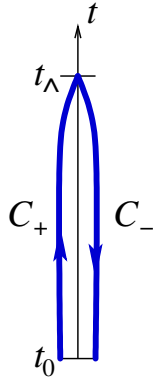
Figure 3.2: Schwinger-Keldysh closed time contour $\mathscr{C} = C_+ \cup C_-$. The remote past t_0 and the far future $t_\wedge$ are usually taken to be $-\infty$ and $+\infty$.

can be written as

$$H = H_0 + V(t), \tag{3.14}$$

where H_0 describes a simple system, and define the interaction picture using this split. The interaction-picture operators $\phi(t)$ are related to the Heisenberg-picture operators ϕ_H by

$$\phi_\mathrm{H}(t) = S(t_0, t)\, \phi(t)\, S(t, t_0). \tag{3.15}$$

Here $S(t', t)$ is the evolution operator

$$S(t', t) = \mathrm{T} \exp \left(i \int_t^{t'} V_0(t'')\, dt'' \right), \tag{3.16}$$

and $V_0(t)$ is the interaction part $V(t)$ of the Hamiltonian in the interaction picture. We will denote $S(+\infty, -\infty)$ simply by S.

The fixed reference time t_0 in (3.15) can be taken to be in the remote past. We may also assume, for illustration, that $|\psi_\mathrm{in}\rangle$ was prepared from the vacuum $|0_\mathrm{in}\rangle$ of H_0 in the remote past, by adiabatic turning-on of the iterations. The correlators are then

$$\langle 0_\mathrm{in}| S^{-1}\, \mathrm{T}(S\, \phi(t_s) \ldots \phi(t_1) |0_\mathrm{in}\rangle . \tag{3.17}$$

Note that the factor of S^{-1} is automatically present, and it serves to evolve the system back from the infinite future to the remote past where $\langle 0_\mathrm{in}|$ was prepared:

$$S^{-1} = [S(+\infty, -\infty)]^{-1} = S(-\infty, +\infty). \tag{3.18}$$

Clearly, the perturbative expansion of (3.17) will involve not just time-ordered two-point functions of ϕ, but also anti-chronologically ordered ones, and unordered ones as well. This proliferation of propagators is best encoded by defining the closed time contour $\mathscr{C}$, with

the factor of S under the time ordering symbol T in (3.17) evolving the system forward in time along C_+, and the factor of S outside of T evolving back along C_-. We introduce the time-ordering symbol $\mathrm{T}_{\mathscr{C}}$ to denote chronological ordering along the entire contour, allowing (3.17) to be succinctly written as

$$\langle 0_{\mathrm{in}}|\mathrm{T}_{\mathscr{C}}(S_{\mathscr{C}}\,\phi(t_s)\ldots\phi(t_1))|0_{\mathrm{in}}\rangle\,, \tag{3.19}$$

with $S_{\mathscr{C}}$ the evolution operator (3.16) along the entire contour $\mathscr{C}$. Only when the final vacuum $|0_{\mathrm{fin}}\rangle$ is given by the initial vacuum up to a possible phase,

$$|0_{\mathrm{fin}}\rangle = e^{i\theta}|0_{\mathrm{in}}\rangle, \tag{3.20}$$

can we replace $\langle 0_{\mathrm{in}}|S^{-1}$ by $e^{i\theta}\langle 0_{\mathrm{fin}}|$ and obtain the standard perturbation theory involving only the Feynman propagators of ϕ. In more general circumstances, however, we cannot replace the initial state $\langle 0_{\mathrm{in}}|$ with a suitable out-state, simply because the final state is not known. We must then follow the general formula (3.17) and evolve the system back using S^{-1}, before closing the correlator on the known initial state.

It is often impractical to work directly with the doubled time contour $\mathscr{C}$. Instead, one can keep the single-valued time t, and double the number of fields, with $\phi_+(t)$ and $\phi_-(t)$ denoting $\phi(t)$ on the C_+ and C_- branch of the Schwinger-Keldysh contour $\mathscr{C}$ at the same value of t. These doubled fields can be used in the path integral representation of the theory. The action that appears in the path integral of the non-equilibrium system is then formally given by

$$S_{\mathrm{SK}} = \int_{-\infty}^{+\infty} dt\,\{\mathcal{L}(\phi_+) - \mathcal{L}(\phi_-)\}\,, \tag{3.21}$$

with $S = \int \mathcal{L}(\phi)$ the original action of the equilibrium system. Note, however, that the compact form (3.21) is somewhat deceiving, and careful arguments involving regulators may be needed to provide the correct treatment of the non-equilibrium path integral (see [64] for details).

3.2. Large-N expansion in quantum systems out of equilibrium

In this section, we put the Schwinger-Keldysh formulation of non-equilibrium systems together with the large-N expansion, and analyze the consequences of the Schwinger-Keldysh formalism for string perturbation theory. In particular, we wish to understand how the Schwinger-Keldysh time contour is perceived by the string worldsheet topologies.

Ribbon diagrams on the Schwinger-Keldysh time contour

First, we formulate Feynman rules out of equilibrium, for our theory of Hermitian traceless matrices $M^a{}_b$, in the adjoint of $SU(N)$. The elements of Feynman graphs again lead to

ribbon diagrams, but now with all vertices and all ends of propagators labeled with $+$ or $-$. The propagators are:

$$+{}^a_b \xrightarrow{\quad d \quad}{}^d_c + \;\; = \;\; \left\langle \mathrm{T}_{\mathscr{C}} \left(M^a_{+b} M^c_{+d} \right) \right\rangle = g^2\, G_{++}{}^{ac}_{\;bd}, \tag{3.22}$$

$$+{}^a_b \xrightarrow{\quad d \quad}{}_c - \;\; = \;\; \left\langle \mathrm{T}_{\mathscr{C}} \left(M^a_{+b} M^c_{-d} \right) \right\rangle = g^2\, G_{+-}{}^{ac}_{\;bd}, \tag{3.23}$$

$$-{}^a_b \xrightarrow{\quad d \quad}{}^d_c + \;\; = \;\; \left\langle \mathrm{T}_{\mathscr{C}} \left(M^a_{-b} M^c_{+d} \right) \right\rangle = g^2\, G_{-+}{}^{ac}_{\;bd}, \tag{3.24}$$

$$-{}^a_b \xrightarrow{\quad d \quad}{}_c - \;\; = \;\; \left\langle \mathrm{T}_{\mathscr{C}} \left(M^a_{-b} M^c_{-d} \right) \right\rangle = g^2\, G_{--}{}^{ac}_{\;bd}. \tag{3.25}$$

The operation $\mathrm{T}_{\mathscr{C}}$ of time-ordering along the contour $\mathscr{C}$ again acts on its arguments by reordering them from the right to the left in the order of increasing contour time, with the flow of time following the direction of the arrows on the contour in Fig. 3.2.

More explicitly, the $\mathrm{T}_{\mathscr{C}}$ time ordering can be understood in terms of the more elementary orderings on the standard time axis parametrized by coordinate time t: The chronological time ordering T along t, and the anti-chronological ordering $\overline{\mathrm{T}}$, in the reverse direction of t. Here we suppress the ${}^{ab}_{cd}$ indices for simplicity, but restore the time dependence, while still suppressing the spatial dependence and all other possible indices and quantum numbers of $M_\pm$:

$$\left\langle \mathrm{T}_{\mathscr{C}} \left(M_+(t) M_+(t') \right) \right\rangle \;\; = \;\; \left\langle \mathrm{T} \left(M(t) M(t') \right) \right\rangle = g^2\, G_F(t,t'), \tag{3.26}$$

$$\left\langle \mathrm{T}_{\mathscr{C}} \left(M_+(t) M_-(t') \right) \right\rangle \;\; = \;\; \left\langle M(t') M(t) \right\rangle = g^2\, G^<(t,t'), \tag{3.27}$$

$$\left\langle \mathrm{T}_{\mathscr{C}} \left(M_-(t) M_+(t') \right) \right\rangle \;\; = \;\; \left\langle M(t) M(t') \right\rangle = g^2\, G^>(t,t'), \tag{3.28}$$

$$\left\langle \mathrm{T}_{\mathscr{C}} \left(M_-(t) M_-(t') \right) \right\rangle \;\; = \;\; \left\langle \overline{\mathrm{T}} \left(M(t) M(t') \right) \right\rangle = g^2\, G_{\overline{F}}(t,t'). \tag{3.29}$$

We thus recognize all four types of propagators in (3.22-3.25) in more elementary terms, as representing the Feynman $i\varepsilon$ propagator G_F, the "anti-Feynman" propagator $G_{\overline{F}}$ (sometimes called the Dyson propagator), and the G-lesser and G-greater propagators $G^<$, $G^>$. For clarity and simplicity, we will keep our $G_{\pm\pm}$ notation of (3.22-3.25) throughout the chapter.

The vertices look the same as in the equilibrium case, except that each vertex is assigned

a $\pm$ sign:

$$-\frac{i}{g^2}\,\delta^{a_2}_{b_1}\delta^{a_3}_{b_2}\delta^{a_1}_{b_3}, \tag{3.30}$$

$$\frac{i}{g^2}\,\delta^{a_2}_{b_1}\delta^{a_3}_{b_2}\delta^{a_1}_{b_3}, \tag{3.31}$$

$$-\frac{i}{g^2}\,\delta^{a_2}_{b_1}\delta^{a_3}_{b_2}\delta^{a_4}_{b_3}\delta^{a_1}_{b_4}, \tag{3.32}$$

$$\frac{i}{g^2}\,\delta^{a_2}_{b_1}\delta^{a_3}_{b_2}\delta^{a_4}_{b_3}\delta^{a_1}_{b_4}, \tag{3.33}$$

$$\vdots$$

The vertical dots at the bottom of this list of vertices represent the possibility of having higher, n-point vertices beyond $n = 4$. These higher-point vertices can be controlled by $1/g^2$, or can have their own independent couplings. These additional choices do not change the universal results of our analysis, and we will often freely assume below, simply for convenience, that such higher-n vertices do exist. Similarly, we assume for simplicity that all vertices have at least three ends; the arguments could be easily extended if one added "2-vertices" and "1-vertices" as well, without altering our conclusions.

Note that because of the Hermiticity of M and the nature of the time ordering along $\mathscr{C}$, we have

$$G_{+-}{}^{ac}_{bd} = G_{-+}{}^{ca}_{db}, \tag{3.34}$$

and there is therefore only one independent propagator that can connect a $+$ vertex to a $-$ vertex. This is reflected in our graphical notation: The propagator on the left side of (3.23), after the ends of the ribbon are exchanged and the indiced swapped, looks identical to the propagator on the left side of (3.24). This means that we will not have to distinguish between G_{+-} and G_{-+} propagators, as long as they are attached to the apprpriate $+$ and $-$ vertices. As a result, each ribbon diagram in non-equilibrium perturbation theory will look like a ribbon diagram of the type we encountered in Section 3.1 at equilibrium, but now with each vertex labeled by a $\pm$ sign.[6]

---

[6]In what follows, when we draw ribbon diagrams we will often put the $\pm$ sign next to the vertex rather than inside the ribbon; this will make some of our diagrams easier to read.

Now we proceed to the analysis of generic ribbon diagrams, and we study how they lead to an expansion of the partition function and correlation functions in terms of the topology of surfaces, generalizing the well-known string perturbation theory away from equilibrium. We will refer to the surfaces representing string worldsheets as "Riemann surfaces" for short, without implying that any geometric structure on them is *a priori* assumed, besides their smooth manifold structure.

First look at string perturbation theory out of equilibrium

In the special case of equilibrium and zero temperature, the Schwinger-Keldysh formalism should correctly reproduce the standard formulation of equilibrium quantum field theory in real time t. This limit is usually taken such that as we sent $t_\wedge \to \infty$, the return part of the Schwinger-Keldysh contour decouples from the calculations of the correlation functions of operators located on the forward branch, and therefore it can be ignored, reproducing standard textbook rules of quantum field theory with the static eternal vacuum. However, remnants of the Schwinger-Keldysh formalism do appear even in this textbook example of vacuum correlation functions in equilibrium at zero temperature, in an almost clandestine way, under a very different name: it reduces to the Cutkosky rules, which are crucial for analyzing unitarity properties of physical amplitudes [72, 73, 74].[7] Indeed, we can take the $t_\wedge \to \infty$ limit for the vacuum correlators in equilibrium at zero temperature, but still allow insertions of observables along both branches of $\mathscr{C}$. The $-$ vertices and operator insertions located on the backward branch C_- behave exactly like those on the "shaded side" from the unitarity cuts. Similarly, the propagators on the "unshaded" or "shaded" sides are simply the equilibrium limits of G_{++} and G_{--}, and the "cut propagators" of the Cutkosky formalism correspond to the equilibrium limit of G_{+-}, where this propagator reduces to the on-shell delta function. Thus, we reproduce the standard Cutkosky rules from the Schwinger-Keldysh formalism: The "shaded" and "unshaded" portions in the Cutkosky rules for Feynman diagrams correspond to the forward and backward branch of the Schwinger-Keldysh time contour, and the cut between the shaded and unshaded region is simply the location of the crossing from the forward branch C_+ to the backward branch C_-, at $t_\wedge \to \infty$.

We now wish to extend the story of the large-N expansion and string theory away from equilibrium. The first guess might be that propagating strings will also exhibit cuts, and that each string worldsheet Σ will consequently be split into two parts – its forward and backward portions Σ^+ and Σ^-, joined along a shared one-dimensional boundary $\partial\Sigma^+ = \partial\Sigma^-$. This common boundary between Σ^+ and Σ^- would then represent the cuts in the worldsheet language. It is one of the central points of this chapter to show that such an expectation is not quite correct. Instead, we will find that the portion of the worldsheet connecting Σ^+ and Σ^- is topologically two-dimensional.

---

[7]This remarkable connection between the Schwinger-Keldysh formalism and the Cutkosky rules seems absent in most textbooks on relativistic quantum field theory. One notable exception, where this relationship is explained in a lucid way, is the recent textbook by Gelis [66].
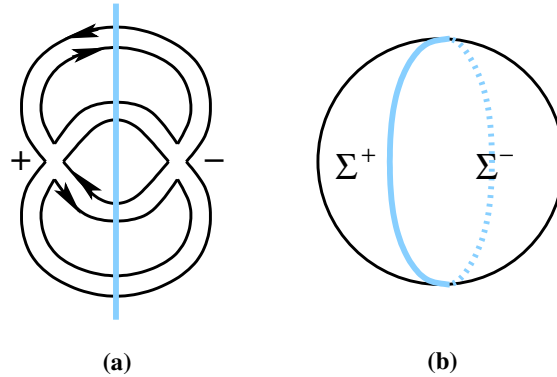
Figure 3.3: An example of a ribbon diagram with cuts, and its associated surface. **(a):** This ribbon diagram has a unique extension of the propagator cuts into the plaquettes. **(b):** The corresponding surface is $\Sigma = S^2$, and the cut decomposes it into two disks Σ^+, Σ^-.

Extending the cuts

Intuitively, the propagators that connect a vertex on the forward portion C_+ of the time contour with a vertex on the C_- portion of the contour represent worldlines of particles that have to cross from C_+ to C_- and therefore pass through the time instant $t_\wedge$ where the two branches meet. This crossing can be usefully denoted in Feynman diagrams by placing cuts across such propagators, indicating the passage through $t_\wedge$. This suggests that in the string picture, such cuts should be perhaps extended from cuts of ribbon diagrams to worldsheet cuts.

Let us first test this guess by considering some simple examples of ribbon diagrams. We begin by placing a cut line across all G_{+-} and G_{-+} propagators,

$$+\,{}^a_b\!\!\begin{array}{c}\longleftarrow\\[-4pt]\longrightarrow\end{array}\!\!{}^d_c\,- \quad .$$

Intuitively, one can think of the cut as indicating where the worldline of the virtual particle, represented by the propagator, crosses over from the forward branch C_+ to the backward branch C_- of the Schwinger-Keldysh time contour $\mathscr{C}$, where the two ends of the propagator are located. If our expectation about cuts of surfaces were correct, such cuts on ribbon propagators should induce uniquely the corresponding cuts on surfaces.

There are indeed many ribbon diagrams for which this works: An example is shown in Fig. 3.3. In such cases, when the cuts across the G_{+-} propagators can be continuously extended across the plaquettes in a unique way, the resulting lines of cuts form a collection of closed circles S^1 on Σ. Moreover, this collection of S^1's separates $+$ regions and $-$ regions in a way which is globally well-defined for the whole surface. Thus, cutting Σ along this collection of S^1's separates Σ into the forward-branch surface Σ^+ and backward-branch Σ^-. The collection of S^1's is then their common boundary, $\partial\Sigma^+ = \partial\Sigma^-$, along which they are glued together to form Σ.
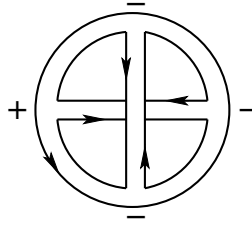
Figure 3.4: A simple example of a ribbon diagram with an ambiguity in how to connect the cuts across the plaquettes. There are two plaquettes: The one on the outside has just two adjacent G_{+-} propagators (thus the two cuts can be connected without ambiguity), while the other plaquette has four adjacent G_{+-} edges, giving two inequivalent ways how to connect the four cuts into two nonintersecting lines.

On the other hand, there are also many ribbon diagrams for which this prescription is incomplete or ambiguous. An example is shown in Fig. 3.4. Upon closer examination, the origin of the ambiguity in this example is clear: There is a plaquette which has more than two G_{+-} propagators adjacent to it (namely four), and there are two inequivalent ways how the corresponding four cuts can be joined into two nonintersecting lines. This makes it clear that the original prescription for extending the cuts across plaquettes to obtain a unique collection of S^1's cuts on Σ works precisely for those ribbon diagrams in which each plaquette has at most two G_{+-} propagators adjacent to it.[8]

How do we systematically resolve this ambiguity? Consider a generic plaquette with at least four G_{+-} propagators adjacent to it. In Fig. 3.5 we have an example with six. There is no unique way how to pairwise connect the six cuts illustrated there to form three nonintersecting lines cutting across the plaquette. In fact, there are five different such pairings, three of which are illustrated in Fig. 3.6. With the increasing number of adjacent G_{+-} the number of possibilities increases rapidly, and we need a new strategy how to extend the cuts through such plaquettes.

In order to forumulate a unique prescription for extending the cuts, we mark the center of each ambiguous plaquette with a dot, and connect all cuts to the dot in the unique way without forming intersections (see Fig. 3.7). This gives a unique prescription, for any ribbon diagram, how to extend the cuts from the G_{+-} propagators to the full diagram and its associated surface Σ. We see that the resulting cut of Σ generally does not correspond to a smooth one-dimensional manifold (which would have to be the union of S^1's), but it is described by a graph consisting of a number of dots connected by lines, and drawn on Σ in a particular way.[9] Given a diagram Δ, we will denote the graph so constructed by $\Gamma(\Delta)$, and refer to it as the "graph of cuts" of the diagram Δ.

---

[8]Of course, in vacuum diagrams considered here, the number of G_{+-} propagators adjacent to any plaquette is always even.

[9]As a general rule, only the centers of those plaquettes which have more than two G_{+-} propagators adjacent to them will be marked with a dot; any plaquette with just two adjacent G_{+-} propagators has an
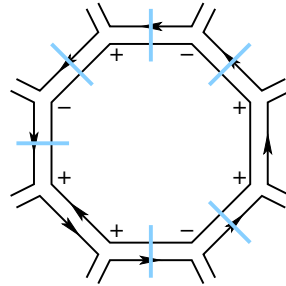
Figure 3.5: An example of a plaquette with six adjacent G_{+-} propagators, indicating their cuts.
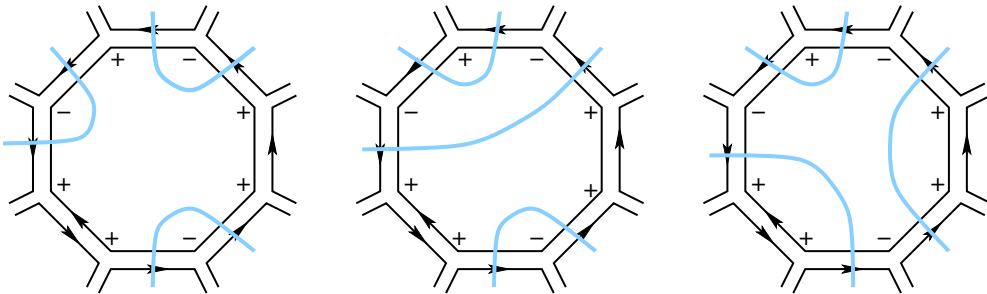
Figure 3.6: Ambiguities in extending the cuts in Fig. 3.5 across the plaquette. In this example, there are five inequivalent ways, of which we show three.
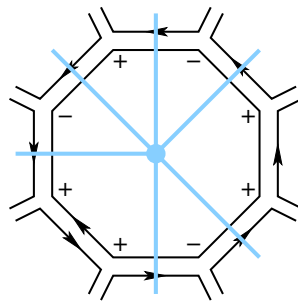
Figure 3.7: The unique extension of the propagator cuts into the plaquette, by marking the center of the plaquette with a dot and connecting all propagator cuts to the dot.

Topology of worldsheets on the Schwinger-Keldysh time contour

One could work in this language of cuts given by graphs on worldsheets, but this representation of the cuts is quite cumbersome. Questions such as: Which graphs are allowed? How

_____

unambiguous cut through it, and no dot is needed in that case.
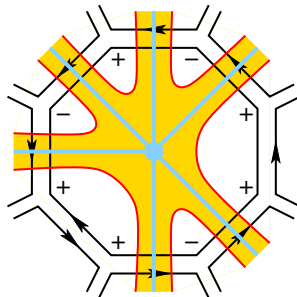
Figure 3.8: The topologically unique thickening of the graph of cuts Γ into a smooth surface with boundaries. The collection of all such thickenings (denoted here in yellow) across all plaquettes forms the smooth wedge region $\Sigma^\wedge$.

are they mapped to the worldsheet? are not easy to answer in this language. For example, not every graph, not even every connected graph, is allowed: It must be bipartite in the sense that it must separate Σ into regions that can be consistently labeled alternately by $+$ and $-$. Moreover, there are way too many allowed graphs, and having to classify them and sum over them would ruin the anticipated simplicity of the topological expansion in string theory. A much clearer picture emerges when we move away from graphs, and replace them with smooth manifolds. Indeed, graphs are complicated, but smooth manifolds are simple (at least in low-enough dimensions).

How do we associate a graph of cuts Γ with a smooth manifold? Consider again one of the ambiguous plaquettes, for example again the one in Fig. 3.7. The graph of cuts across this plaquette is not a smooth manifold, but we can define – in a topologically unique way – its "thickening" into a smooth two-dimensional surface with smooth one-dimensional boundaries, as indicated in the example of Fig. 3.7. Moreover, these two-dimensional thickenings extend smoothly across all adjacent propagators into neighbouring plaquettes, forming a globally well-defined smooth manifold with non-empty smooth boundary. We refer to this manifold as the "wedge region" of Σ, and denote it by $\Sigma^\wedge$.[10] It is this wedge region $\Sigma^\wedge$ that represents the topology of the cuts, connecting Σ^+ and Σ^- into the original smooth surface Σ.

Thus, we have reached one of the main and perhaps most surprising points of this chapter: The turnaround point $t_\wedge$ on the Schwinger-Keldysh contour, where the forward branch C_+ is connected to the backward branch C_-, is from the worldsheet point of view topologically two-dimensional! The cuts connecting the forward and backward parts of Σ are not boundaries between Σ^+ and Σ^-, but are themselves two-dimensional surfaces $\Sigma^\wedge$.

In the remainder of this Section 3.2, we will demonstrate in detail that $\Sigma^\wedge$ can have an arbitrarily complicated topology (*i.e.*, any finite number of connected components, handles,

---

[10]For readers viewing this chapter in color, we note note that the wedge regions $\Sigma^\wedge$ are systematically depicted in our Figures in yellow.

(a)   **(b)**
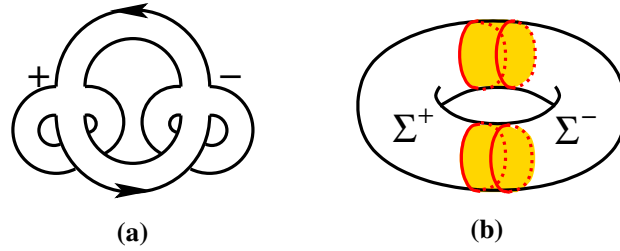
Figure 3.9: An example yielding more than one connected components of $\Sigma^\wedge$. **(a):** A ribbon diagram with $\Sigma = T^2$. **(b):** The corresponding triple decomposition of Σ, with $\Sigma^\pm$ each a cylinder, and $\Sigma^\wedge$ a union of two cylinders.

and boundaries connecting it to Σ^+ and Σ^-), and thefore carries its own genus expansion.

The triple decomposition of Σ

We have just found that the natural way how to think about the "cut" between the forward and backward part of Σ is to represent it by a smooth two-manifold with boundaries, not by a one-dimensional graph. It is this triple decomposition of worldsheets Σ into the forward surface Σ^+, backward surface Σ^-, and the wedge region $\Sigma^\wedge$ which emerges universally from the large-N expansion.

A simple example is the surface associated with the diagram in Fig. 3.3(a), with $\Sigma = S^2$ and the following triple decomposition,

$$ \tag{3.35} $$

Our next task is to classify all possible triple decompositions of Σ that can emerge from actual ribbon diagrams.

First of all, it is easy to find examples where $\Sigma^\wedge$ has more than one connected component, but its graph of cuts is still just a collection of circles. In Fig. 3.9, the graph of cuts $\Gamma(\Delta)$ has two connected components, each isomorphic to S^1, and no vertices. Thus, $\Sigma^\wedge$ consists of two disconnected cylinders (see Fig. 3.9(b)).

The simplest graph of cuts with at least one vertex is the figure-eight graph. It can appear in various ribbon diagrams and also be drawn in various inequivalent ways on surfaces. One example of a ribbon diagram with the figure-eight Γ is in Fig. 3.4, with the associated surface and its triple decomposition depicted in Fig. 3.10. Iterating such constructions shows immediately that connected components of $\Sigma^\wedge$ can have an arbitrarily high number of boundary components.

Next, one wonders about higher genus: Can $\Sigma^\wedge$ with handles also emerge from consistent ribbon diagrams? To show that the answer is yes, consider the diagram in Fig. 3.11. This example gives us an opportunity to introduce a useful mathematical notion, known as the Whitehead reduction of a ribbon diagram: Given a ribbon diagram Δ with two distinct vertices of orders $2+k$ and $2+\ell$ connected by a propagator, define the "Whitehead reduction of Δ" along this propagator by shrinking the propagator to zero length, thus replacing the two vertices with one composite vertex of order $2+k+\ell$. Since we wish to keep track of the information in the triple decomposition of Σ, we allow only those Whitehead reductions that do not change this decomposition, i.e., Whitehead reductions along G_{++} propagators and G_{--} propagators are allowed, but Whitehead reductions along the G_{+-} propagators are not. Two ribbon diagrams that differ by a sequence of allowed Whitehead reductions correspond to the same triple decomposition into Σ^+, Σ^- and $\Sigma^\wedge$.

Returning now to our example from Fig. 3.11, we see that the diagram can be simplified by two Whitehead reductions to that depicted in Fig. 3.12. Both of these diagrams should thus lead to the same triple decomposition of their underlying surface $\Sigma = T^2$, which we can easily determine by direct inspection: Since both Σ^+ and Σ^- will be disks, $\Sigma^\wedge$ has to have two boundaries and a handle, as shown in Fig. 3.13. We conclude that the wedge region can indeed carry a handle.

Combinatorial picture of Σ^+, Σ^- and $\Sigma^\wedge$

In order to prepare the ground for showing that arbitrarily high genera in $\Sigma^\wedge$ can also occur, it will be useful to develop a combinatorial approach to the ribbon diagrams, their associated surfaces Σ and their triple decomposition into Σ^+, Σ^- and $\Sigma^\wedge$.

Consider a surface Σ, obtained from a ribbon diagram Δ. The ribbon diagram provides a cellular decomposition of Σ: The vertices of the ribbon diagram are the zero-dimensional cells, the propagators represent the one-dimensional cells (or edges), and the plaquettes the two-dimensional cells of this cellular decomposition. For cellular decompositions, the Euler
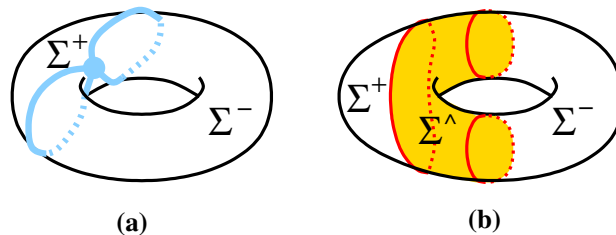
Figure 3.10: The surface Σ that corresponds to the ribbon diagram from Fig. 3.4, and its triple decomposition. **(a):** Σ is the torus, Σ^+ the disk, and Σ^- the cylinder. The cut between them forms a figure-eight graph with one vertex. **(b):** The triple decomposition of Σ; the thickening $\Sigma^\wedge$ of the figure-eight graph is the smooth "pair-of-pants" surface.
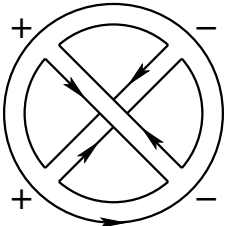
Figure 3.11: A simple ribbon diagram illustrating that $\Sigma^\wedge$ can be of higher genus.

number $\chi(\Sigma)$ of a given surface Σ is simply calculated as $\chi(\Sigma) = V - P + L$, with V the number of vertices, P the number of edges, and L the number of plaquettes. We already used this formula in Eqn. (3.10), in our review of the large-N expansion in equilibrium.

Now we can use the cellular decomposition of Σ implied by Δ to *define* Σ^+, Σ^- and $\Sigma^\wedge$ by assigning the various element of this cellular decomposition to belong to the three parts of the triple decomposition.

First, recall that all vertices in Δ are labeled as either $+$ or $-$, and consequently each propagator is labeled by the two signs indicating the vertices it connects. We will use the
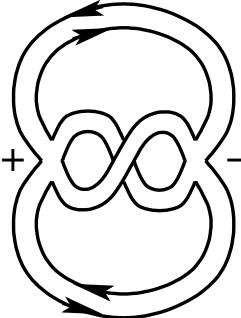
Figure 3.12: This diagram is obtained from that in Fig. 3.11 by Whitehead reduction, therefore it corresponds to the same surface Σ and the same triple decomposition.
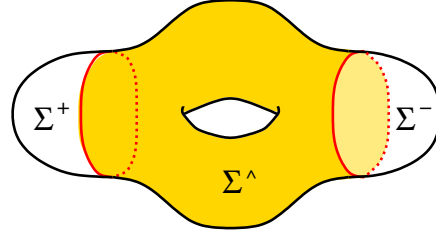
Figure 3.13: Surface $\Sigma = T^2$ corresponding to the ribbon diagrams in Fig. 3.11 and Fig. 3.12, and its triple decomposition. While both Σ^+ and Σ^- are disks, $\Sigma^\wedge$ is a surface with two boundaries and a handle.

following notation:

$$
\begin{aligned}
V_+ &= \text{the number of } + \text{ vertices,} \\
V_- &= \text{the number of } - \text{ vertices,} \\
P_+ &= \text{the number of } G_{++} \text{ propagators,} \\
P_- &= \text{the number of } G_{--} \text{ propagators,} \\
P_{+-} &= \text{the number of } G_{+-} \text{ and } G_{-+} \text{ propagators,} \\
L_+ &= \text{the number of plaquettes (or closed loops) with only } G_{++} \text{ adjacent propagators,} \\
L_- &= \text{the number of plaquettes with only } G_{--} \text{ adjacent propagators,} \\
L_{+-} &= \text{the number of plaquettes with a non-zero number}
\end{aligned}
$$

$$\text{of } G_{+-} \text{ (or } G_{-+}) \text{ adjacent propagators.}$$

We now subdivide the elements of the cellular decomposition of Σ into those belonging to Σ^+, Σ^- and $\Sigma^\wedge$ as follows:

- All $+$ vertices, all G_{++} propagators and all plaquettes with only G_{++} adjacent propagators belong to Σ^+;

- All $-$ vertices, all G_{--} propagators and all plaquettes with only G_{--} adjacent propagators belong to Σ^-;

- All G_{+-} (and G_{-+}) propagators and all plaquettes with a non-zero number of G_{+-} (or G_{-+}) propagators belong to $\Sigma^\wedge$.

This is our combinatorial definition of the triple decomposition of Σ, in terms of the cellular decomposition defined by the underlying ribbon diagram.

We can now define the "cellular Euler numbers" associated with the ingredients of the ribbon diagram Δ that have been assigned to $\Sigma^\pm$ and $\Sigma^\wedge$ as follows:

$$\chi_+(\Delta) = V_+ - P_+ + L_+, \qquad \chi_-(\Delta) = V_- - P_- + L_-, \tag{3.36}$$

and

$$\chi_\wedge(\Delta) = -P_{+-} + L_{+-}. \tag{3.37}$$

It is straightforward to show that the cellular Euler numbers so defined are equivalent to the standard topological definition of the Euler numbers of $\Sigma^\pm$ and $\Sigma^\wedge$ as topological manifolds with boundaries:

$$\chi_+(\Delta) = \chi(\Sigma^+), \qquad \chi_-(\Delta) = \chi(\Sigma^-). \tag{3.38}$$

Indeed, this follows from the simple observation that the elements of the cellular decomposition of Σ that we assigned to Σ^+ and Σ^- form a cellular decomposition of those surfaces with boundaries, and our definition of $\chi_\pm$ in (3.36) coincides with the standard expression for $\chi(\Sigma^\pm)$ in terms of this cellular decomposition.

It is perhaps a little less immediate to see that the cellular Euler number $\chi_\wedge(\Delta)$ defined in (3.37) is also the topological Euler number of the surface $\Sigma^\wedge$ with boundary whose construction we presented in Section 3.2. First of all, the elements of the cellular decomposition of Σ that we assigned to $\Sigma^\wedge$ do *not* give a cellular decomposition of a surface: There are only edges and plaquettes, but no vertices, and these ingredients do not give a closed submanifold in Σ. It is easy, however, to construct an honest cellular decomposition of $\Sigma^\wedge$ by refining the elements that we assigned to $\Sigma^\wedge$. First, add vertices at the ends of all the G_{+-} (and G_{-+}) propagators, and think of them as the points at the boundaries between $\Sigma^\wedge$ and Σ^+ or Σ^-. Then connect these vertices by new edges, with each edge simply following these boundaries within each plaquette, as indicated in Fig. 3.8. The addition of these vertices and edges to the ingredients previously assigned to $\Sigma^\wedge$ defines a cellular decomposition of $\Sigma^\wedge$, as a closed manifold with boundary. Essentially, the new ingredients just add the boundary S^1 components to $\Sigma^\wedge$, without changing the alternating sum of the vertices, edges and plaquettes. We conclude that

$$\chi_\wedge(\Delta) = \chi(\Sigma^\wedge). \tag{3.39}$$

Equipped with this combinatorial picture of the triple decomposition, we can now show that $\Sigma^\wedge$ of arbitrarily high genus can indeed emerge from ribbon diagrams.

Consider a ribbon diagram, constructed from ingredients shown in Fig. 3.14: Two ribbon diagrams with n loose ends. If we glue the end marked 1 with n', 2 with $n'-1$, ... and n with $1'$, the surface Σ associated with the resulting diagram is the sphere. Indeed, in this case we have

$$V_+ = V_- = P_+ = P_- = P_{+-} = n, \quad L_+ = L_- = 1, \tag{3.40}$$

and $L_{+-} = n$, implying that $\chi(\Sigma^+) = \chi(\Sigma^-) = 1$, $\chi(\Sigma^\wedge) = 0$, and $\chi(\Sigma) = 2$. The triple decomposition is the one we found in (3.35): Σ^+ and Σ^- are disks, and $\Sigma^\wedge$ is a cylinder.

On the other hand, if we glue the loose ends in the order indicated in Fig. 3.14, we obtain a surface whose cellular decomposition is characterized by the same numbers as in (3.40), while the number L_{+-} of $+-$ plaquettes changes from n to just 1 if n is odd, and to 2 if n is even. Thus, for odd $n = 2h + 1$ or even $n = 2h + 2$, we see that $\chi(\Sigma^\wedge) = -2h$. Since $\Sigma^\pm$ are disks, $\Sigma^\wedge$ has two boundary components. We conclude that $\Sigma^\wedge$ resulting from the construction in Fig. 3.14 is the surface with two boundaries and h handles (see Fig. 3.15).
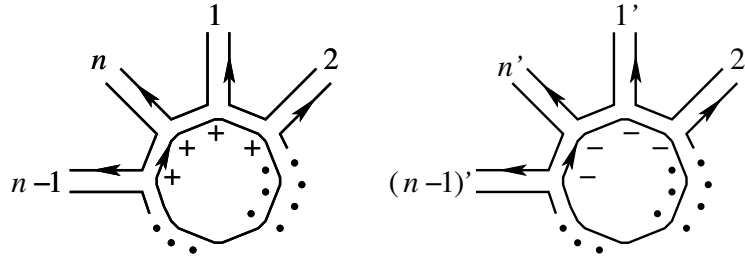
Figure 3.14: Construction of the ribbon diagram whose $\Sigma^\wedge$ is a higher-genus surface with two boundary components, depicted in Figure 3.15. Prepare two ribbon diagrams with n loose ends each as indicated, and connect pairwise the ends labeled by i and i': 1 to $1'$, 2 to $2'$, ..., n to n'. Note that with this order of gluing the ends, the resulting ribbon diagram will have only the total of 3 plaquettes if n is odd, or 4 plaquettes if n is even.

This demonstrates that wedge regions $\Sigma^\wedge$ obtained from ribbon diagrams can have connected components with an arbitrarily high number of handles.

Measure once, cut twice

Our analysis of the large-N expansion of non-equilibrium systems revealed one, perhaps surprising, fact: The time instant $t_\wedge$ where the forward branch of the Schwinger-Keldysh time contour meets the backward branch does not cut the worldsheet Σ into its forward and backward parts Σ^+ and $\Sigma^\wedge$ connected along a common one-dimensional boundary – instead, the worldsheet region $\Sigma^\wedge$ corresponding to $t_\wedge$ is topologically two-dimensional, and even carries its own genus expansion.

Having seen that the wedge region $\Sigma^\wedge$ can have components with arbitrary numbers of boundaries and high genus, there are some natural follow-up questions about $\Sigma^\wedge$ and how it is connected to the forward and backward regions Σ^+ and $\Sigma^\wedge$.
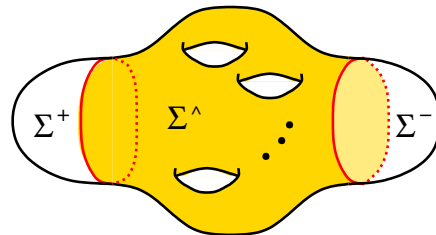
Figure 3.15: The worldsheet topology whose $\Sigma^\wedge$ has h handles and two boundary components, and Σ^+, Σ^- are both disks. This surface is obtained from the ribbon diagram construction depicted in Figure 3.14, with $n = 2h + 1$ or $n = 2h + 2$.

Does $\Sigma^{\wedge}$ always have to have non-empty boundaries with both Σ^{+} and Σ^{-}? The answer is yes, in the following sense: There are certainly ribbon diagrams, such that their assiciated surface is $\Sigma = \Sigma^{+}$ or $\Sigma = \Sigma^{-}$, and $\Sigma^{\wedge}$ is empty. But if $\Sigma^{\wedge}$ is non-empty, it has to have a non-empty boundary both with Σ^{+} and with Σ^{-}. The proof is simple: In the combinatorial description, $\Sigma^{\wedge}$ is built from lines representing G_{+-} propagators, and the $+-$ plaquettes. If $\Sigma^{\wedge}$ is non-empty, it contains at least one G_{+-} propagator. This propagator has to have a place to end, at both ends. On the $+$ side, the propagator can only end at a non-empty boundary with Σ^{+}; similarly, on the $-$ side, it must end on a non-empty boundary with Σ^{-}.

We can summarize this structure in a simple slogan: *Measure once, cut twice!* If you find that Σ has both Σ^{+} and Σ^{-} non-empty, you must cut; and if you cut, you must cut twice. The first "cut" indicates the location within Σ of the boundary between Σ^{+} and $\Sigma^{\wedge}$ (which we denote by $\partial_{+}\Sigma$), and the second "cut" indicates the location of the boundary between $\Sigma^{\wedge}$ and Σ^{-} (which we denote by $\partial_{-}\Sigma$). Of course, $\partial_{+}\Sigma$ is just a collection of n circles and $\partial_{-}\Sigma$ is a collection of n' circles; note that n does not have to equal n'.

It is intriguing to find that the structure of worldsheet "cuts" is so much richer in comparison to the simple propagator cuts known from standard quantum field theory of particle physics.

Dual picture

Ribbon diagrams exhibit a very useful duality property, closely related to what mathematicians call Poincaré duality in topology of manifolds. Each ribbon diagram Δ defines uniquely another, dual ribbon diagram $\Delta^{\star}$, as follows: Each plaquette of Δ is associated with a vertex in $\Delta^{\star}$. Whenever two plaquettes in Δ share an edge, the corresponding vertices in $\Delta^{\star}$ are connected by a ribbon. All ribbons attached to a given vertex in $\Delta^{\star}$ in the same cyclic order as the order of their dual edges around the original plaquette in Δ. As a result, each plaquette in $\Delta^{\star}$ is associated with a unique vertex in Δ. It is easy to see that with this construction, $\Sigma(\Delta^{\star}) = \Sigma(\Delta)$ (and consequently $\chi(\Sigma(\Delta^{\star})) = \chi(\Sigma(\Delta)))$, and $(\Delta^{\star})^{\star} = \Delta$. In particular, the cellular decompositions of Σ provided by a diagram Δ and its dual $\Delta^{\star}$ are dual to each other in the sense of cellular decompositions.

We can use this duality to shed more light on the $\Sigma^{\wedge}$ region. In the combinatorial description of Σ using a ribbon diagram Δ, it was perhaps surprising that we assigned only propagators and plaquettes to $\Sigma^{\wedge}$, *i.e.*, one-dimensional and two-dimensional cells, but no vertices. The dual picture using $\Delta^{\star}$ reveals why that was so: The plaquettes of Δ correspond to vertices in the dual picture, and the G_{+-} propagators that traverse across $\Sigma^{\wedge}$ from the $\partial_{+}\Sigma$ boundary to the $\partial_{-}\Sigma$ boundary turn in the dual picture to lines connecting those vertices. Thus, dualizing the formula (3.37) for the Euler number of $\Sigma^{\wedge}$, we see that contributions to $\chi(\Sigma^{\wedge})$ come only from vertices and propagators of $\Delta^{\star}$, so only zero- and one-dimensional components contribute. These components of $\Delta^{\star}$ of course form nothing other than the graph of cuts $\Gamma(\Delta)$. In this sense, the topological information about $\Sigma^{\wedge}$ can be encoded in cellular data not involving cells of dimension two.

(a)   **(b)**
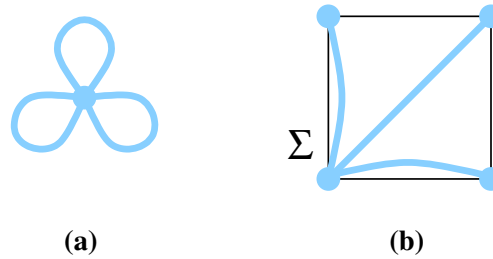
Figure 3.16: Surfaces with distinct $\Sigma^{\wedge}$'s but with the same graph of cuts Γ. In this example, Γ is the trefoil graph. **(a):** Here Γ is drawn on the sphere, and $\Sigma^{\wedge}$ is the sphere with four boundaries. **(b):** Here Σ is the torus, represented as a square with the opposite sides pairwise identified. The indicated graph of cuts is again the trefoil. The triple decomposition of this surface reproduces that of Fig. 3.13.

This does not mean that we should abandon our smooth-surface representation of $\Sigma^{\wedge}$ and revert back to the graph description: The classification of $\Sigma^{\wedge}$ as surfaces with smooth boundaries is much more transparent than the classification of the corresponding graphs and the ways how they can be drawn on surfaces. In particular, without keeping track of how the graph of cuts Γ is drawn on Σ, the graph itself does not contain enough information to reconstruct the topology of $\Sigma^{\wedge}$. Take for example the trefoil graph, depicted in Fig. 3.16(a). This graph can be drawn on the sphere, in a topologically unique way. This configuration indeed corresponds to a particular ribbon diagram, whose $\Sigma = S^2$ and $\Sigma^{\wedge}$ is the sphere with four boudaries. The trefoil graph can also be drawn on a torus, in several inequivalent ways. First, if drawn in a local patch of the torus, it again gives the same $\Sigma^{\wedge}$ as on the sphere. Or it can be drawn such that all three cycles of the trefoil are noncontractible and mutually homotopically inequivalent, as in Fig 3.16(b). This describes the configuration in Fig. 3.12, and $\Sigma^{\wedge}$ is the torus with two boundaries. Of course, both of these $\Sigma^{\wedge}$ topologies (as well as the graph Γ itself) have the same Euler number, $\chi = -2$.

Indeed, this ambiguity is not at all surprising – in order to keep track of how Γ is drawn on Σ, we have just learned that it is natural to interpret it as a ribbon subdiagram of the dual ribbon diagram $\Delta^{\star}$. As a two-dimensional surface with boundaries, this ribbon diagram corresponding to Γ is indeed just the thickening of Γ into $\Sigma^{\wedge}$ that we introduced in Section 3.2.

Grothendieck's *dessins d'enfants* make an appearance

Over its lifetime, string theory has demonstrated an extraordinary ability to make meaningful connections to many diverse areas of modern mathematics. These connections have been very fruitful both for mathematics and physics. In this subsection, we take a brief detour to point out one unexpected connection between the structure of the non-equilibrium string diagrams and objects that have been studied extensively in pure mathematics, under the

name of Grothendieck's *dessigns d'enfants*. Tho readers interested in the physical picture of non-equilibrium string perturbation theory should feel free to skip this subsection and go directly to Section 3.2, where our main results are stated.

Since the notion of *dessins d'enfants* (see, *e.g.*, [75, 76, 77, 78]) was first introduced by Grotendieck in his 1984 *Esquisse d'un Programme*, *dessins* have been found to relate remarkably many diverse areas in pure mathematics (including such arkane concepts as the absolute Galois group[11] and its faithful action on various categories [78]), and it is only fitting that they should appear in string theory.[12] For our purposes, a *dessin d'enfant* can be defined as a connected graph, consisting of a finite number of vertices and lines, and drawn on a two-dimensional surface Σ' such that no two vertices coincide on Σ' and no two lines intersect on Σ', and such that two additional conditions are satisfied: (i) the graph is bipartite in the following sense: each vertex is labeled either black or white, with each line of the graph connecting a black vertex with a white one; and (ii) the complement of the graph in Σ' is topologically a collection of disks.

Now we can show that there is a close relation bewteen *dessins d'enfants* and the wedge-region part of our ribbon graphs. Imagine asking the following question: How do we keep track of only that part of the ribbon diagram that defines the $\Sigma^\wedge$ region of its associated surface? This question is answered as follows. Consider a ribbon diagram Δ, and draw it on its associated surface Σ with triple decomposition Σ^+, Σ^- and $\Sigma^\wedge$. Erase the Σ^+ and $\Sigma^\wedge$ parts of Σ, keeping only the wedge region $\Sigma^\wedge$. Glue in a disk inside each of the boundary components of $\Sigma^\wedge$, place a new vertex in the center of each such disk, and label it $+$ or $-$ depending on whether the disk replaces a boundary with Σ^+ or Σ^-. All ribbon propagators are now ending on the edges of the glued-in disks; extend them to the vertex at the center of the disk, without intersections. This defines a new, "reduced" ribbon diagram, whose associated surface is $\Sigma^\wedge$ with the boundary components filled in with the disks. All detailed information about how the original ribbon diagram extends into the Σ^+ and Σ^- regions has now been erased, so the resulting reduced ribbon diagram encodes only the information about $\Sigma^\wedge$.

We now observe that each such reduced ribbon diagram defines a unique *dessin d'enfant*: Label each $+$ vertex as black, and each $-$ vertex as white, and note that all the axioms of *dessins* are satisfied by our reduced ribbon diagram. In turn, every *dessin d'enfant* is realized by at least one ribbon diagram in this way. More precisely, we can define an equivalence relation on the original ribbon diagrams, by declaring two ribbon diagrams equivalent if they may differ only in their Σ^+ and Σ^- regions, but give the same reduced ribbon diagram when our procedure is followed. Two ribbon diagrams correspond to the same *dessin d'enfant* if they belong to the same equivalence class. For example, the ribbon diagrams in Figs. 3.11 and 3.12 are in the same equivalence class, and the *dessin d'enfant* corresponding to them

---

[11]The absolute Galois group $\mathrm{Gal}(\overline{\mathbb{Q}}/\mathbb{Q})$ is defined as the group of authomorphisms of the algebraic numbers $\overline{\mathbb{Q}}$ which fix the rational numbers $\mathbb{Q}$ [79].

[12]In an unrelatex context, *dessins d'enfants* also appeared previously in string theory in certain brane engineering constructions [80] and Calabi-Yau compactifications [81, 82].

can be drawn like this:

.
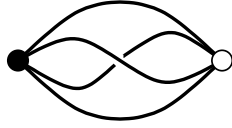
This *dessin* is supposed to be visualized as being drawn on a torus, and the $\Sigma^\wedge$ that corresponds to this *dessin* is depicted in Fig. 3.13.

In turn, two ribbon diagrams from distinct equivalence classes correspond to distinct *dessins*. We conclude that there is a one-to-one correspondence between *dessins d'enfants* and the equivalence classes of all ribbon diagrams defined above, represented by the reduced ribbon diagrams.

We do not have any immediate use in non-equilibrium physics for this connection to *dessins d'enfants*, yet we find it fascinating that they do naturally appear in the structure of non-equilibrium string perturbation theory, and are related so intimately to the most interesting portion $\Sigma^\wedge$ of the worldsheet, associated with the crossing from the forward to the backward branch of the Schwinger-Keldysh time contour.

Non-equilibrium string perturbation theory

After this thorough analysis of the surfaces Σ that can emerge from ribbon diagrams in our large-N theory of matrix degrees of freedom out of equilibrium, we are ready to formulate the main lessons about the dual string theory expansion. Which surfaces contribute to the expansion? If we make no additional assumptions about the dynamics of the large-N system, *i.e.*, assume no "hidden identities" of individual ribbon diagrams (or among groups of ribbon diagrams) that would make some contributions vanish, then as we have seen above, all possible ttriple decompositions of worldsheets result from consistent ribbon diagrams.[13]

In non-equilibrium string perturbation theory, the partition function is expressed as a refined topological expansion over worldsheet surfaces,

$$\mathcal{Z} = \sum_{h=0}^{\infty} \left(\frac{1}{N}\right)^{2h-2} \sum_{\substack{\text{triple decompositions} \\ \chi_+ + \chi_- + \chi_\wedge = 2-2h}} \mathcal{F}_{\Sigma^+,\Sigma^-,\Sigma^\wedge}(\lambda, \dots), \tag{3.41}$$

This formula is the central result of this chapter: In non-equilibrium string theory, the genus expansion into a sum over connected surfaces Σ known from equilibrium is further refined into a sum over triple decomposition of each surface Σ into its forward part Σ^+, backward part Σ^- and the wedge part $\Sigma^\wedge$ which corresponds to the time instant $t_\wedge$ where the two branches C_+ and C_- of the Schwinger-Keldysh time contour meet. We stated the result here

---

[13]For specific systems, there might be additional identities that make some classes of surfaces drop out from the sum; those can be studied on a case-by-case basis. Here we concentrate on the universal predictions about non-equilibrium string perturbation theory, following solely from the topology of the large-N expansion, without any additional dynamical assumptions.
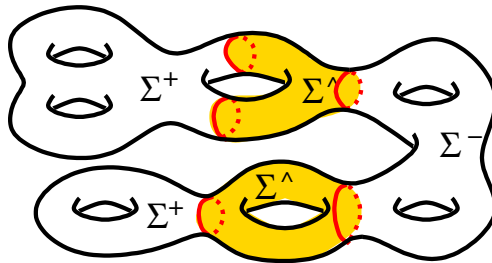
Figure 3.17: A typical string topology contributing to the non-equilibrium string perturbation theory.

for the partition function $\mathcal{Z}$, but the same expansion is expected of correlation functions of local observables as well.

In our derivation of this result from the original large-N system, the individual contribution $\mathcal{F}_{\Sigma^+,\Sigma^-,\Sigma^\wedge}$ of each triple decomposition is weighted by the power of N given by the total Euler number $\chi(\Sigma) = 2 - 2h$. Thus, the term at a fixed order h in the string coupling is further refined into a sum over all triple decompositions of Σ with that genus h into Σ^+, Σ^- and $\Sigma^\wedge$, subject only to the condition that Σ be connected. At this stage, individual triple decompositions are still weighted just by the overall Euler number $\chi(\Sigma)$, with $1/N$ the only parameter of the expansion. This may be the limit of how far the large-N expansion arguments can take us, in predicting the universal properties of the dual string theory.

However, once we identify $1/N$ with the string coupling constant g_s, one can use our experience with critical string theory at equilibrium to speculate that a more refined weighting should be possible. For example, one can imagine dialing different values of the string coupling on the forward and backward branches of the time contour (let's call them g_+ and g_-), or a different value of the string coupling in the asymptotic future at $t_\wedge$ (which we naturally call $g_\wedge$). Indeed, in critical string theory in equilibrium, there are many examples where the string coupling "constant" – being given by the vacuum expectation value of the dilaton field Φ as $g_s = \langle e^\Phi \rangle$ – is dependent on the spacetime location, no longer necessarily equal to a fixed value set by $1/N$. Assuming that on the Schwinger-Keldysh contour g_s can take such three different values $g_\pm$ and $g_\wedge$ in its three different regions, each term in the perturbation theory sum (3.41) would then be weighted by the more refined weight

$$g_+^{-\chi(\Sigma^+)} g_-^{-\chi(\Sigma^-)} g_\wedge^{-\chi(\Sigma^\wedge)}, \tag{3.42}$$

replacing the overall $g_s^{-\chi(\Sigma)}$ that we obtained from the $1/N$ expansion. In order to see whether such a possibility is realized, we would need to know more about the worldsheet dynamics of strings away from equilibrium.

Having shown that all topologies can appear in the triple decompositions of worldsheet surfaces, one can reorganize the question and ask, for a given surface Σ, for a full classification of all its possible triple decompositions. Such decompositions are fully classified in terms of
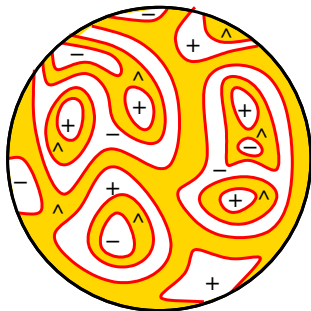
Figure 3.18: Illustration of the possible infinite proliferation of triple decompositions for a given Σ (here illustrated for $\Sigma = S^2$), if connected components of Σ^+ and Σ^- with non-negative Euler number (and no additional insertions of observables inside them) are not identically zero.

the discrete topological data about Σ^+, Σ^- and $\Sigma^\wedge$: Their numbers of handles, and numbers of boundary components. However, without making any additional assumptions about the worldsheet dynamics, the number of distinct triple decompositions of a fixed surface Σ is infinite. This proliferation of decompositions is illustrated for the sphere in Fig. 3.18. We find an infinite number of decompositions of the sphere, with connected components of $\Sigma^\wedge = \Sigma_{0,b}$ given by spheres with b boundaries. Upon closer inspection, we find that the origin of this proliferation is in the existence of components in Σ^+, Σ^- and $\Sigma^\wedge$ whose Euler number χ is non-negative: Indeed, since the Euler number of Σ is the sum of the Euler numbers of its triple decomposition, if only those components that have negative χ were allowed, there would only be a finite number of possible decompositions.

In vacuum diagrams, the components of Σ^+ and $\Sigma^\wedge$ with non-negative Euler numbers are disks and cylinders, while in $\Sigma^\wedge$ it is only the cylinder. When we generalize from vacuum diagrams to correlation functions of local observables on Σ, each insertion counts as a "puncture" in Σ, and contributes an additional -1 to the Euler number. In this case, the additional components of Σ^+ and $\Sigma^\wedge$ causing proliferations in the triple decompositions of Σ are also disks with one puncture. How to deal with such proliferations? There are two main options: (a) allow them to be non-zero and perhaps resum the contributions with non-negative χ to define "renormalized" triple decompositions of Σ, or (b) make an additional assumption about the worldsheet dynamics, declaring that contributions of components of Σ^+ and Σ^- with $\chi \geq 0$ vanish identically.

While Option (a) might be necessary in some circumstances far from equilibrium, Option (b) is something we are familiar with from critical string theory in equilibrium. In critical string theory, string worldsheets inherit a complex structure from dynamics of worldsheet gravity and its symmetries. The $\mathcal{F}_h$ contributions at fixed genus h are given as integrals over moduli spaces of such complex structures. When the worldsheet is a sphere with fewer than three punctures, such contributions vanish identically, since they are suppressed by the infi-

nite volume of a residual worldsheet gauge symmetry. In the language of mathematics, only "stable nodal Riemann surfaces" [83] (*i.e.*, surfaces with punctures and with non-negative Euler numbers) contribute to the amplitudes. This suggests a realization of our Option (b): In theories where the worldsheet dynamics implies additional worldsheet structure (such as the complex structure), one could propose that the boundaries $\partial_+\Sigma$ and $\partial_-\Sigma$ in the triple decomposition should be interpreted geometrically as nodes in the Riemann surface, and expect that the components of Σ^+ and Σ^- which carry non-negative Euler numbers vanish identically, in analogy with critical string theory in equilibrium.

Note that in Option (b), in order to get a finite sum over triple decompositions, it would not be sufficient to assume that just the components of Σ^+ and Σ^- with strictly positive χ (*i.e.*, the disks) vanish identically: There would still be an infinite number of triple decompositions of vacuum diagrams at each order in g_s, starting at genus one.

In fact, the list of topological invariants associated universally with our triple decompositions of Σ is even richer than just $\chi(\Sigma^+)$, $\chi(\Sigma^-)$ and $\chi(\Sigma^\wedge)$. We can define b_+ to be the number of boundary components in the boundary $\partial_+\Sigma$ between Σ^+ and $\Sigma^\wedge$, and similarly b_- as the number of components in the boundary $\partial_-\Sigma$ between Σ^- and $\Sigma^\wedge$. These $b_\pm$ are of course topological invariants, and if we introduce "fugacities" f_+ and f_- for them, we can weigh each triple decomposition of Σ by an additional factor of

$$f_+{}^{b_+} f_-{}^{b_-}. \tag{3.43}$$

Another set of useful invariants are the numbers of connected components in Σ^+, Σ^- and $\Sigma^\wedge$, which we denote by n_+, n_- and $n_\wedge$. Even if Option (a) applies, and the disk and cylinder components of Σ^+ and Σ^- turn out not to be zero, there is one way how to reduce the sum over triple decompositions at each genus h to a finite sum: If we allow only connected Σ^+ and Σ^- to contribute. This can be arranged by introducing "fugacity" parameters γ_+ and γ_- for the numbers of components n_+ and n_-, to weigh the contribution of a given triple decomposition by

$$\gamma_+^{n_+-1}\gamma_-^{n_--1}. \tag{3.44}$$

Presumably, we choose $\gamma_\pm$ to be smaller than one, so that they suppress contributions from higher numbers of connected components of $\Sigma^\pm$. Sending $\gamma_\pm \to 0$ then keeps only the contributions from the connected components in $\Sigma^\pm$.

The question of whether or not the appropriate refined expansion parameters such as $g_\pm$ and $g_\wedge$, $\gamma_\pm$ or $f_\pm$ do naturally appear in a given string theory is likely to depend on the specific examples, and their string dynamics. Since in this chapter we are only focusing on the universal properties independent of any knowledge about the worldsheet dynamics, such questions are outside of the scope of this chapter. Our universal arguments only reveal the universal existence of the topological invariants to which such hypothetical dynamical expansion parameters could be sensitive.
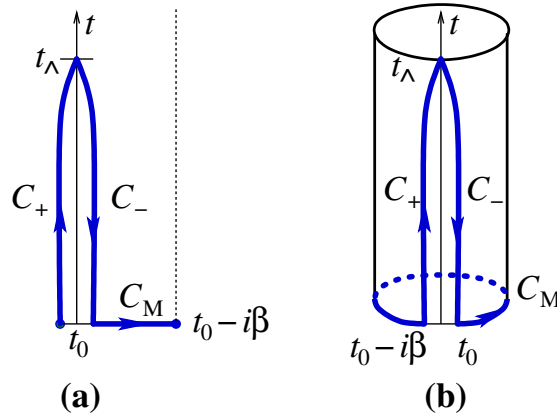
Figure 3.19: **(a):** The Kadanoff-Baym time contour $\mathscr{C}_\beta = C_+ \cup C_- \cup C_M$ in the plane of complexified time, with the dashed line indicating the periodicity of observables by β in the imaginary time direction. **(b):** The KMS periodicity properties suggest that the complexified time can be naturally thought of as a cylinder, on which the KB contour is a closed contour with winding number one.

3.3. Strings on the Kadanoff-Baym time contour

Our analysis of the Schwinger-Keldysh time contour has several straightforward generalizations. In this section, we present the large N expansion of theories on another popular time contour, relevant particularly for systems at finite temperature T at or near equilibrium, known as the Kadanoff-Baym contour[14] [84, 62, 63, 68, 69, 70, 71]. Since the logic of this analysis is a straighforward generalization of our discussion in Section 3.2, we will be relatively brief.

The Kadanoff-Baym contour and finite temperature

The Kadanoff-Baym (KB) contour $\mathscr{C}_\beta$ consists of three segments (see Fig 3.19(a)): Besides the forward and backward branches C_+ and C_- known from the Schwinger-Keldysh contour, there is a third segment CM representing an excursion into the imaginary direction by the amount $-i\beta$. This last segment of the KB contour is referred to as the "Matsubara" segment of the KB contour. Indeed, this Matsubara segment would constitute the entire time contour in the standard imaginary-time approach to equilibrium systems at finite temperature known as the Matsubara formalism. Keeping both the imaginary-time segment and the real-time segments of the KB contour allows us to combine the benefits of the imaginary-time Matsubara formalism with the possibility of studying real-time phenomena at finite temperature. The condition of thermal equilibrium translates into the so-called Kubo-Martin-Schwinger

---

[14]Sometimes this contour is referred to as the Konstantinov-Perel' contour [65].

(KMS) conditions on correlation functions of meaningful quantities. As a consequence of the KMS conditions, the correlation functions are periodic (or antiperiodic) along the imaginary direction of the complexified time; it is therefore natural to think of the KB contour as a closed contour on the cylinder (see Fig 3.19(b)).

Now the fields are tripled: M on the $\mathscr{C}_\beta$ contour can be represented by two fields $M_\pm(t)$ that depend on real time, and one new field $M_{\mathrm{M}}(\tau)$ which depends on the coordinate τ defined as $\tau = -\mathrm{Im}\, t$ along the Matsubara segment C_{M}:

$$M_{\mathrm{M}}{}^a{}_b(\tau) \equiv M^a{}_b(-i\tau). \tag{3.45}$$

With this definition, $\tau \in [0, \beta)$.

This triplication of fields means that we have nine *a priori* distinct propagators, defined using the time ordering $\mathrm{T}_{\mathscr{C}_\beta}$ along the KB contour. They are denoted by ribbons as in (3.22-3.25), but now labeled with three possible indices $+, -, \mathrm{M}$ at each end. The propagators involving the $M_\pm$ fields are as in (3.26-3.29). Then there are four propagators connecting one M_{M} with either M_+ or M_-; these are expressed in terms of the Green's functions $G^\lceil$ and $G^\rceil$ known in the non-equilibrium literature as G-left and G-right [65],

$$\begin{aligned} \langle M_{\mathrm{M}}(\tau) M_\pm(t) \rangle &= g^2\, G^\lceil(\tau, t), &&(3.46) \\ \langle M_\pm(t) M_{\mathrm{M}}(\tau) \rangle &= g^2\, G^\rceil(t, \tau). &&(3.47) \end{aligned}$$

Finally, we have the G_{MM} propagator, familiar from the Matsubara formalism, and given by the two-point function of M_{M} along the Matsubara segment. For clarity, we will again use a uniform two-index notation for all nine propagators in the rest of this section, with the indices running over $+, -, \mathrm{M}$.

The vertices are the same as in (3.30-3.33), except now they are labeled by one of the three indices $+, -, \mathrm{M}$.

Seven-fold decomposition of Σ

In understanding the decomposition of Σ for the KB contour, we will use the same combinatorial approach that worked for us in Section 4.3.

All ribbon diagrams now have vertices labeled by $+, -$ and M. Consider such a diagram Δ. It defines a cellular decomposition of its associated surface Σ. We wish to construct the decomposition of Σ on the KB contour, analogous to the triple decomposition of Σ that we found on the Schwinger-Keldysh contour. We begin by constructing the forward region Σ^+: Combinatorially, we define Σ^+ to be the region whose cellular decomposition consists of all $+$ vertices in Δ, all the G_{++} propagators, and all the plaquettes whose all adjacent propagators are G_{++}. This collection of data indeed defines a cellular decomposition of a surface with boundaries, which will be our Σ^+. Repeating the same with $-$ vertices, propagators and plaquettes defines the backward regionΣ^-. Finally, repeating the same with M vertices, propagators and plaquettes defines Σ^{M}, the "Matsubara region" of Σ.

In complete analogy with Section 4.3, we introduce the following notation:

$$
\begin{aligned}
V_+ &= \text{the number of vertices labeled by } +, \\
P_+ &= \text{the number of } G_{++} \text{ propagators}, \\
L_+ &= \text{the number of plaquettes with all their vertices labeled by } +,
\end{aligned}
$$

(with similar definitions for V_-, P_-, L_-, V_{M}, P_{M} and L_{M}). We define the combinatorial Euler numbers $\chi_\pm$ and χ_{M}, and argue that they are equal to the topological Euler numbers of surfaces with boundaries Σ^+, Σ^- and Σ^{M}:

$$
\begin{aligned}
\chi_+(\Delta) &\equiv V_+ - P_+ + L_+ = \chi(\Sigma^+), \\
\chi_-(\Delta) &\equiv V_- - P_- + L_- = \chi(\Sigma^-), \\
\chi_{\mathrm{M}}(\Delta) &\equiv V_{\mathrm{M}} - P_{\mathrm{M}} + L_{\mathrm{M}} = \chi(\Sigma^{\mathrm{M}}).
\end{aligned}
$$

Next we try to repeat our definition of $\Sigma^{\wedge}$, and define the regions of Σ that correspond to the parts of the KB contour where two of the regions Σ^+, Σ^- or Σ^{M} connect. First, we define region Σ^{+-} by assigning to it all G_{+-} and G_{-+} propagators in Δ, and all the plaquettes with at least one adjacent G_{+-} or G_{-+} propagator but no adjacent M vertices. We denote by V_{+-}, P_{+-} and L_{+-} the numbers of vertices, propagators and plaquettes so assigned to Σ^{+-}. Next, we similarly define regions $\Sigma^{+\mathrm{M}}$ and $\Sigma^{-\mathrm{M}}$ by repeating the same steps which defined Σ^{+-}.

Precisely as in the case of $\Sigma^{\wedge}$ in Section 4.3, these combinatorial data contain no vertices, and they do not define a cellular decomposition of the three surfaces. We can still define the cellular Euler numbers

$$
\begin{aligned}
\chi_{+-}(\Delta) &\equiv V_{+-} - P_{+-} + L_{+-}, \\
\chi_{+\mathrm{M}}(\Delta) &\equiv V_{+\mathrm{M}} - P_{+\mathrm{M}} + L_{-\mathrm{M}}, \\
\chi_{-\mathrm{M}}(\Delta) &\equiv V_{-\mathrm{M}} - P_{-\mathrm{M}} + L_{-\mathrm{M}},
\end{aligned}
$$

and ask whether they are equal to the topological Euler numbers of the surfaces Σ^{+-}, $\Sigma^{+\mathrm{M}}$ and $\Sigma^{-\mathrm{M}}$. In contrast to the Schwinger-Keldysh case, here we find that these three surfaces are in general *not* manifolds with smooth boundaries, but instead they are manifolds with corners. Compared to the Schwinger-Keldysh case studied in Section 4.3, the novelty here is that the combinatorial ingredients of Δ assigned to the six distinct region do not yet generally cover all of Σ. We must add yet another region, $\Sigma^{+-\mathrm{M}}$, to which we assign all the plaquettes which have adjacent indices of all three types $+$, $-$ and M. The number of such plaquettes will be denoted by $L_{+-\mathrm{M}}$. With the addition of $\Sigma^{+-\mathrm{M}}$, each combinatorial element of the cellular decomposition of Σ has been accounted for and assigned to exactly one region, and we have defined a partition of Σ into seven parts.

Let us take a closer look at the $\Sigma^{+-\mathrm{M}}$ component. Its combinatorial Euler number will be simply the number of the plaquettes assigned to $\Sigma^{+-\mathrm{M}}$,

$$
\chi_{+-\mathrm{M}}(\Delta) = L_{+-\mathrm{M}}. \tag{3.48}
$$
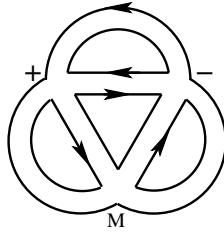
Figure 3.20: A simple ribbon diagram with a seven-fold decomposition of Σ.

In contrast to the other six regions, which can be topologically complicated with arbitrarily high genus, the topology of $\Sigma^{+-\mathrm{M}}$ is quite simple: Since it contains only plaquettes, and no propagators or vertices of the original ribbon diagram Δ, it consists topologically of a collection of disconnected disks, one for each plaquette. The entire topology of $\Sigma^{+-\mathrm{M}}$ is thus completely fixed in terms of its Euler number $\chi_{+-\mathrm{M}} = L_{+-\mathrm{M}}$, which simply counts the total number of the disconnected disks.

A simple example of the seven-fold decomposition of Σ associated with a ribbon diagram Δ, for which all seven parts of this decomposition are non-empty, is given in Fig. 3.20. It also provides an example where Σ^{+-}, $\Sigma^{+\mathrm{M}}$ and $\Sigma^{-\mathrm{M}}$ are not smooth manifolds, but manifolds with corners, as one can verify by evaluating their Euler numbers.

The decomposition patterns for Σ can get even more complicated when one considers time contours with more than three segments. An extension to such contours is not just a mindless mathematical exercise, as such contours can be physically well-motivated: For example, the contour relevant for thermofield dynamics has four segments (see Fig. 3.21). In the case with $k > 3$ segments of the time contour, we introduce an index $i = 1, \ldots k$ and iterate our combinatorial construction for $k = 3$ from earlier in this section to construct regions Σ^i, Σ^{ij}, $\ldots \Sigma^{i_1 \ldots i_k}$. It is best to think of them as antisymmetric in the indices. The one simplifying feature is that starting from $\Sigma^{ij\ell}$, all higher-order regions consists solely of isolated plaquettes of Δ, and are therefore topologically simple, just as our $\Sigma^{+-\mathrm{M}}$ above. Unfortunately, the Σ^{ij}'s are again manifolds with corners.

Manifolds with corners are rather awkward, and it would be much preferrable to work only with manifolds with smooth boundaries. One can avoid using the manifolds with corners in the following way. First, we define a coarser decomposition of Σ into just four parts: Keeping Σ^+, Σ^- and Σ^{M}, and assigning all the rest of Σ to be the fourth region $\widehat{\Sigma}$. In our example from Fig. 3.20, $\widehat{\Sigma}$ is a sphere with three boundaries. $\widehat{\Sigma}$ can be viewed as a manifold with a smooth boundary, using the same arguments that we used in Section 4.3 for $\Sigma^\wedge$.

This four-fold decomposition is rather crude, since it loses track of the regions corresponding to just two segments of the time contour meeting, such as Σ^{+-}. We can restore this refinement by the following slight modification of our previous rules:

- All + vertices, all G_{++} propagators and all the plaquettes which have only G_{++} adjacent propagators define region Σ^+; analogously for Σ^- and Σ^{M}.

- All G_{+-} (and G_{-+}) propagators and all the plaquettes that have at least one G_{+-} (or G_{-+}) adjacent propagator define region $\widetilde{\Sigma}^{+-}$; analogously for $\widetilde{\Sigma}^{+M}$ and $\widetilde{\Sigma}^{-M}$.

Clearly, all the combinatorial ingredients in Δ have been assigned. The Σ^+, Σ^- and Σ^M regions are defined as before, and they do not share any plaquettes with each other or any other region. The novelty is in the $\widetilde{\Sigma}$ regions: They can be interpreted as surfaces with smooth boundaries, but they can now overlap over disks. Their union is $\widehat{\Sigma}$. The seventh region Σ^{+-M} of the seven-fold decomposition is the collection of all the disks in Σ over which at least two of the $\widetilde{\Sigma}$ components overlap.[15] In our example from Fig. 3.20, $\widetilde{\Sigma}^{+-}$, $\widetilde{\Sigma}^{+M}$ and $\widetilde{\Sigma}^{-M}$ are all disks, overlapping over two disks, as indicated in Fig. 3.22.

To conclude this section, we point out that the dual picture of the ribbon diagrams developed in Section 3.2 gives an interesting perspective also on the seven-fold decomposition of Σ associated with the Kadanoff-Baym contour. Going from the original ribbon diagram Δ to its dual diagram $\Delta^\star$ reveals that while Σ^+, Σ^- and Σ^M are effectively two-dimensional (since they are built from vertices, lines and plaquettes of $\Delta^\star$), Σ^{+-}, Σ^{+M} and Σ^{-M} are effectively one-dimensional, built only from vertices and lines of $\Delta^\star$. This is reminiscent of what we saw in the triple decomposition on the Schwinger-Keldysh contour in Section 3.2. In the seven-fold decomposition, this pattern goes one step further, and Σ^{+-M} is found to be effectively zero-dimensional, since it is built only from vertices in $\Delta^\star$ and therefore represents just a finite collection of points in this dual picture.

---

[15]These new decomposition rules can be extended straightforwardly to the case of time contours with k components. One defines regions Σ^i and $\widetilde{\Sigma}^{ij}$ for $i, j = 1, \ldots k$ and $i < j$ in analogy with the $k = 3$ case. They are all manifolds with smooth boundaries. Then $\widehat{\Sigma} = \bigcup \Sigma^{ij}$, and all the higher $\Sigma^{i_1 \ldots i_s}$ with $s \geq 3$ correspond the the collection of disks where the appropriate $\widetilde{\Sigma}^{ij}$'s overlap.
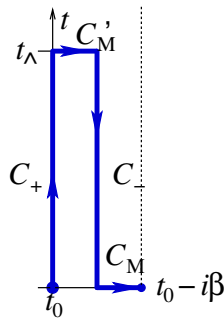
Figure 3.21: The time contour relevant for thermofield dynamics, as a physically motivated example of a contour with four segments [85, 62, 63].
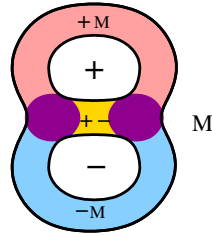
Figure 3.22: The surface associated with the diagram in Fig. 3.20, and its decomposition into Σ^+, Σ^-, Σ^{M}, $\widetilde{\Sigma}^{+-}$, $\widetilde{\Sigma}^{+\mathrm{M}}$ and $\widetilde{\Sigma}^{-\mathrm{M}}$. The three $\widetilde{\Sigma}$'s overlap over two disks. All components are manifolds with smooth boundaries, and $\widehat{\Sigma} = \widetilde{\Sigma}^{+-} \cup \widetilde{\Sigma}^{+\mathrm{M}} \cup \widetilde{\Sigma}^{-\mathrm{M}}$ is the sphere with three boundaries.

3.4. Other generalizations

Our analysis can be naturally extended from the theory of closed oriented strings to theories containing unoriented and/or open strings. Since this generalization is straightforward, we will be brief.

Unoriented strings

Until now, we assumed the matrix degrees of freedom to be Hermitian and traceless, in the adjoint representation of the symmetry group $SU(N)$. We can replace the unitary group $SU(N)$ with another sequence of simple groups that allows a large-N limit – either orthogonal $SO(N)$ or symplectic $Sp(N)$. Our story then naturally generalizes and involves unoriented surfaces.

For $SO(N)$ or $Sp(N)$, Feynman rules and their ingredients are essentially the same as in the $U(N)$ case, except that the ribbons now do not carry arrows on their edges,

$$\pm{}^{a}_{b}\!\!\underline{\qquad\qquad}{}^{d}_{c}\pm \quad,$$

The arrows were needed in the $SU(N)$ case to distinguish between the upper indices and the lower indices of M, which correspond to inequivalent representations $\mathbf{N}$ and $\overline{\mathbf{N}}$. In contrast, for $SO(N)$ and $Sp(N)$ the upper and lower indices correspond to the same representation, and can be freely raised and lowered using the invariant quadratic form of $SO(N)$ or $Sp(N)$. Hence, in Feynman diagrams we no longer have to keep track of the difference between the left and right edge of the ribbons, as reflected by the absence of arrows in the notation. The matrices M are antisymmetric for $SO(N)$ and symmetric traceless for $Sp(N)$; this difference is immaterial for our arguments, and both cases will lead to the same topological expansion in non-equilibrium string perturbation theory. (See also Footnote 3 above for a clarification of the tracelessness condition relevant to the $Sp(N)$ case.)
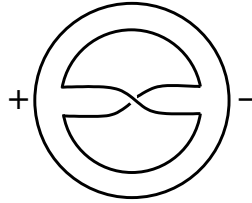
Figure 3.23: A typical ribbon diagram involving a twist in one of the propagators. The resulting surface is nonorientable, in this case the projective sphere $\mathbb{RP}^2$. In its triple decomposition, Σ^+ and Σ^- are both disks, and $\Sigma^\wedge$ is the sphere with two boundaries and a crosscap.

Similarly, the vertices are
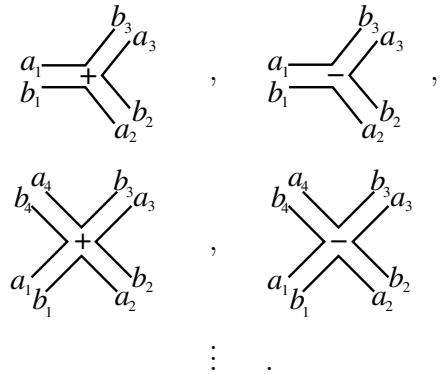
The dots here stand again for the list of higher n-point vertices, which are allowed but kept implicit.

Since the edges of the ribbons are no longer oriented, the propagators and vertices can now be connected with an additional twist (see Fig. 3.23). The resulting surfaces are then unoriented.

Recall how the classification of closed oriented surfaces extends to the case of closed unoriented surfaces. Besides the number h of handles, such surfaces Σ can also have c crosscaps.[16] With any nonzero c, Σ is nonorientable. In the classification of topologically inequivalent Σ's, the two non-negative integers h and c are not independent. Instead, there is one identity that fully describes their redundancy: Σ with h handles and $3 + c$ crosscaps (and b boundary components, should those be present) is topologically equivalent to Σ with $h + 1$ handles and $c + 1$ crosscaps (and b boundary components),

$$\Sigma_{h,c+3,b} = \Sigma_{h+1,c+1,b}, \tag{3.49}$$

_____

[16]The crosscap is defined by removing a disk from Σ, which creates an S^1 boundary, and then pairwise identifying the opposite points on this boundary; see, _e.g._, [86].

for all $h = 0, 1, \ldots$ and $c = 0, 1, \ldots$ (and $b = 0, 1, \ldots$). In equilibrium string theory, the genus expansion is over all inequivalent topologies, classified now by h and c subject to this one identity. Each surface contributes at order $g_s^{-\chi(\Sigma)}$ in the string coupling, with the Euler number now given by

$$\chi(\Sigma) = 2 - 2h - c. \tag{3.50}$$

Note that in contrast to the case of closed oriented strings, (i) there are generally several distinct topologies contributing at a given order in g_s, and (ii) there are now surfaces that contribute at odd orders in g_s. All this is of course extremely well-undestood in the case of critical string theory [86].

The results of our analysis for $SU(N)$ in Section 3.2 extend directly to unoriented string theory. Each surface Σ contributing to the non-equilibrium perturbative expansion again exhibits a triple decomposition into the forward region Σ^+, backward region Σ^- and the wedge region $\Sigma^\wedge$, glued together along common boundaries $\partial_+\Sigma$ and $\partial_-\Sigma$ to form Σ, the only novelty being that each of the three regions of the triple decomposition can now be orientable or nonorientable. With this one exception, the story parallels that of Section 3.2.

Coupling to vector degrees of freedom: Open string theory

Another natural generalization involves the presence of both matrix and vector degrees of freedom, in the adjoint and fundamental representation of one of the large-N sequences $SU(N)$, $SO(N)$ or $Sp(N)$. This generalization leads to surfaces with boundaries, or in other words, a theory of both closed and open strings. For simplicity we concentrate on the $SU(N)$ case, which makes the strings oriented; the $SO(N)$ and $Sp(N)$ cases will lead to a description in terms of unoriented closed and open strings.

Adding the degrees of freedom Ψ^a in the fundamental representation $\mathbf{N}$ (with its conjugate $\bar{\Psi}_b$ in the anti-fundamental $\overline{\mathbf{N}}$) adds new terms to the action,

$$S(M, \Psi) = \int \left(\bar{\Psi}_a \dot{\Psi}^a + g' \bar{\Psi}_a M^a{}_b \Psi^b + g'' \bar{\Psi}_a M^a{}_b M^b{}_c \Psi^c + \ldots \right). \tag{3.51}$$

To the Feynman rules for M, this will add a propagator for Ψ and new vertices. In equilibrium, the new propagator is the two-point function $\langle \Psi^a \bar{\Psi}_b \rangle$, which is now denoted by an oriented single line. When we take the system away from equilibrium, the Schwinger-Keldysh time contour is again that of Fig. 3.2, and it leads to the doubling of fields $\Psi_\pm$, $\bar{\Psi}_\pm$. The non-equilibrium propagators thus have each end again labeled by a choice of a $\pm$ sign,[17]

$$\pm \; \overset{a \qquad b}{\longrightarrow} \; \pm \quad .$$

---

[17]In the quadratic part of (3.51), we again only displayed the term with the time derivative, keeping all the other terms bilinear in Ψ and $\bar{\Psi}$ (such as masses, terms with spatial derivatives, or with more time derivatives) implicit, to keep the notation simple and to reflect the universality of our arguments. The propagator (3.52) of course contains the full information about all such terms.

In $S(M.\Psi)$ in (3.51), the "..." denote interactions with higher powers of M.[18] Besides the original vertices of the theory with the matrix degrees of freedom $M_\pm$, there are now new vertices,
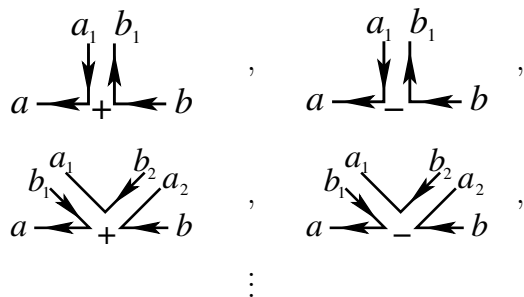
which describe the interaction between $M_\pm$, $\Psi_\pm$ and $\bar{\Psi}_\pm$ on the Schwinger-Keldysh contour. Our conclusions about the topology of the large-N expansion will be unaffected by whether we choose to think of Ψ as fermions or bosons: Only some signs in individual diagrams change, but the features of the topological expansion remain the same.

Consider for simplicity vacuum Feynman diagrams; the extension to n-point correlators is straightforward. With the vector degrees of freedom Ψ present, any Feynman diagram Δ will now be associated with a surface Σ with boundaries. The prescription for constructing Σ from Δ is exactly the same as in Section 3.1. Following this prescription leaves us with boundaries, each boundary component traced by a closed loop made of the $\Psi\bar{\Psi}$ propagators. Thus, the dual string theory contains closed and open oriented strings.

In equilibrium string theory of oriented closed and open strings, the sum over topologies extends over the topologically inequivalent oriented surfaces $\Sigma_{h,b}$ with boundaries, fully classified by the number of handles h and boundaries b which are non-negative integers and without redundancies. Taking the coupled system of M, Ψ away from equilibrium shows that our conclusions from Section 3.2 hold again: The sum over topologies $\Sigma_{h,b}$ is refined to a sum over triple decompositions Σ^+, Σ^- and $\Sigma^\wedge$ of each $\Sigma_{h,b}$.

At first, it might appear a little awkward that we are supposed to split a surface $\Sigma_{h,b}$ which itself has boundaries, into three regions: Some of the cuts may cut across the boundaries of $\Sigma_{h,b}$. However, this seemingly intricate issue is easy to deal with, by invoking one of the classic techniques with a proven record in critical string theory in equilibrium [87, 88, 89], in the context of D-branes and orientifolds: Treat each worldsheet surface Σ with boundaries (and/or crosscaps) as a $\mathbb{Z}_2$ orbifold of a closed oriented surface $\bar{\Sigma}$, *i.e.*, $\Sigma = \bar{\Sigma}/\mathbb{Z}_2$, with $\mathbb{Z}_2$ an orientation-reversing involution of $\bar{\Sigma}$. The boundaries of Σ correspond to the lines of $\mathbb{Z}_2$ fixed points of the involution. The triple decomposition of Σ is then simply defined as a triple decomposition of the closed oriented cover $\bar{\Sigma}$ (in the sense of Section 3.2), consistent with the

---

[18]In the theory of M alone, our interactions were all single-trace, and here we also assume that all the interactions between Ψ and M are of the "single-trace" type – only those monomials that do not factorize into the product of two singlets are admitted. This in particular implies that the vector degrees of freedom appear quadratically, and all the new vertices have just two single-line ends. This simplification indeed occurs in various important examples, and in particular mimics the behavior of quarks in QCD.

$\mathbb{Z}_2$ symmetry. With this trick, our conclusions of Section 3.2 extend straightforwardly from oriented closed theories to theories with closed and open strings, orientable or nonorientable.

Chapter 4

Non-Equilibrium Strings and the Keldysh Rotation

4.1. Introduction

In our previous chapter, to which this chapter is a sequel, we studied the structure of the large-N expansion of non-equilibrium systems with matrix degrees of freedom using the Schwinger-Keldysh formalism, and its dual description in terms of strings. The goal of [7] was to use this duality to identify some of the first elements of the universal calculus for non-equilibrium string perturbation theory.

We limited our attention in [7] to the "forward-backward" (henceforth referred to as "$\pm$") representation of the Schwinger-Keldysh formalism: The system is evolved along an oriented closed time contour $\mathscr{C}$, which consists of a forward component C_+ evolving from an early time t_0 to a late time $t_\wedge$, followed by the backward component C_- going back from $t_\wedge$ to t_0. This leads to a doubling of fields as functions of the single coordinate time t: For each field ϕ, we denote by $\phi_+(t)$ the values of ϕ on C_+, and by $\phi_-(t)$ the values of ϕ on C_-.

It is well known (see for example [67, 58, 64, 90, 91]) that many important physical features of the Schwinger-Keldysh formalism for non-equilibrium systems are revealed in a different representation, involving a simple but very useful field redefinition. Instead of the $\phi_\pm$ fields, this representation uses their sum and difference,

$$\phi_{\text{cl}} \;=\; \frac{1}{2}(\phi_+ + \phi_-), \tag{4.1}$$

$$\phi_{\text{qu}} \;=\; \phi_+ - \phi_-. \tag{4.2}$$

The variables ϕ_{cl} and ϕ_{qu} are often referred to as "classical" and "quantum" [64, 90, 91], even though they of course both represent fluctuating fields. This field redefinition is usually referred to as the "Keldysh rotation," since its idea goes back to [6]. It leads to remarkable simplifications. First, in the $\pm$ formalism, there are four nonzero propagators $G_{\pm\pm}$ satisfying one sum-rule identity

$$G_{++} + G_{--} = G_{+-} + G_{-+}. \tag{4.3}$$

The implications of this identity are often obscure in individual Feynman diagrams. After the Keldysh rotation, only three propagators are nonzero:

$$\langle \phi_{\mathrm{qu}}(t')\, \phi_{\mathrm{cl}}(t)\rangle_0 \equiv G_A(t', t), \tag{4.4}$$

$$\langle \phi_{\mathrm{cl}}(t')\, \phi_{\mathrm{qu}}(t)\rangle_0 \equiv G_R(t', t), \tag{4.5}$$

$$\langle \phi_{\mathrm{cl}}(t')\, \phi_{\mathrm{cl}}(t)\rangle_0 \equiv G_K(t', t), \tag{4.6}$$

$$\langle \phi_{\mathrm{qu}}(t')\, \phi_{\mathrm{qu}}(t)\rangle_0 \equiv 0. \tag{4.7}$$

Thus, in the Keldysh-rotated basis, the sum rule equivalent to (4.3) is automatically satisfied, reducing the number of diagrams that need to be summed. The second – and physically more important – simplification is that in the Keldysh basis, the information about the dynamics and the information about the state have been decoupled from each other: The mixed propagators G_A and G_R are state-independent, and the entire information about the state is carried by G_K. In contrast, in the $\pm$ formalism all four propagators $G_{\pm\pm}$ are sensitive to both the dynamics and the state. These features of the Keldysh formalism make not only practical calculations more efficient, but also the physical picture more direct and easier to interpret.

To illustrate this well-known usefulness of the Keldysh rotation, consider the example of a relativistic scalar field of mass m in thermal equilibrium at temperature T. In the $\pm$ formalism, the momentum-space propagators (in the mostly-minus spacetime metric signature) are

$$G_{++}(p) = \frac{i}{p^2 - m^2 + i\epsilon} + 2\pi\, n_{\mathrm{B}}(|p^0|)\, \delta(p^2 - m^2),$$

$$G_{--}(p) = \frac{-i}{p^2 - m^2 - i\epsilon} + 2\pi\, n_{\mathrm{B}}(|p^0|)\, \delta(p^2 - m^2),$$

$$G_{+-}(p) = 2\pi\left[\theta(-p^0) + n_{\mathrm{B}}(|p^0|)\right] \delta(p^2 - m^2),$$

$$G_{-+}(p) = 2\pi\left[\theta(p^0) + n_{\mathrm{B}}(|p^0|)\right] \delta(p^2 - m^2),$$

where

$$n_{\mathrm{B}}(\omega) = \frac{1}{\exp(\omega/T) - 1} \tag{4.8}$$

is the Bose-Einstein distribution function. After the Keldysh rotation, we get just three nonzero propagators,

$$\langle \phi_{\mathrm{qu}}\, \phi_{\mathrm{cl}}\rangle_0 = \frac{i}{p^2 - m^2 + i\,\mathrm{sign}(p^0)\epsilon} \equiv G_A(p), \tag{4.9}$$

$$\langle \phi_{\mathrm{cl}}\, \phi_{\mathrm{qu}}\rangle_0 = \frac{i}{p^2 - m^2 - i\,\mathrm{sign}(p^0)\epsilon} \equiv G_R(p), \tag{4.10}$$

$$\langle \phi_{\mathrm{cl}}\, \phi_{\mathrm{cl}}\rangle_0 = 2\pi\left[\tfrac{1}{2} + n_{\mathrm{B}}(|p^0|)\right] \delta(p^2 - m^2) = \pi \coth\left(\frac{|p^0|}{2T}\right) \delta(p^2 - m^2) \equiv G_K(p). \tag{4.11}$$

As promised, the quantum-to-quantum propagator vanishes identically, the mixed propagators become the advanced and retarded propagators G_A and G_R which only know about the dynamics but not about the state, and all the information about the initial density matrix is stored in the classical-to-classical propagator G_K.

The Keldysh rotation also has a number of closely related cousins, which appear across a multitude of diverse areas of physics, always with similar simplifying results. In the Larkin-Ovchinnikov representation [92], popular in non-equilibrium condensed matter [58, 64], another unitary transformation is performed on the fields; the same three propagators appear, but the propagator 2×2 matrix is now upper triangular, with G_A and G_R on the diagonal, and G_K in the upper-right corner. In the closely related Langreth-Wilkins representation [93] (see [71] for a review), popularized by the influential lecture [94] and now wide-spread in use in non-equilibrium physics of mesoscopic systems [65], a non-unitary field transformation is performed such that the propagator matrix stays upper triangular as in the Larkin-Ovchinnikov representation, but with the G_K propagator replaced by $G^<$. The Keldysh rotation (4.1) and (4.2) also plays a prominent role in the theory of the decoherence functional of Gell-Mann and Hartle [95],[1] which is instrumental in the description of the quantum-to-classical transition in the sum-over-histories approach to quantum systems, including those involving the dynamical spacetime geometries of quantum gravity and cosmology. In this chapter, we will concentrate on the original Keldysh rotation in its original context, but we expect that our results can be extended straightforwardly to such closely related cases as well.

In [7], we used the $\pm$ version of the Schwinger-Keldysh formalism to derive some universal implications of the large-N expansion for the dual string theory. We found that, in comparison to strings at equilibrium, the string perturbation expansion is further refined, with each worldsheet Σ subdivided into a triple decomposition,

$$\Sigma = \Sigma^+ \cup \Sigma^\wedge \cup \Sigma^-. \tag{4.12}$$

Here the forward part Σ^+ is associated with the forward part C_+ of the time contour, and similarly for the backward part Σ^- and C_-. The "end of time" wedge region $\Sigma^\wedge$ is associated with the meeting point of C_+ and C_- at $t_\wedge$, and it provides a bridge between Σ^+ and Σ^-. Remarkably, each of the three parts of this triple decomposition of Σ has its own associated genus expansion.

In view of the importance of the Keldysh-rotated version of the Schwinger-Keldysh formalism, in this chapter we extend our analysis of the large-N expansion and string theory to this Keldysh-rotated case. Our results were briefly announced in [98], which also contains a brief summary of the results of [7] in the $\pm$ formalism. Here we provide our detailed arguments and proofs justifying the statements announced in [98], and we also present additional results not advertised in [98]. Our analysis of the large-N expansion again reveals an intriguing refinement of string worldsheet diagrams. This time, however, the subdivision of worldsheets is not into the tree parts as observed in the $\pm$ formalism – instead, we will

---

[1]In this context, the rotation acts on two alternative histories $\phi_+(t)$ and $\phi_-(t)$ of the system that enter the decoherence functional; see also [96, 97] for the earlier and closely related concept of an influence functional.

find a subdivision distinct from (4.12):

$$\Sigma = \Sigma^{\text{cl}} \cup \Sigma^{\text{qu}}, \tag{4.13}$$

with the worldsheet Σ composed of a "classical" part Σ^{cl}, and its "quantum embellishments" Σ^{qu}. Each of the two parts of Σ is again associated with its own genus expansion.

The resulting picture of non-equilibrium string perturbation theory that emerges in the Keldysh-rotated formalism is by no means a straightforward consequence of the worldsheet picture established in [7] in the $\pm$ formalism based on the triple decomposition (4.12). This is not entirely unexpected: Whereas in the language of the original matrix degrees of freedom, the Keldysh rotation is a rather simple change of variables, the worldsheet dual theories before and after the rotation should not be related in any simple way, for the following reason. On the side of the matrix degrees of freedom, the Keldysh rotation mixes the values of M on the forward and backward branches C_+ and C_- of the time contour for the same value of t. The simplicity of this mixing relies crucially on the existence of a canonical identification of the time evolution parameter t along C_+ and C_-. In contrast, things are not this simple on the worldsheets: Even in the absence of knowing any details of the worldsheet dynamics, we anticipate some form of worldsheet diffeomorphism invariance, which makes any identification of the worldsheet time coordinate τ on Σ^+ and Σ^- non-canonical at best, and impossible globally if Σ^+ and Σ^- are of different topology (which they typically are). The worldsheet representations before and after the Keldysh rotation will be related by a complicated resummation of many ribbon diagrams, and for these reasons, we do not anticipate any simple procedure for deriving one worldsheet picture from the other. This is indeed the perspective supported by the main results of this chapter.

4.2. Large-N expansion after the Keldysh rotation

As in [7], we start with a theory of $N \times N$ Hermitian matrix degrees of freedom $M^a{}_b(t, \ldots)$, which may be spacetime fields, or just quantum mechanical degrees of freedom; we only display the dependence on time, with the dependence on space and possible other quantum numbers playing only a spectator role in our arguments and therefore kept implicit. In this way, our results will be universal, in particular independent of whether the theory is relativistic or not. We further assume that the theory has an $SU(N)$ symmetry, and that the original action of the theory takes the single-trace form,

$$S(M) = \frac{1}{g^2} \int dt \, \text{Tr} \left(\dot{M}^2 + M^3 + M^4 + \ldots \right). \tag{4.14}$$

We studied this theory on the Schwinger-Keldysh time contour $\mathscr{C}$ in detail in Section 2 of [7], and analyzed its large-N expansion with the fixed 't Hooft coupling $\lambda \equiv g^2 N$, using the $\pm$ formalism.[2] In the $\pm$ formalism, $M(t)$ becomes doubled to $M_\pm(t)$, and the action is

---

[2]As in [7], it would be easy to generalize all our arguments to the case of more than one independent 't Hooft coupling, controlling different interaction terms in $S(M)$. We concentrate on one λ for simplicity. Also, as in [7], we keep the dependence on spatial coordinates and spatial derivatives in the action implicit.

formally of the form

$$S_{\mathrm{SK}}(M_\pm) = S(M_+) - S(M_-), \tag{4.15}$$

which needs to be augmented by the appropriate boundary conditions: the correct rules at the meeting point $t_\wedge$ between the two branches of $\mathscr{C}$, and the information about the initial state at t_0 if different from the vacuum.

Now we perform the Keldysh rotation of the fields: As in (4.1) and (4.2), we define M_{cl} and M_{qu}. Each of these fields continues to carry the adjoint representation of our symmetry group. In order to avoid notational clutter and too many subscripts and superscripts, we will use M to denote the "classical" matrix field M_{cl},

$$M(t) = \frac{1}{2}\left(M_+(t) + M_-(t)\right), \tag{4.16}$$

and $\mathscr{M}$ to denote the "quantum" matrix field M_{qu}:

$$\mathscr{M}(t) = M_+(t) - M_-(t). \tag{4.17}$$

After the Keldysh rotation, the action S_{SK} becomes

$$S_{\mathrm{SK}} = \frac{1}{g^2} \int dt\, \mathrm{Tr}\left(K(M,\mathscr{M}) + 3\, M^2 \mathscr{M} + \frac{1}{4}\mathscr{M}^3 + 4\, M^3 \mathscr{M} + M\mathscr{M}^3 + \dots\right). \tag{4.18}$$

The structure of the quadratic kinetic term $K(M,\mathscr{M})$ is such that it gives the three propagators that we discussed in Section 4.1, as we will see again when we look at the Feynman rules below. This form of the action would naturally generalize if we added higher polynomial interactions to $S(M)$, or allowed independent couplings to control different terms in $S(M)$. Note, however, that the number of $\mathscr{M}$'s in each monomial interaction term in (4.18) will always be odd.

Feynman rules for the ribbon diagrams after Keldysh rotation

Feynman rules for the ribbon diagrams after the Keldysh rotation are as follows. The quadratic kinetic term $K(M,\mathscr{M})$ in (4.18) yields three propagators,[3]

$$\begin{array}{cc} \substack{a \\ b} \quad = \quad \substack{d \\ c} \end{array} \quad = \quad \langle M^a{}_b \, \mathscr{M}^c{}_d \rangle_0, \tag{4.19}$$

$$\begin{array}{cc} \substack{a \\ b} \quad \quad \substack{d \\ c} \end{array} \quad = \quad \langle \mathscr{M}^a{}_b \, M^c{}_d \rangle_0, \tag{4.20}$$

$$\begin{array}{cc} \substack{a \\ b} \quad \quad \substack{d \\ c} \end{array} \quad = \quad \langle M^a{}_b \, M^c{}_d \rangle_0. \tag{4.21}$$

We use the notation popular in the non-equilibrium field theory literature (see, *e.g.*, [64]): The dotted line denotes the "quantum" end of a propagator, and the full line denotes the "classical" end. Here we have just extended this convention to ribbons.

---

[3]In our notation, we use the subscript "0" in $\langle \dots \rangle_0$ to distinguish the bare propagators from the full 2-point functions $\langle \dots \rangle$ which we will be studying below.

The vertices are

$$= \quad \frac{N}{\lambda}(\dots), \qquad (4.22)$$

$$= \quad \frac{N}{\lambda}(\dots) \qquad (4.23)$$

at three points, and

$$= \quad \frac{N}{\lambda}(\dots), \qquad (4.24)$$

$$= \quad \frac{N}{\lambda}(\dots), \qquad (4.25)$$

$$\vdots$$

at four points. As in [7], the vertical dots at the end of this list stand for higher n-point vertices, which we allow to be present for full generality, but do not depict explicitly. Note that they all have to satisfy one restriction: The number of quantum ends at each vertex always has to be odd, a feature that follows from the general structure of (4.18).

The precise numerical values of the vertices can be easily extracted from (4.18) (or appropriate generalizations thereof). The horizontal dots "$(\dots)$" on the right-hand sides of (4.22-4.25) refer to all the group-theory as well as momentum- and frequency-dependent factors which do not depend on N and λ; their details are unimportant for our arguments. The only important fact for our analysis is that all the vertices are proportional to N when λ is held fixed. Similarly, in that regime, all the propagators (4.19)-(4.21) are proportional to $1/N$.

We summarize the rules for building consistent Feynman diagrams:

- Quantum ends of propagators are attached to quantum ends of vertices;

- Classical ends of propagators are attached to classical ends of vertices;

- The following rule is a simple consequence of causality: If there is a closed loop consisting of a sequence of only G_A (or only G_R) propagators, the diagram is identically zero

and will be systematically ignored.[4] Note that in order for the diagram to be identically zero, the closed loop in question does *not* have to surround just one plaquette.

Signpost notation for the Feynman diagrams

Before we proceed to the analysis of the large-N expansion, we find it convenient to introduce a slightly different graphical notation for the non-equilibrium Feynman diagrams, which will simplify the look of the diagrams and allow us to develop some useful intupdflateition. This new notation will also simplify our proofs and other arguments below.

Recall that in the $\pm$ formalism, it was very convenient that the ribbon diagrams looked just like those in equilibrium, with all the additional information carried solely by the vertices: Each vertex was labeled by a sign choice $\pm$. The type of propagator connecting two given vertices was then uniquely determined by the signs at the vertices. At first glance, the Feynman rules after the Keldysh rotation do not share the same simplicity. We will develop a more useful prescription in several simple steps. First, it is rather awkward to deal with dotted versus undotted halves of propagators – we will encode the same information by using regular undotted lines for all the ribbon edges, but placing a "bulk arrow" in the middle of the ribbon propagator pointing in the direction from the quantum end to the classical end of the propagator. The classical-to-classical propagators G_K do not get any "bulk arrow" mark. In the next step, one can pull each arrow from the middle of the propagator to the quantum end of the propagator, and associate this arrow with the adjacent vertex instead. In this way, each vertex is uniquely assigned a collection of arrows rooted at the vertex and pointing in the directions of various attached propagators. This collection of arrows rooted at the same vertex is reminiscent of a signpost at trail intersections. For the lack of a better term, from now on we will refer to this collection of arrows at a given vertex as a "signpost", and this notation as the "signpost notation".[5]

---

[4]Strictly speaking, such diagrams are not illegal, but since they identically vanish, leaving them systematically out will significantly reduce the number of diagrams that need to be drawn for any process. Also, we do not expect that such diagrams should be independently reproduced on the string-theory side of the duality between the large-N theory and string theory.

[5]A somewhat similar notation, using arrows to indicate the G_A and G_R propagators, has been used in the literature (for example see [67]). The novelty of our signpost notation is that we assign the arrows to the vertices, not the propagators. Note also the different status of the edge arrows reflecting the $SU(N)$ group structure, and the signpost arrows reflecting the non-equilibrium ingredients in our diagrams: We often indicate graphically only one edge arrow per each closed edge loop or each open edge segment in a given diagram, and do not put edge arrows on all individual propagators, to avoid notational clutter in the figures. On the other hand, the location and direction of each signpost arrow carries important information and such arrows cannot be conveniently left out.

In this new signpost notation, our three-point vertices (4.22, 4.23) look as follows,

$$\text{(4.26)}$$

$$\text{(4.27)}$$

$$\text{(4.28)}$$

while the four-point vertices (4.24, 4.25) are

$$\text{(4.29)}$$

$$\text{(4.30)}$$

$$\vdots \qquad .$$

Note that the propagators do not require any additional notation – each propagator is uniquely determined by the two signposts at the vertices it connects. The rules for building consistent diagrams can now be rewritten solely as restrictions on the signposts allowed at the vertices of the ribbon diagrams:

- At each vertex, the signpost carries an odd number of arrows, each pointing into a distinct propagator.

- The signposts are such that each propagator can have at most one arrow pointing into it from the adjacent vertices.

- Starting from any vertex, follow the signpost instructions: Follow any of the adjacent propagators which has an arrow pointing into it; repeat this process at each vertex you visit. If after n such steps you return to the vertex you started from, the diagram is identically zero and will be systematically omitted. (See an example in Fig. 4.1.) This rule is the rephrasing of the analogous rule we encoutered above in the original notation.

It will be useful to formalize the prescription for traveling along a ribbon diagram Δ in the direction of the arrows, as follows: We define an *admissible path* on Δ from a vertex
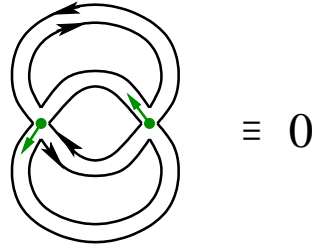
Figure 4.1: An example of a signpost ribbon diagram which vanishes identically. Note that in this example, the closed path made of G_A propagators that makes this diagram vanish is not surrounding just one plaquette.

v_1 to another vertex v_2 to be a collection of consecutive propagators and vertices, obtained by starting at v_1, choosing an arrow from the signpost at v_1, moving in the direction of this chosen arrow along the attached propagator to the next vertex, and repeating the steps at each signpost encountered along the way, until we reach v_2. As a consequence of this definition, there is always at least one admissible path going through any given vertex of Δ. Also, for any pair v_1, v_2 of vertices, there might be one or more distinct admissible paths connecting them, or none at all.

All vacuum diagrams vanish identically

To practice the use of our new notation and to show its efficiency, we will now prove that all vacuum diagrams are zero. Begin at any vertex, and imagine being a traveler who follows the arrows at all signposts, *i.e.*, travels along an *admissible path* as defined above. Since the number of arrows at each vertex is odd, there is at least one arrow at your original location. Follow that arrow, and repeat the step at each new vertex you visit. Again, since there is at least one arrow at each vertex, this procedure makes sense at each step. If after a finite number of steps you return to a vertex you already visited, by our rules the diagram is declared to be zero identically. Since for a vacuum diagram, there are no external legs at which you could end up after a finite number of steps, to prevent the diagram from being zero you would have to travel forever, visiting an infinite number of new vertices. Since in our analysis we only consider Feynman diagrams with a finite number of vertices, this concludes the proof.

Thus, we reach our first conclusion about the universal structure of non-equilibrium string perturbation theory in the Keldysh-rotated form:

$$\mathcal{Z} = \sum_{h=0}^{\infty} \left(\frac{1}{N}\right)^{2h-2} \mathcal{F}_h(\lambda, \ldots) = 0; \tag{4.31}$$

the sum of all the 0-point diagrams vanishes identically.[6] This is an example of the effi-

---

[6] Note that as in [7] and [98], we continue denoting the sum over all *connected* ribbon diagrams by $\mathcal{Z}$.

ciency of the Keldysh-rotated formalism, which must be reproduced by any candidate for the description of the worldsheet dynamics of the string.

4.3. Large N and string worldsheets: Classical and quantum surfaces

We are now ready to demonstrate that for each ribbon diagram Δ in the Keldysh-rotated formalism, its associated Riemann surface $\Sigma(\Delta)$ can be naturally decomposed into a classical part Σ^{cl} plus its quantum "embellishment" part Σ^{qu}. This will be done in two steps: First, we define for each diagram its "classical foundation" $\widehat{\Sigma}^{\text{cl}}$: a surface whose topology is generally simpler (or at least not more complicated) than that of Σ. The full surface Σ is then obtained by replacing a collection of non-overlapping disks on $\widehat{\Sigma}^{\text{qu}}$ with the quantum "embellishments". However, since we have just shown that all vacuum diagrams vanish, we cannot use vacuum diagrams to illustrate our arguments as we did in the $\pm$ representation [7] – we will need n-point correlation functions.

Adding external sources

In what follows, we mostly concentrate for simplicity on diagrams which contribute to the two-point correlator of $\mathscr{M}$ and M,

$$\langle \mathscr{M}^a{}_b M^c{}_d \rangle = \langle \mathscr{M}^a{}_b M^c{}_d \rangle_0 + \dots, \tag{4.32}$$

an equation represented graphically as follows,

$$\tag{4.33}$$

where the "..." denote all the loop corrections. In fact, in order to eliminate the loose indices at the ends of the propagators, it will be better to couple $M^a{}_b$ and $\mathscr{M}^a{}_b$ to their conjugate sources, $J^b{}_a$ and $\mathscr{J}^b{}_a$, and encode the two-point function (and all higher n-point functions) in $SU(N)$ singlets such as

$$J^b{}_a \langle \mathscr{M}^a{}_b M^c{}_d \rangle \mathscr{J}^d{}_c. \tag{4.34}$$

Note that it is the *classical* source J that couples to the *quantum* field $\mathscr{M}$, and the *quantum* source $\mathscr{J}$ to the *classical* field M. This follows from the fact that in the $\pm$ formalism, the coupling to sources adds the following term to the full action (4.15),

$$\int dt \, \text{Tr} \left(J_+ M_+ - J_- M_- \right). \tag{4.35}$$

As usual, the sum $\mathscr{Z}$ over *all* diagrams, connected or not, is related to $\mathcal{Z}$ by $\mathcal{Z} = \log \mathscr{Z}$.

With the standard definitions

$$
\begin{aligned}
J_{\text{cl}} &\equiv J = \frac{1}{2}(J_+ + J_-), \\
J_{\text{qu}} &\equiv \mathscr{J} = J_+ - J_-,
\end{aligned}
\tag{4.36}
$$

the coupling in (4.35) indeed adds to the Keldysh-rotated action (4.18) the following source term,

$$
\int dt \, \text{Tr} \, (J\mathscr{M} + \mathscr{J} M).
$$

In our ribbon diagrams, we will graphically denote the external sources as follows,

$$
J : \qquad J \; \text{} \quad ,
$$

$$
\mathscr{J} : \qquad \mathscr{J} \; \text{} \quad .
$$

Using this notation, the expression in (4.34) is graphically represented by

$$
J \; \text{} \; \mathscr{J}.
\tag{4.37}
$$

On the string dual side, the insertions of the singlets $J\mathscr{M}$ and $\mathscr{J} M$ will correspond to marked points on the surface Σ.

In the full theory, one is more appropriately interested in correlation functions of n local composite operators $\mathcal{O}_i(M, \mathscr{M})$ (with $i = 1, \ldots, n$) that are *singlets* of the $SU(N)$ symmetry. It is such operators that can be expected to be associated with simple local vertex-operator insertions on the worldsheets in the dual string theory. The sources J and $\mathscr{J}$ that we use to form the singlets $J\mathscr{M}$ and $\mathscr{J} M$ can be simply seen as placeholders for the insertions of such more complicated singlet operators $\mathcal{O}_i$, and we use them solely for the convenience of our presentation.

Reduction of Σ to its classical foundation $\widehat{\Sigma}^{\text{cl}}$

Each ribbon diagram Δ can be associated with a unique surface Σ, constructed by simply forgetting the non-equilibrium signposts at the vertices and following the prescription for Σ that worked in equilibrium. Restoring the signposts will then equip Σ with some additional structure, and we expect the topological sum over surfaces of genus h to be correspondingly refined.

How do we identify the refined structure that is naturally induced on Σ by the restoration of the non-equilibrium data? There is one physically well-motivated decomposition of each non-equilibrium ribbon diagram Δ, which induces a natural decomposition of Σ. Recall first that the information about the *state* is carried by the Keldysh propagators G_K, but not the G_A and G_R propagators and the vertices. It is then natural to define an operation which acts on a ribbon diagram Δ by "forgetting" the G_K propagators: Erasing all the G_K propagators

from a ribbon diagram should leave a subdiagram $\widehat{\Delta}$, in which the information about the state of the system has been erased. Note that since every vertex of Δ has at least one arrow at its signpost, no vertices are erased in the process of ddforming $\widehat{\Delta}$. Some of the vertices of $\widehat{\Delta}$ will have fewer attached legs than their counterparts in Δ. In particular, some vertices in the reduced diagram $\widehat{\Delta}$ might become "1-vertices" or "2-vertices," but each vertex still has at least one propagator attached to it. Even to such generalized diagrams, one can still apply the standard process of constructing an associated compact surface without boundaries (by gluing in a disk to fill each closed loop). We will denote this surface by $\widehat{\Sigma}^{\mathrm{cl}}$ and refer to as the "classical foundation" of Σ. By design, the expectation is that even on the string side, the classical foundation $\widehat{\Sigma}^{\mathrm{cl}}$ should be encoding the information about the dynamics but not about the state of the original system.

Note that $\widehat{\Sigma}^{\mathrm{cl}}$ is either topologically simpler than Σ, or at most topologically equivalent to Σ. In technical terms, the increasing topological complexity of surfaces is measured by the decreasing value of their Euler number. It turns out that the Euler number of the classical foundation $\widehat{\Sigma}^{\mathrm{cl}}$ is always greater than or equal to the Euler number of Σ. We postpone the proof of this statement until Section 4.3, after we define more precisely the decomposition of Σ into its classical and quantum part.

Topology of the classical foundation $\widehat{\Sigma}^{\mathrm{cl}}$

First, we will show that the classical foundations $\widehat{\Sigma}^{\mathrm{cl}}$ that emerge from consistent diagrams can be arbitrarily topologically complicated, as two-dimensional orientable surfaces without boundaries. Since such two-dimensional surfaces are topologically classified by their non-negative integer genus n, we need to show that $\widehat{\Sigma}^{\mathrm{cl}}$ for all possible n arise from consistent ribbon diagrams. We will prove this statement by constructing a sequence of ribbon diagrams which contain no G_K propagators, implying that their associated surface Σ is identical to its classical foundation, $\widehat{\Sigma}^{\mathrm{cl}} = \Sigma$, and with Σ of arbitrarily high genus. We will illustrate this on the two-point functions with the $J\mathscr{J}$ external source insertions.

First, consider the diagram in Fig. 4.2. It is planar, contains only G_A and G_R propagators, and $\Sigma = \widehat{\Sigma}^{\mathrm{cl}}$ is a two-sphere. Following the cutting and re-gluing procedure on the two indicated propagators as described in Fig. 4.2 gives Σ which is a two-torus, again isomorphic to $\widehat{\Sigma}^{\mathrm{cl}}$.

In the next step, we iterate this procedure to form any higher genus surface Σ, again isomorphic to its classical foundation $\widehat{\Sigma}^{\mathrm{cl}}$: Starting with the planar ladder diagram with $2n+1$ rungs as indicated in Fig. 4.3, we cut the $2n$ indicated rungs, and re-glue them in the opposite order. Counting the number of plaquettes, propagators and vertices of the resulting non-planar diagram demonstrates that its associated surface is of genus n. Since there were no G_K propagators involved, the classical foundation $\widehat{\Sigma}^{\mathrm{cl}}$ is isomorphic to Σ, and therefore also of genus n.

Decomposition of Σ into its classical and quantum parts $\Sigma^{\mathbf{cl}}$ and $\Sigma^{\mathbf{qu}}$

When we restore the G_K propagators in a given ribbon diagram Δ, we reconstruct the full surface Σ from the classical foundation $\widehat{\Sigma}^{\mathrm{cl}}$. This process defines a decomposition of the original surface Σ into its quantum and classical parts, which we denote by Σ^{cl} and Σ^{qu}. Both Σ^{cl} and Σ^{qu} will be two-dimensional surfaces whose boundaries consist of a collection of S^1, along which Σ^{cl} and Σ^{qu} are glued together. The classical foundation $\widehat{\Sigma}^{\mathrm{cl}}$ is then related to Σ^{cl} simply by gluing in disks into each boundary component of Σ^{cl}. For an algorithmic definition of this decomposition of Σ for any given ribbon diagram Δ, we now refer to a more precise combinatorial description.

Combinatorial picture of $\widehat{\Sigma}^{\mathbf{cl}}$, $\Sigma^{\mathbf{cl}}$ and $\Sigma^{\mathbf{qu}}$

Begin with a ribbon diagram Δ in the Keldysh-rotated formalism. The collection of vertices, propagators and closed loops (which we refer to as "plaquettes") in Δ provides a simplicial decomposition of the associated surface Σ. We subdivide this combinatorial data associated with Δ as follows:

- All vertices belong to Σ^{cl}.

- All G_A and G_R propagators belong to Σ^{cl}.

- All plaquettes that have no adjacent G_K propagators belong to Σ^{cl}.

- All G_K propagators belong to Σ^{qu}.

- All plaquettes with at least one adjacent G_K propagator belong to Σ^{qu}.

This assigns each building block of the cellular decomposition of Σ to either Σ^{cl} or Σ^{qu}. (Perhaps the only exception is the treatment of the external source insertions, to which we return in Section 4.3.) What is less clear is that Σ^{cl} and Σ^{qu} can be naturally interpreted as smooth surfaces, connected to each other along a common boundary which is topologically

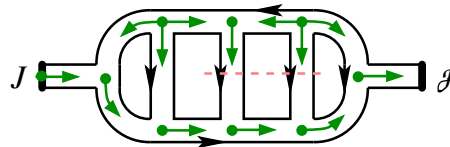Figure 4.2: An example of a ribbon diagram without any G_K propagators; thus, the associated surface Σ has no quantum embellishments, and $\widehat{\Sigma}^{\mathrm{cl}} = \Sigma$, the two-pointed sphere. Cutting the two propagators inside this diagram across the indicated dashed line, and re-gluing them in the opposite order, turns $\Sigma = \Sigma^{\mathrm{cl}}$ into a two-pointed torus.
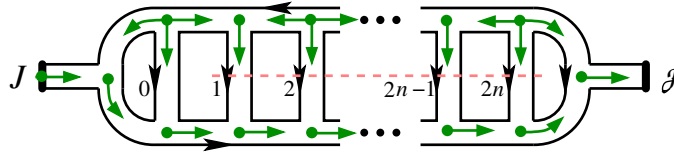
Figure 4.3: A construction that yields a higher-genus Σ with no quantum embellishments. Starting from this planar diagram, cut the propagators labeled 1 to $2n$ across, along the indicated dashed line, and re-glue them in the opposite order: 1 to $2n$, 2 to $2n-1$, ..., $2n$ to 1. This gives a ribbon diagram associated with $\Sigma = \Sigma^{\mathrm{cl}}$ of genus n.

just a collection of S^1's. That it is indeed so can be demonstrated by an equivalent definition of the decomposition of Σ into Σ^{cl} and Σ^{qu}, which works plaquette-by-plaquette, and follows a similar plaquette-by-plaquette definition of the triple decomposition of Σ in terms of the widened cuts in the $\pm$ formalism studied in detail in [7, 98].

Plaquette-by-plaquette construction of a smooth Σ^{qu}

Begin by placing a transverse line segment across the middle of each G_K propagator, and widen this cut into a segment of a two-dimensional ribbon. Inside each plaquette, connect all such line segments entering the plaquette to the marked center inside the plaquette. Widening the resulting graph gives a unique portion of a smooth surface with boundaries inside the plauqette, a portion which connects smoothly to other such portions of a smooth surface with boundaries across each adjacent G_K propagator (see Fig. 4.4 for illustrations). Their union thus defines a smooth surface with a smooth boundary consisting of a number of S^1's. It is easy to see that this surface is topologically canonically equivalent to our Σ^{qu} as defined combinatorially above.

Another natural perspective on the plaquette-by-plaquette construction is obtained when we switch from the original ribbon diagram Δ to its dual ribbon diagram $\Delta^\star$. (We reviewed this duality of ribbon diagrams in Section 2.8 of [7], and used it there to study the triple decomposition of Σ in the $\pm$ formalism.) In this dual picture, the widened cut across each G_K propagator in Δ represents a certain ribbon propagator of $\Delta^\star$, and their connection to the marked center inside a plaquette with at least one adjacent G_K propagator represents a vertex in $\Delta^\star$. The collection of all such propagators and vertices of $\Delta^\star$ that have been assigned to Σ^{qu} thus represents a ribbon subdiagram in $\Delta^\star$, and therefore has a natural interpretation as a topologically smooth surface with boundaries. This surface is precisely the surface Σ^{qu} that we obtained from the plaquette-by-plaquette prescription.

Given our combinatorial definition of Σ^{cl} and Σ^{qu}, it is natural to define the following combinatorial Euler numbers associated with the combinatorial ingredients defining the decomposition,

$$\chi_{\mathrm{cl}}(\Delta) = V - P_{\mathrm{cl}} + L_{\mathrm{cl}}, \qquad \chi_{\mathrm{qu}}(\Delta) = -P_{\mathrm{qu}} + L_{\mathrm{qu}}. \tag{4.38}$$
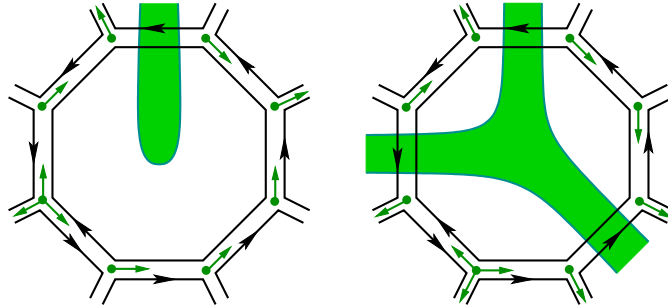
Figure 4.4: Two examples illustrating the direct plaquette-by-plaquette construction of Σ^{qu} as a surface with smooth boundaries. For those readers viewing this figure in color, the portions of Σ^{qu} so constructed are denoted in green.

Here V is the number of vertices in Δ, P_{qu} the number of its Keldysh propagators, $P_{\mathrm{cl}} = P - P_{\mathrm{qu}}$ the number of its non-Keldysh propagators, P_{cl} the number of plaquettes with no adjacent G_K propagators, and P_{qu} the number of the plaquettes with at least one G_K propagator. By repeating the steps used in the $\pm$ formalism in [7], it is straightforward to show that these combinatorial Euler numbers reproduce the Euler characteristics of the smooth surfaces Σ^{cl} and Σ^{qu},

$$\chi_{\mathrm{cl}}(\Delta) = \chi(\Sigma^{\mathrm{cl}}), \qquad \chi_{\mathrm{qu}}(\Delta) = \chi(\Sigma^{\mathrm{qu}}). \tag{4.39}$$

The sum of the two is of course the Euler number of Σ, simply given in terms of the number of handles h as $\chi(\Sigma) = 2 - 2h$.

We can now return to the statement we made in Section 4.3, that the topology of the classical foundation $\widehat{\Sigma}^{\mathrm{cl}}$ is simpler than that of the full surface Σ. The notion of "topological simplicity" of a surface Σ is quantified by the Euler number $\chi(\Sigma)$: The simpler the topology of the surface, the greater its Euler number. We wish to show that

$$\chi(\widehat{\Sigma}^{\mathrm{cl}}) \geq \chi(\Sigma). \tag{4.40}$$

The proof is now simple, because we can rely on the features of the decomposition of each Σ as $\Sigma^{\mathrm{cl}} \cup \Sigma^{\mathrm{qu}}$. Consider the connected components of Σ^{qu}, one by one. Each such component has some number b of boundaries, $b \geq 1$, along which it connects to Σ^{cl}. Its Euler number is $\leq 2 - b$. Replace this connected component with b disks; the Euler number of the replacement is b. Since $b \geq 1$, the Euler number of the replacement is always greater than or equal to the Euler number of the original connected component of Σ^{qu}. By definition, the classical foundation $\widehat{\Sigma}^{\mathrm{cl}}$ is obtained from Σ by performing this replacement procedure with all connected components of Σ^{qu}. Using the additivity property of the Euler number, this demonstrates that the Euler number of $\widehat{\Sigma}^{\mathrm{cl}}$ must be greater than or equal to that of Σ, thus proving (4.40).
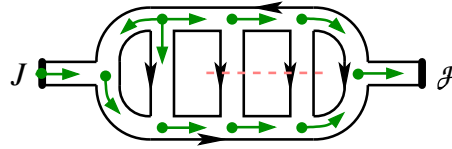
Figure 4.5: An example of a ribbon diagram with two G_K propagators, whose Σ is again a two-pointed sphere, and $\Sigma^{\mathrm{cl}} = \Sigma$. In this case, the quantum embellishment Σ^{qu} is a disk. Cutting the two indicated propagators along the dashed line and regluing them in the opposite order gives Σ which is a two-pointed torus, with Σ^{cl} a two-pointed sphere, and Σ^{qu} a torus with one boundary.
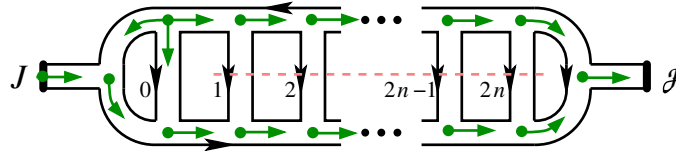
Figure 4.6: The construction of a surface with a higher-genus quantum embellishment Σ^{qu}. The indicated diagram gives Σ a two-pointed sphere, with Σ^{qu} a disk, just like in Fig. 4.5. Cutting propagators labeled 1 to $2n$ and regluing them back in the opposite order as in Fig. 4.3 yields Σ which is a two-pointed surface with n handles, $\widehat{\Sigma}^{\mathrm{cl}}$ a two-pointed sphere, and Σ^{qu} with n handles and one boundary.

Note that according to this definition of topological complexity of a surface, we find that the collection of n disconnected spheres is simpler than a collection of n' spheres if $n > n'$. This is a consequence of our definition of topological complexity that we can live with.

Topology of the quantum embellishments Σ^{qu}

In our next step, we show that arbitrarily complicated topologies of the quantum embellishment surfaces Σ^{qu} can appear from consistent ribbon diagrams. We will prove this statement by constructing a sequence of ribbon diagrams whose quantum embellishments Σ^{qu} are connected surfaces with one boundary and an arbitrarily high genus.

This constrction is illustrated in Figs. 4.5 and 4.6: First, we construct a surface whose classical foundation is an S^2 with two marked points at which the sources are inserted, and the quantum part Σ^{qu} is a torus with one boundary. Then we iterate this process, and construct a surface whose Σ^{qu} has any number of handles and one boundary.

Next we need to show that Σ^{qu} can have connected components with more than one boundary component. Examples of ribbon diagrams with this feature are easy to find if we consider higher $2n$-point correlation functions. Consider the diagram in Fig. 4.7, which contributes to the 4-point function with the external sources $J \mathcal{J} J \mathcal{J}$. This diagram is

connected and planar, therefore the surface Σ associated with it is the sphere (with four marked points corresponding to the insertions of the two J's and two $\mathscr{J}$'s.). Its Σ^{qu} is a cylinder, and this diagram thus shows that connected components of Σ^{qu} can have more than one boundary.

One can also use this 4-point function to find diagrams whose Σ^{qu} are connected, have two boundaries, and an arbitrary number h of handles: Simply replace the one G_K propagator in Fig. 4.7 by $2h + 1$ propagators, glue them to the bottom horizontal ribbon in the order from 1 to $2h + 1$, and to the top horizontal ribbon in the reverse order, from $2h + 1$ to 1. This resulting ribbon diagram will have $2h + 1$ propagators, and just one plaquette. Its Σ^{qu} is a connected surface with two boundaries and h handles.

This process can be easily extended to construct examples whose Σ^{qu} is connected and has more than two boundaries. One of the simplest ribbon diagrams whose Σ^{qu} is connected and with three boundaries is depicted in Fig. 4.8, and involves a 6-point function. (In fact, an even simpler ribbon diagram with the same properties would result from removing any one of the three G_K propagators in Fig. 4.8.) Clearly, by iterating this construction to $2b$-point functions, one easily obtains examples whose Σ^{qu} has b boundary components.

Is it necessary to go to such higher-point functions in order to find examples with connected components of Σ^{qu} having high numbers b of boundaries, or do such Σ^{qu} appear already in the 2-point function? The answer is that they do appear, but in order to find examples of ribbon diagrams that contribute to the 2-point function and whose Σ^{qu} has a connected component with more than one boundary, one must look a bit harder, to non-planar diagrams. Consider the diagram in Fig. 4.9. It has been designed such that it only has one G_K propagator. It leads to Σ^{qu} which has two boundary components. The process clearly iterates, and gives examples of Σ^{qu} which are connected and have an arbitrary number b of boundary components, even in the case of the 2-point function.

Locations of the external sources

Besides the internal number of vertices, propagators and closed loops, our Feynman diagrams inevitably contain a non-zero number of external source insertions. The external sources can be either classical J, or quantum $\mathscr{J}$. In order to complete the combinatorial rules proposed
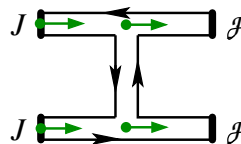
Figure 4.7: This diagram is planar, and Σ is an S^2 with four marked points. The classical foundation $\widehat{\Sigma}^{\mathrm{cl}}$ consists of two disconnected S^2's, each with two marked points. The quantum embellishment Σ^{qu} is a cylinder: Combinatorially, it is constructed from one G_K propagator and the one plaquette of this diagram, and has two boundaries.
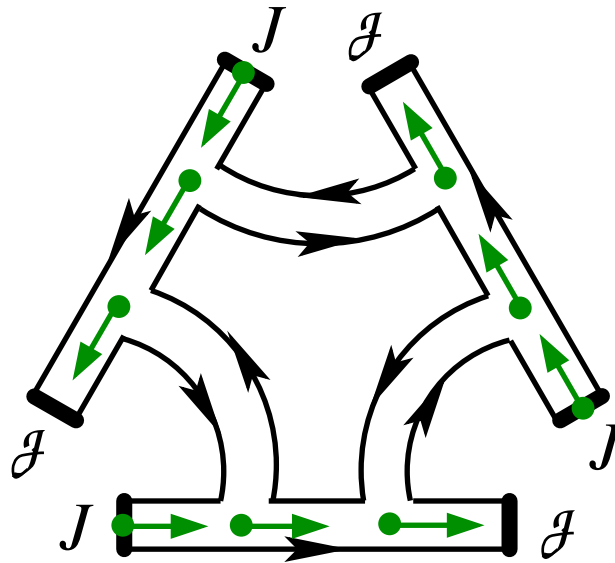
Figure 4.8: **(a):** This ribbon diagram is again planar and contributes to a 6-point function. **(b):** Its associated surface Σ is an S^2 with six marked points. $\widehat{\Sigma}^{\mathrm{cl}}$ consists of a collection of three S^2's with two marked points each, and Σ^{qu} is the "pair of pants" surface, with no handles and three boundary components.

in Section 4.3 to define the decomposition of Σ to Σ^{cl} and Σ^{qu}, we must decide how to assign the external sources to the two parts of this decomposition.

Since the classical source J can never be attached to the G_K propagator, it would appear natural to assign the insertion of J always to Σ^{cl}. With the quantum source $\mathscr{J}$, the story is not so clear: We can choose to assign it always to Σ^{qu}, or we can choose to assign it to either Σ^{qu} or Σ^{cl}, depending on whether it is attached to the G_K propagator or the G_A propagator. Which of these two choices, if any, is more natural?

Perhaps the most natural and elegant answer is to simply admit that the external source insertions are not a part of Σ, and therefore do not have to be assigned to either Σ^{cl} or Σ^{qu}. This picture is further supported by the fact that in critical string theory, the insertions of
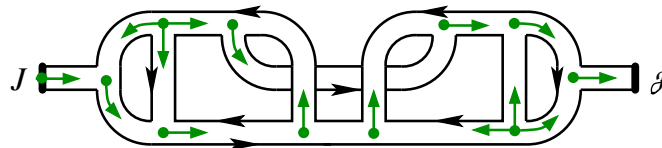
Figure 4.9: The construction of a surface Σ that contributes to the $J\langle \mathscr{M}\, M \rangle \mathscr{J}$ two-point function, and whose Σ^{qu} is a cylinder. Here $\Sigma = T^2$, and its classical foundation is $\widehat{\Sigma}^{\mathrm{cl}} = S^2$.

(a)   (b)

Figure 4.10: Illustration of a quantum source $\mathscr{J}$ attached to a G_K propagator, and its location on Σ. **(a):** This diagram is planar and Σ is a four-pointed sphere. One of the external quantum sources $\mathscr{J}$ is connected to a G_K propagator. **(b):** Following our rules for the plaquette-by-plaquette construction of Σ^{qu}, we find the decomposition of Σ depicted here, with one $\mathscr{J}$ isolated inside a disk component of Σ^{cl}.

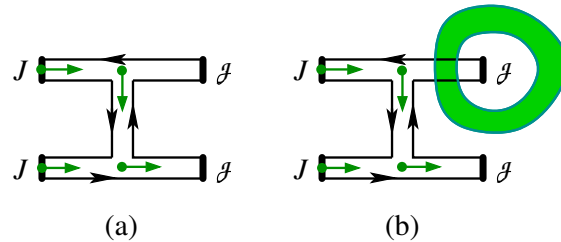the vertex operators correspond to the "punctures" in the Riemann surface, points which have been removed from Σ. This agrees with the observation that each such "puncture" contributes -1 to the Euler number $\chi(\Sigma)$: In the combinatorial picture, creating a puncture means removing a vertex in the cellular decomposition of Σ, resulting in the subtraction of 1 from the overall Euler number. On surfaces with complex structures (such as those in critical string theory in Euclidean worldsheet signature), a puncture can be viewed as an infinitesimally small boundary, and therefore contributes the same amount to $\chi(\Sigma)$. For Σ with h handles, b boundaries and n punctures, the Euler number is then

$$\chi(\Sigma) = 2 - 2h - b - n. \tag{4.41}$$

This is indeed the expression relevant for the counting of the powers of N in our large-N expansion.

Even if we agree not to consider the source insertions a part of Σ, a small ambiguity remains: How do we treat the plaquettes in the ribbon diagram, immediately surrounding the source insertions? To see a simple example of the possible ambiguity, consider Fig. 4.10. If we follow our plaquette-by-plaquette prescription, one of the quantum sources ends up surrounded by a small disk with no other source insertions, which by our rules is assigned to Σ^{cl}. This punctured disk is surrounded by Σ^{qu}. Wouldn't it be more natural and economical to assign this small disk (and its puncture, representing the $\mathscr{J}$ insertion) to Σ^{qu}?

We believe that the answer is no, and that the straightforward plaquette-by-plaquette definition of the decomposition is both natural and most economical. If the diagram in Fig. 4.10 were the only one with the $\mathscr{J}$ insertion surrounded by a disk assigned to Σ^{cl}, it would make sense to re-assign it to Σ^{qu} and end up with a simplified sum over surface decompositions. However, there is an entire family of diagrams with the same decomposition into Σ^{cl} and Σ^{qu}, of which the example in Fig. 4.10 is only the lowest-order representative, with fewest vertices inside this punctured disk. Another example is given in Fig. 4.11. The existence of such higher-order diagrams suggests that it is natural to follow the simple rules of
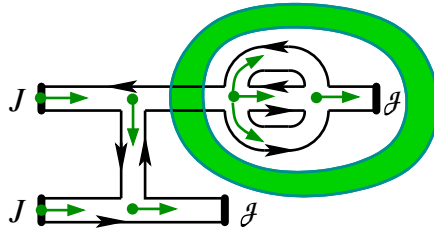
Figure 4.11: Another ribbon diagram that leads to the same Σ^{cl} and Σ^{qu} as the example in Fig. 4.10.

our plaquette-by-plaquette definition of the decomposition of Σ: According to that definition, every internal vertex in a given ribbon diagam is always inside Σ^{cl} – there is an open disk in Σ which contains the vertex and is entirely in Σ^{cl}. It is then natural to extend this picture also to the 1-vertices associated with the vertex insertions: Even if the puncture in Σ that corresponds to the source insertion is technically not a part of Σ, it has a neigborhood in Σ with the topology of a punctured disk, which intersects only one propagator of the ribbon diagram. The logic of the plaquette-by-plaquette construction suggests that this punctured disk should be assigned to Σ^{cl}.

Thus, the extension of the plaquette-by-plaquette construction to the ribbon diagrams with external source insertions suggests that all insertions of both J and $\mathscr{J}$ should be naturally interpreted as punctures in Σ^{cl}. This is the definition of the decomposition of Σ with punctures into its classical and quantum part which we adopt for the rest of this chapter: All punctures of Σ will always belong to Σ^{cl}.

4.4. Non-equilibrium string perturbation theory after the Keldysh rotation

Thus, we arrive at the form of the topological genus expansion in non-equilibrium string perturbation theory, in the Keldysh-rotated form. Consider again the sum over all *connected* ribbon diagrams in our generic large-N non-equilibrium system with matrix degrees of freedom, and with n_{cl} insertions of the classical source J and n_{qu} insertions of the quantum source $\mathscr{J}$. This amplitude can be written as

$$\mathcal{A}_{n_{\mathrm{cl}},n_{\mathrm{qu}}}(N,\lambda,\ldots)\, J^{n_{\mathrm{cl}}}\, \mathscr{J}^{n_{\mathrm{qu}}}. \tag{4.42}$$

The coefficients $\mathcal{A}_{n_{\mathrm{cl}},n_{\mathrm{qu}}}(N,\lambda,\ldots)$ can then be expanded in the powers of $1/N$, leading to the string dual description as a sum over connected worldsheet topologies, each with $n_{\mathrm{cl}} + n_{\mathrm{qu}}$ punctures.

For notational simplicity, we introduce the generating functional $\mathcal{Z}(J,\mathscr{J})$ of the amplitudes (4.42), defined as a formal sum of (4.42) over all n_{cl} and n_{qu}, and refer to $\mathcal{Z}(J,\mathscr{J})$
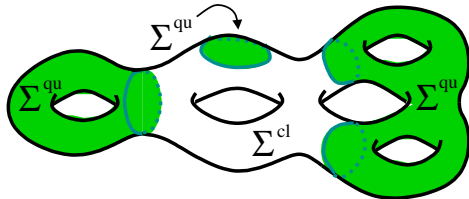
Figure 4.12: A typical surface Σ contributing to (4.43), and its decomposition into the classical foundation $\widehat{\Sigma}^{\mathrm{cl}}$ and the quantum embellishment Σ^{qu}. In this example, Σ is a surface with five handles, and with three $\mathscr{J}$ sources inserted at three marked points. Its classical foundation $\widehat{\Sigma}^{\mathrm{cl}}$ is a torus with three marked points, and its Σ^{qu} consists of three disconnected components: A torus with one boundary, a surface with two handles and two boundaries, and a disk.

as the "partition function" for short. In this language, we can now summarize the main results of this chapter as follows: The large-N expansion of the partition function for the non-equilibrium system in the Keldysh-rotated version of the Schwinger-Keldysh formalism takes the form of a sum over surface topologies, refined to

$$\mathcal{Z}(J, \mathscr{J}) = \sum_{h=0}^{\infty} \left(\frac{1}{N}\right)^{2h-2} \sum_{\substack{\text{double decompositions} \\ \chi(\Sigma^{\mathrm{cl}})+\chi(\Sigma^{\mathrm{qu}})=2-2h}} \mathcal{F}_{\Sigma^{\mathrm{cl}},\Sigma^{\mathrm{qu}}}(J, \mathscr{J}; \lambda, \ldots). \tag{4.43}$$

In this non-equilibrium case, the sum over the surface topologies goes over all double decompositions of Σ into Σ^{cl} and Σ^{qu}, such that Σ is the connected surface of genus h, and with $n_{\mathrm{cl}} + n_{\mathrm{qu}}$ marked points inside Σ^{cl} corresponding to the insertions of n_{cl} classical sources J and n_{qu} quantum sources $\mathscr{J}$.

We have already demonstrated that $\mathcal{Z}(0,0) = 0$ identically. In fact, this observation can be extended from the vacuum diagrams to the more general case of all diagrams with non-zero J but zero $\mathscr{J}$,

$$\mathcal{Z}(J, 0) = 0. \tag{4.44}$$

The proof is simple: Consider a ribbon diagram with at least one vertex. There is at least one arrow at the signpost at that vertex. Follow any admissible path starting in the direction of this arrow. In a diagram with a finite number of vertices, this path must end in a finite number of steps. The only place where an admissible path can end is at a $\mathscr{J}$ source insertion. Thus, for the diagram to be non-zero, there must be at least one $\mathscr{J}$ attached. There are no diagrams that would contribute to a correlation function with n classical sources J, if there is not at least one $\mathscr{J}$ source insertion, thus proving (4.44). Of course, this proof is perturbative in nature, as are all our arguments based on the perturbative expansion in terms of the underlying perturbative ribbon diagrams.

These vanishing identities have a clear physical interpretation familiar from the field-theory side of the non-equilibrium system: Setting the quantum source $\mathscr{J}$ to zero is equiv-

alent in the original $\pm$ formalism to setting the sources J_+ and J_- on the $C_\pm$ parts of the Schwinger-Keldysh contour equal to each other. When this is done, the probe of the system by J_+ on the forward branch is exactly undone by the compensating probe by J_- on the return path, and all the diagrams contributing to such a process are identically zero. On the string side, this is reflected by the statement of (4.44): All contributions from the worldsheets Σ without at least one $\mathscr{J}$ insertion vanish identically.

In fact, this statement about non-equilibrium string perturbation expansion can be further refined: For the amplitude associated with a given decomposition of Σ into Σ^{cl} and Σ^{qu} to be non-zero, each connected component of Σ^{cl} must have at least one $\mathscr{J}$ insertion. The proof is a simple generalization of the argument we used to prove (4.44): Each connected component of Σ^{cl} has at least one vertex. There is at least one allowed path that begins at this vertex. This allowed path stays within the same connected component of Σ^{cl}, and it has to end somewhere after a finite number of steps. Since it can only end at an $\mathscr{J}$ insertion, each connected component of Σ^{cl} must have at least one such insertion.

Note that (4.44) can be interpreted as the boundary condition for solving the full generating functional of the correlation functions (4.43). Finding that (4.44) is valid represents an important check of self-consistency for any $\mathcal{Z}(J, \mathscr{J})$ in non-equilibrium string theory.

Resummation of the perturbative expansion

The decomposition of the string worldsheet Σ into its classical and quantum parts suggests a reorganization of the perturbative expansion in string theory: We can first perform the sum over the topologically inequivalent classical foundations $\widehat{\Sigma}^{\mathrm{cl}}$, and then sum over all quantum embellishments that can be added to a given $\widehat{\Sigma}^{\mathrm{cl}}$. This resummation leads to the following expression, equivalent to (4.43):

$$
\mathcal{Z}(J, \mathscr{J}) = \sum_{\widehat{\Sigma}^{\mathrm{cl}}} \left(\frac{1}{N}\right)^{-\chi(\widehat{\Sigma}^{\mathrm{cl}})} \left\{ \sum_{b=0}^{\infty} \left(\frac{1}{N}\right)^{b} \left[\sum_{\Sigma_b^{\mathrm{qu}}} \left(\frac{1}{N}\right)^{-\chi(\Sigma_b^{\mathrm{qu}})} \mathcal{F}_{\widehat{\Sigma}^{\mathrm{cl}}, b, \Sigma_b^{\mathrm{qu}}}(J, \mathscr{J}; \lambda, \ldots) \right] \right\}.
$$
(4.45)

Here Σ_b^{qu} denotes a quantum embellishment surface, not necessarily connected, with b boundary components. The first sum in (4.45) is over the classical foundations, which are closed surfaces, also not necessarily connected. The second sum in (4.45) is over the number b of disks excised in the classical foundation $\widehat{\Sigma}^{\mathrm{cl}}$, in order to form Σ^{cl} (and over the distributions of such excisions among the connected components of $\widehat{\Sigma}^{\mathrm{qu}}$). The third sum in (4.45) is over all possible topologically inequivalent quantum embellishment surfaces Σ^{qu} which have b boundary components, and can therefore be glued to Σ^{cl} to form the full surface Σ. These ingredients are subjected to just one overall constraint: The resulting Σ must be connected.

The resummation of the non-equilibrium string perturbation expansion in the form (4.45) exhibits one somewhat unpleasant feature: For a given classical foundation $\widehat{\Sigma}^{\mathrm{cl}}$, the sum over inequivalent Σ^{qu} topologies is not finite, even at a fixed order in the string coupling $1/N$. This infinity of inequivalent topologies contributing at the same order in $1/N$ for a given

$\widehat{\Sigma}^{\mathrm{cl}}$ has a simple origin: Disconnected components of Σ^{qu} with the topology of a disk. One can excise any number m of disks from $\widehat{\Sigma}^{\mathrm{qu}}$ and replace them with such disconneted disk components of Σ^{qu}, without changing the Euler number of Σ and thus the order in $1/N$ at which this surface contributes to the partition function.

This feature suggests performing yet another resummation: For a given $\widehat{\Sigma}^{\mathrm{cl}}$, we can split the sum over all quantum embellishments in (4.45) into two steps: First the sum over any number of connected components of Σ^{qu} with the disk topology, followed by the sum over all components of Σ^{qu} whose Euler number is ≤ 0 (and which are therefore not disks). For a given classical foundation $\widehat{\Sigma}^{\mathrm{cl}}$, the first step defines a "renormalized" surface obtained by summing over all possible quantum embellishments by disks, and the second sum over topologically nontrivial quantum embellishments at each order in $1/N$ is then a finite sum over finitely many topologically distinct quantum embellishments of the renormalized $\widehat{\Sigma}^{\mathrm{cl}}$.

For specific models, or in specific circumstances, it might happen that the sum over quantum embellishments of each connected component of $\widehat{\Sigma}^{\mathrm{cl}}$ by disks becomes finite. Indeed, we shall see two such examples in Section 4.5, where we consider classical and stochastic limits of the general non-equilibrium quantum systems: In Section 4.5, we will find an example where all quantum embellishments vanish identically; and in Section 4.5, we will encounter another example, in which each connected component of Σ^{cl} can have at most one boundary component, which implies that the sum over its disk embellishments terminates at order one in the number of disks.

Worldsheet decompositions before and after the Keldysh rotation

We can now compare and contrast the worldsheet decompositions of Σ in non-equilibrium string perturbation theory in the original forward-backward formulation and in the formulation after the Keldysh rotation.

In the $\pm$ formalism, there is a symmetry between the forward and backward parts of the Schwinger-Keldysh contour, which implies a symmetry between the forward and backward parts Σ^+ and Σ^- of the triple decomposition of the worldsheet. In particular, their combinatorial definitions in terms of the ingredients in the underlying ribbon diagram reflect this symmetry. The remaining part, $\Sigma^\wedge$, has a different standing: It represents the part of the worldsheet associated with the instant of time where the forward and backward branches of the Schwinger-Keldysh contour meet. $\Sigma^\wedge$ does carry its own topological genus expansion, and in this sense it is topologically two-dimensional. Still, as we discussed in [98], its combinatorial definition suggests that $\Sigma^\wedge$ may be interpreted as geometrically one-dimensional.

In the Keldysh-rotated formulation, there is no symmetry between the classical and quantum component Σ^{cl} and Σ^{qu} of the two-fold decomposition of the worldsheet surface Σ: As we saw, the primary ingredient in this decomposition is the classical foundation $\widehat{\Sigma}^{\mathrm{cl}}$, which is topologically simpler or at most equivalent to Σ. Starting with this classical foundation, Σ is formed by adding the quantum embellishments represented by Σ^{qu}. Both Σ^{cl} and Σ^{qu} can have topologies of any genus, but there is no similarity or symmetry between them.

In fact, there appears to be a certain parallel between Σ^{cl} of the Keldysh-rotated formalism, and the Σ^+ and Σ^- components of the $\pm$ formalism of [7]. Analogously, the quantum part Σ^{qu} in the Keldysh-rotated formalism is somewhat reminiscent of the wedge region $\Sigma^{\wedge}$ of the $\pm$ formalism. Indeed, note an intriguing similarity between the combinatorial definition of Σ^{qu} in the Keldysh-rotated formalism as given in Section 4.3, and the worldsheet region $\Sigma^{\wedge}$ at the "end of time" in the $\pm$ formalism of [7]: In both instances, these surfaces are built solely from propagators and plaquettes, and no vertices in the original ribbon diagram. Thus, in the Poincaré dual ribbon diagram, Σ^{qu} and $\Sigma^{\wedge}$ are both built from vertices and lines only, which can make them appear geometrically one-dimensional. Yet, topologically they correspond to two-dimensional surfaces and carry their own genus expansion, as we demonstrated in Section 4.3.

4.5. Classical limits of non-equilibrium systems and string theory

In non-equilibrium theory in the Keldysh form, there are several popular approximations, which represent various classical limits of the system. In this section, we study the consequences of taking such limits for the string perturbation expansion. Besides the interst in studying the string-theory side of such approximations for their own sake, this section serves one additional purpose: We will see that our results will give further justification to our terminology, and in particular clarify why it makes sense to refer the two parts Σ^{cl} and Σ^{qu} as the "classical" and "quantum" part of the worldsheet Σ.

The classical limit

The first popular approximation is one in which we consider the quantum field ϕ_{qu} (or, in our matrix case, $\mathscr{M}$) to be small compared to ϕ_{cl} (in our case M), expand the action up to linear order in the quantum field $\mathscr{M}$ and then integrate $\mathscr{M}$ out (see, *e.g.*, [64, 90, 91, 99]).

$$S_{\mathrm{SK}} = \frac{1}{g^2} \int dt \, \mathrm{Tr} \left(M \, G_R^{-1} \mathscr{M} + \mathscr{M} \, G_A^{-1} \, M + 3 \, M^2 \mathscr{M} + 4 \, M^3 \mathscr{M} + \ldots \right). \qquad (4.46)$$

Integrating $\mathscr{M}$ yields a delta function, which makes the remaining dynamical field M satisfy its classical equation of motion,

$$\ddot{M}(t) = -V'(M(t)). \qquad (4.47)$$

(Here V is the potential that contains all the cubic and higher interaction terms of the original action, and we have kept all the spatial-momentum dependence in the equation implicit.) Thus, in this limit, all fluctuations (both quantum and thermal) are infinitely suppressed. This is the reason why this approximation is usually invoked to justify the terminology "classical" and "quantum" for the fields M and $\mathscr{M}$: The "classical" field M in

this "classical" approximation satisfies the classical equation of motion, and the "quantum" field has been integrated out.

What does this approximation look like in the string-theory representation? Consider the general ribbon diagrams in this approximation. First, linearizing the cubic and higher interaction terms in the action (4.18) in the quantum field $\mathscr{M}$ means that we drop all vertices with more than one arrow at their signpost. Note a curious consequence: In this classical approximation, there is no free will left for our hypothetical travelers following admissible paths on a given ribbon diagram! Indeed, the choice of an admissible direction at each vertex along the path is uniquely determined by the single arrow at its signpost, and all admissible paths are completely deterministic.

Linearizing the quadratic term in (4.18) means that we keep only the mixed propagators G_A and G_R, dropping all the G_K propagators. This step is familiar: This is how we defined the reduction from the full surface Σ to its classical foundation $\widehat{\Sigma}^{\text{cl}}$ in Section 4.3. However, not all classical foundations of the original theory will appear: Only those diagrams whose every vertex has just one arrow at its signpost will survive the linearization procedure.

It is now easy to show that all such ribbon diagrams will be collections of trees. Each of the trees is rooted by one $\mathscr{J}$ insertion. The collection of all allowed paths that end at this $\mathscr{J}$ form the branches of the tree. The deterministic feature of the allowed paths discussed above ensures that there are indeed no closed loops in this tree. Tree diagrams are planar, and therefore Σ is just a collection of spheres.

Thus, we reach a very pleasing conclusion: In the classical limit of the original non-equilibrium quantum system, the partition function $\mathscr{Z}(J, \mathscr{J})$ as given by the sum over worldsheet topologies automatically reduces itself to a sum over string worldsheet surfaces with only spherical topologies! For each term, the number of S^2's is equal to the number of $\mathscr{J}$ external insertions. Moreover, all these surfaces have no quantum embellishments Σ^{qu}, and therefore are equivalent to their classical foundation $\widehat{\Sigma}^{\text{qu}}$. In equilibrium closed string theory, summing over only spherical topologies is the hallmark of taking the classical limit. It is nice to see that taking the classical limit of the non-equilibrium system matches the process of taking the classical limit on the string side as well. We believe that this result provides some intuitive justification for the terminology we introduced for the decomposition of Σ into its "classical" and "quantum" part Σ^{cl} and Σ^{qu}.

Classical stochastic limit and the Martin-Siggia-Rose method

In this approximation, we take the semiclassical limit $\hbar \to 0$ but keep the classical thermal fluctuations. This is achieved by restoring the dependences on $\hbar$ in the Schwinger-Keldysh action (4.18), exposing the system to an environment by coupling it to a thermal bath of harmonic oscillators, and taking the classical limit while keeping the temperature T fixed (see, *e.g.*, [64], Chapters 3.2 and 4, for details). Note that this approximation will not require the M degrees of freedom to be in equilibrium, only the bath.

It turns out that keeping the dependence on non-zero T is equivalent to keeping not only the linear terms but also the terms *quadratic* in $\mathscr{M}$ in our expansion of the action(4.18).

The classical action (4.46) is then modified to

$$S_{\text{SK}} = \frac{1}{g^2} \int dt \, \text{Tr} \left(M \, G_R^{-1} \mathcal{M} + \mathcal{M} \, G_A^{-1} \, M + 3 \, M^2 \mathcal{M} + 4 \, M^3 \mathcal{M} + \ldots + i\gamma T \mathcal{M}^2 \right). \quad (4.48)$$

Here γ is a constant that characterizes the spectral density of the Ohmic bath modelling the environment (see [64]). This constant γ also appears in the additive friction terms in the G_A and G_R propagators, terms which were absent in these propagators in the classical limit of Section 4.5; these additional terms do not influence our treatment of the Feynman rules, ribbon diagrams and our conclusions.

In order to see in what sense this action (4.48) represents a classical stochastic system, it is convenient to use the Hubbard-Stratonovich transformation in the path integral,

$$e^{-\gamma T \int dt \, \text{Tr}\left(\mathcal{M}^2\right)} = \int \mathcal{D}\xi(t) \, e^{-\int dt \, \text{Tr}\left(\frac{1}{\gamma T}\xi^2 - 2i\xi(t)\mathcal{M}(t)\right)}, \quad (4.49)$$

so that we can trade the term quadratic in $\mathcal{M}$ for a linear coupling between $\mathcal{M}$ and a new, typically Gaussian, field ξ. In our case, both $\mathcal{M}(t)$ and $\xi(t)$ are $SU(N)$ matrices (with all additional dependences on the spatial coordinates or other quantum numbers again kept implicit, as has been the case throughout our analysis).

Since $\mathcal{M}$ now appears only linearly, it can be again integrated out to give a delta function localized on the stochastic classical equation of motion for M,

$$\ddot{M}(t) = -\gamma \dot{M} - V'(M(t)) + \xi(t). \quad (4.50)$$

In this classical equation, $\xi(t)$ serves as a stochastic noise, with a Gaussian distribution represented by the path integral (4.49). Note the presence of the friction term $-\gamma \dot{M}$, which appears due to the dependence of G_A and G_R on γ mentioned above. The famous Martin-Siggia-Rose method [100] for dealing with stochastic systems reverses this construction [101, 102]: It starts with a Langevin equation analogous to (4.50), and reintroduces the quantum field $\mathcal{M}$ to represent the system in the path integral language.

Now we will use the action (4.48) of this classical stochastic limit of the original system of matrix degrees of freedom, to see the implications of this approximation on the dual string side.

First note that in this limit, all vertices in the surviving ribbon diagrams are again allowed to have just one arrow at their signpost, just as in the classical limit discussed in Section 4.5. In particular, the following conclusions about the classical foundation $\widehat{\Sigma}^{\text{cl}}$ of the surfaces associated with the surviving ribbon digrams stay the same:

- All admissible paths on the ribbon diagrams are completely deterministic;

- The reduced ribbon diagram that defines the classical foundation $\widehat{\Sigma}^{\text{cl}}$ is a collection of trees (with one tree per each $\mathscr{J}$ source insertion), and its each connected component is therefore planar;
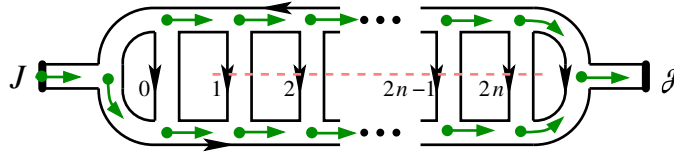
Figure 4.13: An example a ribbon diagram that follows the rules of the stochastic classical approximation with action (4.48). Note the deterministic nature of the amissible paths on this diagram. Cutting across the indicated $2n$ rungs and re-gluing them as in Fig. 4.6 yields a ribbon diagram whose surface Σ has n handles, while its classical foundation is still $\widehat{\Sigma}^{\mathrm{cl}} = S^2$. The non-trivial topology is entirely contained in the quantum part Σ^{qu}, which is a surface with n handles and one boundary.

- The classical foundation $\widehat{\Sigma}^{\mathrm{cl}}$ is either a sphere, or a collection of disconnected spheres (with one S^2 for each connected tree component of the associated reduced ribbon diagram);

- The number of connected components S^2 of $\widehat{\Sigma}^{\mathrm{cl}}$ is equal to the number of $\mathscr{J}$ source insertions in the diagram.

In contrast to the zero-temperature classical limit studied in Section 4.5, however, there is now a non-zero remnant of the classical-to-classical G_K propagator, due to the presence of the $\mathscr{M}^2$ term in (4.48) linear in T. Thus, the worldsheets Σ contributing in this stochastic classical limit will still contain quantum embellishments, but their classical foundations will be collections of S^2's.

Restoring now all the G_K propagators in the reduced diagram, the surface Σ can have an arbitrarily high number of handles, as we show in Fig. 4.13. However, this nontrivial topology of Σ is now solely due to the quantum embellishments: Leaving out the G_K propagators reduces any original ribbon diagram of this approximation to a collection of trees, implying that the classical foundation $\widehat{\Sigma}^{\mathrm{cl}}$ is always a collection of two-spheres. In addition, one can similarly show that each connected component of Σ^{cl} is a disk (*i.e.*, it has only one boundary S^1 connecting it to Σ^{qu}), or the entire Σ is an S^2 with no quantum embellishments.

We see that even in the stochastic classical limit, there continues to be a meaningful sense in which the "classical" limit in the non-equilibrium system (as defined by (4.48)) means also a "classical" limit in the sense of the dual string theory, where the "classical" string limit is conventionally understood as the summation over worldsheets with only spherical topology [103] and possibly with marked points. This time, however, this classical string limit applies only to the *classical foundation* of Σ, while the higher-genus quantum embellishments Σ^{qu} represent the classical thermal or stochastic fluctuations in the original matrix system.

Chapter 5

Conclusion

There are several possible directions for future research. Here, we organize them based on the chapter they are most relevant to.

5.1. Future Work on the Weak Gravity Conjecture

This chapter comprises a proof of the weak gravity conjecture, obtained from studying the macroscopic entropy of gauged scalars on a semiclassical near-extremal black hole background. Our choice of renormalization conditions allows us to safely neglect non-linear metric backreaction. The quantum corrected entropy violates the second law if the conjecture is not satisfied. When the conjecture is satisfied, the black hole near extremality decays rapidly due to Schwinger pair production, which allows the theory to evade the troubling thermodynamic violation. Therefore, we establish that it is necessary that a weak gravity conjecture is obeyed.[1]. Our calculation demonstrates that entropy inequalities may discriminate between effective field theories that live in the landscape versus the swampland. Although effective field theories that violate the weak gravity conjecture do not obviously violate unitarity, positivity, or causality, the violation of the second law indicates that *some* sickness lurks within them. In conclusion, we propose that a violation of the second law modulo backreaction indicates an IR obstruction to a UV completion in a unified theory [104].

Our analysis does not truly address weak gravity in effective field theory or on arbitrary perturbations of the black hole background. We only consider the minimally gauged, minimally coupled quadratic action of the $D = 4$ gauged scalar. A follow-up chapter [105] bridges the gap: we address the conjecture in arbitrary dimensions and non-minimal interactions, including non-renormalizable terms. We limited our analysis here to the minimal quadratic action for ease of presentation and because we could obtain an exact result. We extend our result to actions with higher dimension operators and to actions with multiple scalars in

---

[1]We leave it to future work to determine if it is *sufficient*.

[105]. In particular, we prove the generalized electric weak gravity conjecture of [26] in our follow-up chapter.

It would be worthwhile to extend our methodology to arbitrary p-form gauge fields. For example, while it is expected that there is a weak gravity conjecture for $p > 1$, it is unclear if $p = 0$ axions are subject to a weak gravity conjecture. If they are, then there are direct implications for inflationary model building. In particular, large field axion inflation would violate the $p = 0$ weak gravity conjecture [29].

Although our results directly apply to the weak gravity conjecture, they might also apply to the Ooguri-Vafa conjecture [106].[2] Ooguri and Vafa claim that there are no stable non-supersymmetric AdS vacuua whose cosmological constant is supported by a flux. If true, then the conjecture has serious implications for non-supersymmetric AdS/CFT. Large-N brane constructions and Kaluza-Klein compactifications include extremal particles in the bulk spectrum. Our result demonstrates a conflict between thermodynamics and non-supersymmetric, gauged extremal particles, suggesting a route to proving the conjecture.

The extensions aforementioned do not capture the full potential of our methodology. We propose that the armamentarium of entropy technology at our disposal may define new, undiscovered constraints on effective field theories compatible with quantum gravity. Our follow-up chapter provides minor evidence in favor of the proposal [105]. The power of the methodology lies within the relative ease of calculating macroscopic entropy of IR field content in semi-classical gravitational backgrounds. One may remain agnostic as to the full UV completion of the effective theory. Nonetheless, if the effective theory violates known entropy inequalities in the IR, then there exists some obstruction to a UV completion.

5.2. Future Work on the Large-N Expansion and Strings Out of Equilibrium

In this chapter, we studied the large-N expansion in non-equilibrium quantum systems with matrix degrees of freedom on the Schwinger-Keldysh time contour, to derive universal features of the perturbative expansion in the dual string theory. In equilibrium, the standard loop expansion in the powers of the string coupling g_s takes the form of a sum over inequivalent worldsheet topologies Σ, fully classified (in the case of closed oriented strings) by the number of handles on Σ. In non-equilibrium string theory, we found that this topological expansion is further refined: Each surface Σ undergoes a triple decomposition into region Σ^+ on the forward branch of the Schwinger-Keldysh time contour, Σ^- on the backward branch of the time contour, and the wedge region $\Sigma^\wedge$ which corresponds to the instant in time where the two branches meet. Surprisingly, $\Sigma^\wedge$ is itself a topologically two-dimensional region, with arbitrarily complicated topology and its own genus expansion. The perturbative sum over worldsheet topologies Σ now includes a sum over all triple decompositions.

---

[2]See also [107].

These findings are quite universal, since they follow just from the robust features of the large-N Feynman diagrams, without any assumptions about the (unknown) worldsheet dynamics of the dual theory. In this sense, we expect that any candidate string-theory dual should consistently reproduce this refined structure of string perturbation theory.

The next challenge is to find concrete realizations of the refined string perturbation theory in examples where the worldsheet dynamics is known or can be worked out. At least three natural testing grounds suggest themselves: One is noncritical string theory in low spacetime dimensions, which is nonperturbatively described by the appropriate continuum limit of matrix models. Another example, where a lot is known about both sides of the large-N/string-theory duality and our ideas can presumably be tested, is the most-studied example of AdS/CFT correspondence, given by $\mathcal{N} = 4$ supersymmetric Yang-Mills theory and its Type IIB superstring $AdS_5 \times S^5$ dual. Finally, critical superstring theory in asymptotically flat spacetimes should also provide interesting tests. In fact, the insights of this chapter may also be relevant for equilibrium superstring perturbation theory, in the context of extending the beautiful methods of Cutkosky rules and Refs. [73, 72, 74] for proving unitarity of amplitudes to string theory. These methods have been surprisingly out of reach in the first-quantized approach to string theory (see [108] for the relevant discussion), and progress on these issues so far seems to require string field theory [109].

We mainly hope that the results of this chapter will help to pave the way towards the development of non-equilibrium string theory, enlarging the scope of physical systems that can be described by a string-theory dual.

5.3. Future Work on the Keldysh Rotation and Non-equilibrium String Theory

In this chapter we found that, as anticipated, the calculus of non-equilibrium string perturbation theory looks quite different in the Keldysh representation, in comparison to its form in the original $\pm$ formalism that we found in [7]. In both cases, the large-N expansion is organized into a sum over surfaces Σ of increasing topological complexity, just as in the standard string perturbation theory at equilibrium. In contrast to equilibrium, however, in both representations of non-equilibrium string perturbation theory the surfaces Σ are found to carry a more refined structure (besides just the genus of Σ) which is universal for all systems. It is this additional structure that is quite different between the two non-equilibrium representations.

In the $\pm$ formalism, the worldsheet surfaces Σ exhibit a triple decomposition, into their forward branch Σ^+, a backward branch Σ^- and the "wedge" region $\Sigma^\wedge$ which corresponds to the crossing from the forward to the backward portion of the Schwinger-Keldysh time contour. In contrast, in the Keldysh representation, each surface Σ consists of a classical foundation $\widehat{\Sigma}^{\mathrm{cl}}$, which is further decorated by the quantum portion Σ^{qu} of the surface.

In [7], we also studied the structure of non-equilibrium string perturbation theory, and

the refinement of the worldsheet decompositions, for closed time contours with more than two segments, most notably for the Kadanoff-Baym contour relevant for systems at finite temperature. Besides the forward branch C_+ and the backward branch C_-, this time contour has a third segment $\mathbf{C}_\mathrm{M}$ (sometimes called the "Matsubara" segment), which extends along the imaginary direction by the amount $\beta = 1/T$ set by the temperature. We have not generalized the results of the Keldysh rotation to this case, simply because the status of this third segment is different than that of $C_\pm$. However, one can certainly imagine a hybrid formalism, in which the Keldysh rotation has been performed on the fields taking values on $C_\pm$, leaving the Matsubara segment intact. Such a hybrid formalism has indeed been used extensively in the theory of non-equilibrium many-body systems (see [71] for a review). The fields in this hybrid formalism would consist of the classical and quantum fields $M(t)$ and $\mathscr{M}(t)$ that we studied in this chapter, plus the Matsubara field $M_\mathrm{M}(\tau)$ that we used in Section 3 of [7]. By combining the results of [7] and those of the present chapter, it should be possible to derive the form of the worldsheet decomposition in this hybrid formalism for non-equilibrium systems with a string dual.

Effectively, our analysis in [7] and in the present chapter produced a set of rules which can be viewed almost as axioms, and which are so universal that we expect any string theory out of equilibrium to be consistent with them: In the $\pm$ description, the instant in time where the forward and backward contours meet is perceived from the worldsheet perspective as topologically two-dimensional, and carries its own genus expansion; the sum over surfaces is refined into a sum over their triple decompositions. In the Keldysh rotated description, each part of the two-fold decomposition of the worldsheet surface into its classical foundation and quantum embellishments carries its own independent genus expansion. Due to their universal nature, these axioms are arguably not very strong, and therefore not very helpful in determining any specific details of the worldsheet dynamics. We hope, however, that they may at least provide some guidance in the future search for the worldsheet description, in particular examples of interest.

It will be interesting to see which of the two representations of the string-theoretic dual description of large-N non-equilibrium systems will be more useful from the perspective of the worldsheet theory. Perhaps the answer might even depend on the large-N system in question, and the kind of string theory which happens to be dual to it. We leave these fascinating questions open for future investigations.

Bibliography

[1] Jan Zaanen et al. *Holographic Duality in Condensed Matter Physics*. Cambridge Univ. Press, 2015.

[2] Sean A. Hartnoll, Andrew Lucas, and Subir Sachdev. "Holographic quantum matter". In: (2016). arXiv: `arXiv:1612.07324 [hep-th]`.

[3] Petr Hořava. "Stability of Fermi surfaces and K-theory". In: *Phys. Rev. Lett.* 95 (2005), p. 016405. DOI: `10.1103/PhysRevLett.95.016405`. arXiv: `arXiv:hep-th/0503006`.

[4] Andrea Cappelli et al., eds. *The Birth of String Theory*. Cambridge, UK: Cambridge Univ. Press, 2012.

[5] Julian S. Schwinger. "Brownian motion of a quantum oscillator". In: *J. Math. Phys.* 2 (1961), pp. 407–432. DOI: `10.1063/1.1703727`.

[6] L.V. Keldysh. "Diagram technique for nonequilibrium processes". In: *Zh. Eksp. Teor. Fiz.* 47 (1964), pp. 1515–1527.

[7] Petr Hořava and Christopher J. Mogni. "Large-N expansion and string theory out of equilibrium". In: (2020). eprint: `arXiv:2008.11685` (hep-th).

[8] P. Hájiček. "Time loop formalism in quantum field theory". In: *The Second Marcel Grossmann Meeting on the Recent Developments of General Relativity*. 1979, p. 483.

[9] R.D. Jordan. "Effective Field Equations for Expectation Values". In: *Phys. Rev. D* 33 (1986), p. 444. DOI: `10.1103/PhysRevD.33.444`.

[10] Steven Weinberg. "Quantum contributions to cosmological correlations". In: *Phys. Rev. D* 72 (2005), p. 043514. DOI: `10.1103/PhysRevD.72.043514`. arXiv: `arXiv:hep-th/0506236`.

[11] Steven Weinberg. "Quantum contributions to cosmological correlations. II. Can these corrections become large?" In: *Phys. Rev. D* 74 (2006), p. 023508. DOI: `10.1103/PhysRevD.74.023508`. arXiv: `arXiv:hep-th/0605244`.

[12] Steven Weinberg. "Effective field theory for inflation". In: *Phys. Rev. D* 77 (2008), p. 123541. DOI: `10.1103/PhysRevD.77.123541`. arXiv: `arXiv:0804.4291 [hep-th]`.

[13] Daniel Baumann and Liam McAllister. *Inflation and String Theory*. Cambridge University Press, 2015. arXiv: `arXiv:1404.2601 [hep-th]`.

[14] Jan de Boer, Michal P. Heller, and Natalia Pinzani-Fokeeva. "Holographic Schwinger-Keldysh effective field theories". In: *JHEP* 05 (2019), p. 188. DOI: 10.1007/JHEP05(2019)188. arXiv: arXiv:1812.06093 [hep-th].

[15] Felix M. Haehl, R. Loganayagam, and Mukund Rangamani. "Schwinger-Keldysh formalism. Part I: BRST symmetries and superspace". In: *JHEP* 06 (2017), p. 069. DOI: 10.1007/JHEP06(2017)069. arXiv: arXiv:1610.01940 [hep-th].

[16] Felix M. Haehl, R. Loganayagam, and Mukund Rangamani. "Schwinger-Keldysh formalism. Part II: thermal equivariant cohomology". In: *JHEP* 06 (2017), p. 070. DOI: 10.1007/JHEP06(2017)070. arXiv: arXiv:1610.01941 [hep-th].

[17] C. P. Herzog and D. T. Son. "Schwinger-Keldysh propagators from AdS/CFT correspondence". In: *JHEP* 03 (2003), p. 046. DOI: 10.1088/1126-6708/2003/03/046. arXiv: arXiv:hep-th/0212072.

[18] Gerard 't Hooft. "A planar diagram theory for strong interactions". In: *Nucl. Phys. B* 72 (1974), p. 461. DOI: 10.1016/0550-3213(74)90154-0.

[19] Gerard 't Hooft. "A two-dimensional model for mesons". In: *Nucl. Phys. B* 75 (1974), pp. 461–470. DOI: 10.1016/0550-3213(74)90088-1.

[20] Alexander M. Polyakov. "A few projects in string theory". In: *Les Houches Summer School on Gravitation and Quantizations, Session 57*. 1993, p. 783. arXiv: hep-th/9304146.

[21] Juan Martin Maldacena. "The Large N limit of superconformal field theories and supergravity". In: *Adv. Theor. Math. Phys.* 2 (1998), p. 231. DOI: 10.1023/A:1026654312961. arXiv: arXiv:hep-th/9711200.

[22] Nima Arkani-Hamed et al. "The string landscape, black holes and gravity as the weakest force". In: *JHEP* 06 (2007), p. 060. eprint: hep-th/0601001.

[23] Ben Heidenreich, Matthew Reece, and Tom Rudelius. "Evidence for a Lattice Weak Gravity Conjecture". In: (2016). arXiv: 1606.08437 [hep-th].

[24] Tom Banks, Matt Johnson, and Assaf Shomer. "A Note on Gauge Theories Coupled to Gravity". In: *JHEP* 09 (2006), p. 049. DOI: 10.1088/1126-6708/2006/09/049. arXiv: hep-th/0606277 [hep-th].

[25] Horacio Casini. "Relative entropy and the Bekenstein bound". In: *Class.Quant.Grav.* 25 (2008), p. 205021. DOI: 10.1088/0264-9381/25/20/205021. arXiv: 0804.2182 [hep-th].

[26] Clifford Cheung and Grant N. Remmen. "Naturalness and the Weak Gravity Conjecture". In: *Phys. Rev. Lett.* 113 (2014), p. 051601. DOI: 10.1103/PhysRevLett.113.051601. arXiv: 1402.2287 [hep-ph].

[27] Clifford Cheung and Grant N. Remmen. "Infrared Consistency and the Weak Gravity Conjecture". In: *JHEP* 12 (2014), p. 087. DOI: 10.1007/JHEP12(2014)087. arXiv: 1407.7865 [hep-th].

[28] Daniel Harlow. "Wormholes, Emergent Gauge Fields, and the Weak Gravity Conjecture". In: *JHEP* 01 (2016), p. 122. DOI: 10.1007/JHEP01(2016)122. arXiv: 1510.07911 [hep-th].

[29] Ben Heidenreich, Matthew Reece, and Tom Rudelius. "Weak Gravity Strongly Constrains Large-Field Axion Inflation". In: *JHEP* 12 (2015), p. 108. DOI: 10.1007/JHEP12(2015)108. arXiv: 1506.03447 [hep-th].

[30] Ben Heidenreich, Matthew Reece, and Tom Rudelius. "Sharpening the Weak Gravity Conjecture with Dimensional Reduction". In: *JHEP* 02 (2016), p. 140. DOI: 10.1007/JHEP02(2016)140. arXiv: 1509.06374 [hep-th].

[31] Raphael Bousso et al. "Proof of a Quantum Bousso Bound". In: *Phys.Rev.* D90.4 (2014), p. 044002. DOI: 10.1103/PhysRevD.90.044002. arXiv: 1404.5635 [hep-th].

[32] Raphael Bousso et al. "Entropy on a null surface for interacting quantum field theories and the Bousso bound". In: *Phys.Rev.* D91.8 (2015), p. 084030. DOI: 10.1103/PhysRevD.91.084030. arXiv: 1406.4545 [hep-th].

[33] Raphael Bousso et al. "A Quantum Focussing Conjecture". In: (2015). arXiv: 1506.02669 [hep-th].

[34] Raphael Bousso et al. "Proof of the Quantum Null Energy Condition". In: *Phys. Rev.* D93.2 (2016), p. 024017. DOI: 10.1103/PhysRevD.93.024017. arXiv: 1509.02542 [hep-th].

[35] Shamik Banerjee et al. "Logarithmic Corrections to N=4 and N=8 Black Hole Entropy: A One Loop Test of Quantum Gravity". In: *JHEP* 11 (2011), p. 143. DOI: 10.1007/JHEP11(2011)143. arXiv: 1106.0080 [hep-th].

[36] Sayantani Bhattacharyya, Binata Panda, and Ashoke Sen. "Heat Kernel Expansion and Extremal Kerr-Newmann Black Hole Entropy in Einstein-Maxwell Theory". In: *JHEP* 08 (2012), p. 084. DOI: 10.1007/JHEP08(2012)084. arXiv: 1204.4061 [hep-th].

[37] Ashoke Sen. "Logarithmic Corrections to N=2 Black Hole Entropy: An Infrared Window into the Microstates". In: *Gen. Rel. Grav.* 44.5 (2012), pp. 1207–1266. DOI: 10.1007/s10714-012-1336-5. arXiv: 1108.3842 [hep-th].

[38] Shamik Banerjee, Rajesh Kumar Gupta, and Ashoke Sen. "Logarithmic Corrections to Extremal Black Hole Entropy from Quantum Entropy Function". In: *JHEP* 03 (2011), p. 147. DOI: 10.1007/JHEP03(2011)147. arXiv: 1005.3044 [hep-th].

[39] Ashoke Sen. "Quantum Entropy Function from AdS(2)/CFT(1) Correspondence". In: *Int. J. Mod. Phys.* A24 (2009), pp. 4225–4244. DOI: 10.1142/S0217751X09045893. arXiv: 0809.3304 [hep-th].

[40] Ashoke Sen. "Logarithmic Corrections to Schwarzschild and Other Non-extremal Black Hole Entropy in Different Dimensions". In: *JHEP* 04 (2013), p. 156. DOI: 10.1007/JHEP04(2013)156. arXiv: 1205.0971 [hep-th].

[41]   William Cottrell, Gary Shiu, and Pablo Soler. "Weak Gravity Conjecture and Extremal Black Holes". In: (2016). arXiv: `1611.06270 [hep-th]`.

[42]   Shahar Hod. "A proof of the weak gravity conjecture". In: (2017). arXiv: `1705.06287 [gr-qc]`.

[43]   Matthew D. Schwartz. *Quantum Field Theory and the Standard Model*. Cambridge University Press, 2014. ISBN: 1107034736, 9781107034730.

[44]   Dmitri V. Vassilevich. "Heat kernel expansion: User's manual". In: *Phys.Rept.* 388 (2003), pp. 279–360. DOI: `10.1016/j.physrep.2003.09.002`. arXiv: `hep-th/0306138 [hep-th]`.

[45]   Sergey N. Solodukhin. "Entanglement entropy of black holes". In: *Living Rev.Rel.* 14 (2011), p. 8. arXiv: `1104.3712 [hep-th]`.

[46]   B. Pioline and J. Troost. "Schwinger pair production in AdS(2)". In: *JHEP* 03 (2005), p. 043. DOI: `10.1088/1126-6708/2005/03/043`. arXiv: `hep-th/0501169 [hep-th]`.

[47]   Aron C. Wall. "A proof of the generalized second law for rapidly changing fields and arbitrary horizon slices". In: *Phys.Rev.* D85.6 (2012), p. 104049. DOI: `10.1103/PhysRevD.87.069904,10.1103/PhysRevD.85.104049`. arXiv: `1105.3445 [gr-qc]`.

[48]   Juan M. Maldacena, Jeremy Michelson, and Andrew Strominger. "Anti-de Sitter fragmentation". In: *JHEP* 02 (1999), p. 011. eprint: `hep-th/9812073`.

[49]   Godfrey Reggio, Philip Glass, and Ron Fricke. *Koyaanisqatsi,* IRE. 1982.

[50]   Gerard 't Hooft. *Under the Spell of the Gauge Principle,* Chapter 6. World Scientific, 1994.

[51]   Sidney R. Coleman. "1/N". In: *17th International School of Subnuclear Physics: Pointlike Structures Inside and Outside Hadrons*. 1980.

[52]   Sidney Coleman. *Aspects of Symmetry: Selected Erice Lectures*. Cambridge: Cambridge University Press, 1985. ISBN: 978-0-521-31827-3.

[53]   Juan Martin Maldacena. "TASI 2003 lectures on AdS/CFT". In: *Theoretical Advanced Study Institute in Elementary Particle Physics (TASI 2003): Recent Trends in String Theory*. 2003, p. 155. arXiv: `arXiv:hep-th/0309246`.

[54]   Laurence G. Yaffe. "Large N limits as classical mechanics". In: *Rev. Mod. Phys.* 54 (1982), p. 407. DOI: `10.1103/RevModPhys.54.407`.

[55]   Robert C. Penner. *Decorated Teichmüller theory*. European Mathematical Society, 2012. ISBN: 978-3-03719-075-3.

[56]   E. M. Lifshitz and L. P. Pitaevskii. *Landau and Lifshitz Course of Theoretical Physics, Volume 10: Physical Kinetics*. Pergamon Press, 1981.

[57]   J. Rammer and H. Smith. "Quantum field-theoretical methods in transport theory of metals". In: *Rev. Mod. Phys.* 58 (1986), p. 323. DOI: `10.1103/RevModPhys.58.323`.

[58] Jorgen Rammer. *Quantum field theory of non-equilibrium states*. Cambridge: Cambridge University Press, 2007.

[59] G. D. Mahan. *Many-Particle Physics, Third Edition*. Plenum Press, 2000.

[60] Kuang-chao Chou et al. "Equilibrium and nonequilibrium formalisms made unified". In: *Phys. Rept.* 118 (1985), pp. 1–131. DOI: 10.1016/0370-1573(85)90136-X.

[61] Michel Le Bellac. *Thermal Field Theory*. Cambridge: Cambridge University Press, 1996. ISBN: 978-0-511-88506-8, 978-0-521-65477-7.

[62] Ashok K. Das. *Finite Temperature Field Theory*. New York: World Scientific, 1997. ISBN: 978-981-02-2856-9, 978-981-4498-23-4.

[63] Ashok K. Das. "Topics in finite temperature field theory". In: (2000). arXiv: arXiv: hep-ph/0004125.

[64] A. Kamenev. *Field Theory of Non-Equilibrium Systems*. Cambridge: Cambridge University Press, 2011.

[65] G. Stefanucci and R. van Leeuwen. *Nonequilibrium Many-Body Theory of Quantum Systems*. Cambridge: Cambridge University Press, 2013.

[66] François Gelis. *Quantum Field Theory: From Basics to Modern Topics*. Cambridge University Press, 2019. ISBN: 978-1-108-48090-1, 978-1-108-57590-4.

[67] G.A. Vilkovisky. "Expectation values and vacuum currents of quantum fields". In: *Lect. Notes Phys.* 737 (2008), p. 729. arXiv: arXiv:0712.3379 [hep-th].

[68] Václav Špička, Bedřich Velický, and Anděla Kalvová. "Long and short time quantum dynamics: I. Between Green's functions and transport equations". In: *Physica* E 29 (2005), p. 154.

[69] Václav Špička, Bedřich Velický, and Anděla Kalvová. "Long and short time quantum dynamics: II. Kinetic regime". In: *Physica* E 29 (2005), p. 175.

[70] Václav Špička, Bedřich Velický, and Anděla Kalvová. "Long and short time quantum dynamics: III. Transients". In: *Physica* E 29 (2005), p. 196.

[71] Václav Špička, Bedřich Velický, and Anděla Kalvová. "Electron systems out of equilibrium: Nonequilibrium Green's function approach". In: *Int. J. Mod. Phys.* B 28 (2014), p. 1430013. DOI: 10.1142/S0217979214300138.

[72] Gerard 't Hooft and M.J.G. Veltman. "Diagrammar". In: *NATO Sci. Ser. B* 4 (1974), pp. 177–322. DOI: 10.1007/978-1-4684-2826-1_5.

[73] M.J.G. Veltman. "Unitarity and causality in a renormalizable field theory with unstable particles". In: *Physica* 29 (1963), pp. 186–207. DOI: 10.1016/S0031-8914(63) 80277-3.

[74] M.J.G. Veltman. *Diagrammatica: The Path to Feynman rules*. Cambridge University Press, 2012. ISBN: 978-1-139-24339-1, 978-0-521-45692-0.

[75] Leila Schneps. *The Grothendieck Theory of Dessins d'Enfants, LMS Lecture Note Series **200***. Cambridge University Press, 1994.

[76] Sergei K. Lando and Alexander K. Zvonkin. *Graphs on Surfaces and Their Applications*. Springer-Verlag, 2004.

[77] Pierre Guillot. "An elementary approach to dessins d'enfants and the Grothendieck-Teichmüller group". In: (2013). arXiv: `arXiv:1309.1968[math.GR]` [math.GR].

[78] Gareth A. Jones and Jurgen Wolfart. *Dessins d'Enfants on Riemann Surfaces*. Springer, 2016.

[79] Norbert A'Campo, Lishen Ji, and Athanase Papadopoulos. "Actions of the absolute Galois group". In: (2016). arXiv: `arXiv:1603.03387` [math.GT].

[80] Sownak Bose, James Gundry, and Yang-Hui He. "Gauge theories and dessins d'enfants: beyond the torus". In: *JHEP* 01 (2015), p. 135. DOI: `10.1007/JHEP01(2015)135`. arXiv: `arXiv:1410.2227` [hep-th].

[81] Yang-Hui He, John McKay, and James Read. "Modular subgroups, dessins d'enfants and elliptic K3 surfaces". In: *J. Comput. Math.* 16 (2013), pp. 271–318. DOI: `10.1112/S1461157013000119`. arXiv: `arXiv:1211.1931` [math.AG].

[82] Yang-Hui He. "Calabi-Yau varieties: from quiver representations to dessins d'enfants". In: (2016). arXiv: `arXiv:1611.09398` [math.AG].

[83] Enrico Arbarello, Maurizio Cornalba, and Phillip A. Griffiths. *Geometry of Algebraic Curves, Volume II*. Springer, 2011. ISBN: 978-3-540-69392-5.

[84] Leo P. Kadanoff and Gordon Baym. *Quantum Statistical Mechanics: Green's Function Methods in Equilibrium and Nonequilibrium Problems*. New York: W.A. Benjamin, 1962.

[85] A.J. Niemi and G.W. Semenoff. "Finite temperature quantum field theory in Minkowski space". In: *Annals Phys.* 152 (1984), p. 105. DOI: `10.1016/0003-4916(84)90082-4`.

[86] J. Polchinski. *String Theory. Vol. 1: An introduction to the bosonic string*. Cambridge University Press, 1998. ISBN: 978-0-511-25227-3, 978-0-521-67227-6, 978-0-521-63303-1.

[87] Petr Hořava. "Strings on worldsheet orbifolds". In: *Nucl. Phys. B* 327 (1989), p. 461. DOI: `10.1016/0550-3213(89)90279-4`.

[88] Petr Hořava. "Background duality of open string models". In: *Phys. Lett. B* 231 (1989), p. 251. DOI: `10.1016/0370-2693(89)90209-8`.

[89] Augusto Sagnotti. "Open strings and their symmetry groups". In: *NATO Advanced Summer Institute on Nonperturbative Quantum Field Theory (Cargese Summer Institute)*. 1987, p. 0521. arXiv: `arXiv:hep-th/0208020`.

[90] Alex Kamenev. "Many-body theory of non-equilibrium systems". In: (2004). eprint: `arXiv:cond-mat/0412296`.

[91] Alex Kamenev and Alex Levchenko. "Keldysh technique and nonlinear sigma-model: Basic principles and applications". In: *Adv. Phys.* 58 (2009), p. 197. DOI: `10.1080/00018730902850504`. eprint: `arXiv:0901.3586` (cond-mat.other).

[92] A.I. Larkin and Yu.N. Ovchinnikov. "Nonlinear conductivity of superconductors in the mixed state". In: *JETP* 41 (1975), p. 960.

[93] David C. Langreth and John W. Wilkins. "Theory of Spin Resonance in Dilute Magnetic Alloys". In: *Phys. Rev. B* 6 (1972), pp. 3189–3227. DOI: `10.1103/PhysRevB.6.3189`.

[94] D. C. Langreth. "Linear and nonlinear response theory with applications". In: *Linear and Nonlinear Electron Transport in Solids*. Ed. by J. T. Devreese and V. E. van Doren. Plenum Press, 1976.

[95] Murray Gell-Mann and James B. Hartle. "Classical equations for quantum systems". In: *Phys. Rev. D* 47 (1993), p. 3345. DOI: `10.1103/PhysRevD.47.3345`. arXiv: `arXiv:gr-qc/9210010`.

[96] R.P. Feynman and F.L. Vernon Jr. "The Theory of a general quantum system interacting with a linear dissipative system". In: *Annals Phys.* 24 (1963), p. 118. DOI: `10.1016/0003-4916(63)90068-X`.

[97] Richard Phillips Feynman and Albert Roach Hibbs. *Quantum mechanics and path integrals*. International series in pure and applied physics. New York, NY: McGraw-Hill, 1965.

[98] Petr Hořava and Christopher J. Mogni. "String perturbation theory on the Schwinger-Keldysh time contour". In: (2020). eprint: `arXiv:2009.03940` (hep-th).

[99] A.H. Mueller and D.T. Son. "On the Equivalence between the Boltzmann equation and classical field theory at large occupation numbers". In: *Phys. Lett. B* 582 (2004), pp. 279–287. DOI: `10.1016/j.physletb.2003.12.047`. eprint: `arXiv:hep-ph/0212198`.

[100] P.C. Martin, E.D. Siggia, and H.A. Rose. "Statistical Dynamics of Classical Systems". In: *Phys. Rev. A* (1973), pp. 423–437. DOI: `10.1103/PhysRevA.8.423`.

[101] De Dominicis, C. "Techniques de renormalization de la théorie des champs et dynamique des phénomènes critiques". In: *J. Phys. (Paris) Colloques* 37 (1976), pp. C1–247. DOI: `10.1051/jphyscol:1976138`.

[102] Hans-Karl Janssen. "On a Lagrangean for classical field dynamics and renormalization group calculations of dynamical critical properties". In: *Zeitsch. Phys. B* 23.4 (1976), p. 377. DOI: `10.1007/BF01316547`.

[103] Michael B. Green, J.H. Schwarz, and Edward Witten. *Superstring Theory. Vol. 1: Introduction*. Cambridge Monographs on Mathematical Physics. Cambridge U. Press, 1988. ISBN: 978-0-521-35752-4.

[104]   Allan Adams et al. "Causality, analyticity and an IR obstruction to UV completion". In: *JHEP* 10 (2006), p. 014. DOI: `10.1088/1126-6708/2006/10/014`. arXiv: `hep-th/0602178 [hep-th]`.

[105]   Zachary Fisher and Christopher J. Mogni. (to appear).

[106]   Hirosi Ooguri and Cumrun Vafa. "Non-supersymmetric AdS and the Swampland". In: (2016). arXiv: `1610.01533 [hep-th]`.

[107]   Ben Freivogel and Matthew Kleban. "Vacua Morghulis". In: (2016). arXiv: `1610.04564 [hep-th]`.

[108]   Edward Witten. "The Feynman $i\epsilon$ in string theory". In: *JHEP* 04 (2015), p. 055. DOI: `10.1007/JHEP04(2015)055`. arXiv: `arXiv:1307.5124 [hep-th]`.

[109]   Roji Pius and Ashoke Sen. "Cutkosky rules for superstring field theory". In: *JHEP* 10 (2016). [Erratum: JHEP 09, 122 (2018)], p. 024. DOI: `10.1007/JHEP10(2016)024`. arXiv: `arXiv:1604.01783 [hep-th]`.